Univerzita Karlova
Přírodovědecká fakulta

Studijní program: Chemie
Studijní obor: Makromolekulární Chemie

Nanočástice citlivé na vnější podněty obsahující fenylboronové spojky jako potenciální nosiče léčiv

Stimuli - responsive nanoparticles with boronic ester linkages as a potential carrier for drug delivery

Diplomová práce

Školitel: Ing. Mariusz Uchman, Ph.D
Konzultant: doc. RNDr. Pavel Matějíček, Ph.D

Praha, 2020

Prohlášení:

Prohlašuji, že jsem závěrečnou práci zpracovala samostatně a že jsem uvedla všechny použité informační zdroje a literaturu. Tato práce ani její podstatná část nebyla předložena k získání jiného nebo stejného akademického titulu.

V Praze, dne 03.06.2020

I would like to thank to my supervisor Ing. Mariusz Uchman, Ph.D., to my advisor doc. RNDr. Pavel Matějíček, Ph.D., and to my counselor doc. RNDr. Miroslav Štěpánek, Ph.D. for the opportunity to be the part of the Soft Matter family since the beginning of my journey in Charles University. The door to their office was always open whenever I had a question about my research, and their advices guided, encouraged and motivated me. I would also like to thank to my colleagues for their continuous help and permanently good mood in our laboratory. Special thanks go to my nearest family and to my boyfriend for providing me support throughout my years of study.

Abstrakt

Diplomová práce se zabývá přípravou polymerních systémů citlivých na vnější podněty pro medicínské aplikace založených na postpolymerizační funkcionalizaci trojblokového terpolymeru poly(styren)-*b*-poly(4-vinyl pyridin)-*b*-poly(ethylen oxid) pomocí funkčních skupin schopných vázat dioly 2-bromethyl-4-fluorofenylboronovou kyselinou a 2-bromethyl-fenylboronovou kyselinou. Byl vyvinut plně reprodukovatelný a kontrolovatelný postup kvaternizace N-skupiny 4-pyridinylového kruhu uvedenými funkčními skupinami a výtěžek kvaternizační reakce byl určen pomocí ^{11}B a ^{1}H NMR a infračervené spektroskopie. Dále byl vypracován protokol reprodukovatelné přípravy stabilních polymerních nanočástic ve vodných pufrech o různém pH vzniklých samoskládáním těchto funkcionalizovaných trojblokových terpolymerů. Struktura a chování připravených nanočástic byly studovány pomocí statického, dynamického a elektroforetického rozptylu světla a kryogenní transmisní elektronové mikroskopie. S ohledem na možné aplikace byl pomocí absorpční a fluorescenční spektroskopie zkoumána vazba modelového léčiva Alizarinu na fenylboronové funkční skupiny připravených nanočástic. Byla důkladně studována vazba Alizarinu na polymerní částice a jeho uvolňování vlivem změny vnějších podmínek jako pH a koncentrace cukrů a příbuzných diolů.

Abstract

This thesis deals with the post-polymerization functionalization of a pH-responsive poly(styrene)-*b*-poly(4-vinyl pyridine)-*b*-poly(ethylene oxide) triblock terpolymer with stimuli responsive and diol-binding 2-bromomethyl-4-fluorophenylboronic acid and 2-bromomethyl-phenylboronic acid suitable for biomedical applications. A reproducible method of quaternization of poly(4-vinyl pyridine) block with prescriptible quaternization ratio was developed and the reaction yield was analyzed by ^{11}B, ^{1}H NMR and infrared spectroscopy. A reproducible self-assembly protocol for stable nanoparticles from functionalized stimuli-responsive triblock terpolymer was found, and the nanoparticles were studied by static, dynamic and electrophoretic light scattering, and cryogenic transmission electron microscopy. Fluorescence and UV-VIS spectroscopy measurements were performed for description of boron-ester linkages formation and hydrolysis with model drug Alizarin as a study of encapsulation and release reactions together with sugar sensing reactions for potential drug delivery.

Abbreviations

AL – Alizarin

ALfree – Alizarin molecules in water

ARS – Alizarin Red S

ATP – adenosine triphosphate

C – ascorbic acid

CONTIN – constrained inverse Laplace transform routine

Cryo-TEM – cryogenic transmission electron microscopy

DLS – dynamic light scattering

F – fructose

FID – free induction decay

FPBA – 2-bromomethyl-4-fluorophenylboronic acid

FT-IR – Fourier-transform infrared spectroscopy

G – galactose

IR – infrared

LCST – lower critical solution concentration

LS – light scattering

NIR – near infrared

NMR – nuclear magnetic resonance

PBA – 2-bromomethyl phenylboronic acid

PEO – poly(ethylene oxide)

PNIPAAm – poly(*N*-isopropylacrylamide)

PS – poly(styrene)

PVPQ – quaternized poly(vinyl pyridine)

Pyr – pyridine

P2VP – poly(2-vinyl pyridine)

P4VP – poly(4-vinyl pyridine)

SLS – static light scattering

SVE – poly(styrene)-*b*-poly(4-vinyl pyridine)-*b*-poly(ethylene oxide)

UV – ultraviolet

VIS – visible

Content

1. Introduction

Block copolymers in selective solvent spontaneously undergo microphase separation by forming micelles. The limitation of AB diblock copolymers self-assembly into only spherical micelles, cylindrical nanoparticles and bilayers drives the effort of research towards investigation of triblock terpolymers self-assembly. The incorporation of a third block that can be either solvophilic or solvophobic to AB diblocks promises more elaborate structures of nanoparticles, that find potential use in drug delivery as a transport vehicle.

Triblock terpolymer nanoparticles can be used in drug delivery, but their composition must be tailored, which is a technically demanding task. For such purpose, creating stimuli-responsive polymer blocks and above all incorporating of functional groups into triblock chains may generate smart triblock nanocarriers, thereby increasing their specificity and responsiveness to drug delivery pathways. However, the polymerization of a polymer rich in functional groups may be difficult and time consuming. Moreover, the control over the functionalization of a polymer during the polymerization process is highly unpredictable.

For this reason, we propose in this thesis a new approach for the inclusion of a functional group into the poly(styrene)-*b*-poly(4-vinyl pyridine)-*b*-poly(ethylene oxide) triblock terpolymer through a quick and controllable post-polymerization modification. This approach enabled us to quaternize predetermined and controlled number of 4-vinyl pyridine units of a triblock with stimuli responsive and diol-binding phenylboronic acid. ^{11}B, ^{1}H NMR and infrared spectroscopy confirmed the reproducibility of the specific quaternization reaction yield. Light scattering techniques and cryo-TEM imaging showed reproducibility of self-assembly protocol for preparation of stable nanoparticles. Overall, UV-VIS and fluorescence spectroscopy showed the high responsiveness to sugars and red/ox environment of such a boronic acid-modified stimuli-responsive triblock. Accordingly, our findings show the potential of using this polymer as a carrier for a diol-containing anti-cancer drug with a prescriptible drug molar ratio in the drug delivery field.

2. Overview of the literature

Triblock terpolymers can self-assemble into nanoparticles and can be potentially used in drug delivery. The field of drug transport is technically demanding; thus, the polymer composition has to be designed carefully. The polymer structure and functionality strongly influence nanoparticle behavior in physiological environment. In one hand, the composition in terms of order, length and solubility of blocks plays a key role in nanoparticles shape.[1, 2, 3] In other hand, the sensitivity to external stimuli through stimuli-responsive blocks and the introduction of functional groups to the polymeric structure can add a smart estate to triblocks and make them more attractive for the drug delivery field.[4, 5] Following section serves as a guideline throughout the structural variables affecting nanoparticles shape and architecture. Moreover, it shows effect of inclusion of the stimuli-responsive block into the polymeric structure and it further explains the effectivity of functionalization of polymer by post polymerization reactions.

2.1. Triblock terpolymer structure

The architecture of nanostructures can be planned right from the start of triblock terpolymer polymerization. Triblock terpolymers consist of one solvophilic block and two incompatible solvophobic block but we know also triblocks with two solvophilic blocks and one solvophobic block. In both cases the incompatibility between individual blocks ensures spontaneous microphase separation and formation of three types of domains (e.g., core-shell-corona) within one nanostructure when transferred to selective solvent. The position of each block in triblock terpolymers in hand with block length and solubility affects the distribution of domains within one nanostructure. In other words, we can make different triblock terpolymers issued from three types of blocks by altering order of blocks in a triblock terpolymer.

2.1.1. Order of blocks in triblock terpolymers

The block order in triblocks plays a crucial role in self-assembly by affecting the nanoparticle shape and thus, also its application. Blocks in triblock terpolymers can be organized not only in linear triblocks but also in non-linear triblocks.[1, 2, 8] Self-assembled

blends of two diblock copolymers with one identical block can also be considered as an alternative to triblock terpolymers systems. This part will be mainly focused on linear triblock terpolymers self-assembly and also examples of non-linear systems and blends used for formation of nanoparticles.

Linear triblock terpolymers

First of all, linear triblock terpolymers involve the important part of triblock self-assembly studies. There are principally three possibilities of blocks ordering, the ABC type, BAC type and ACB type, where A usually stands for solvophilic block, C for solvophobic block and B can act as either the less solvophilic block than the A or the less solvophobic than C block.[1, 8]

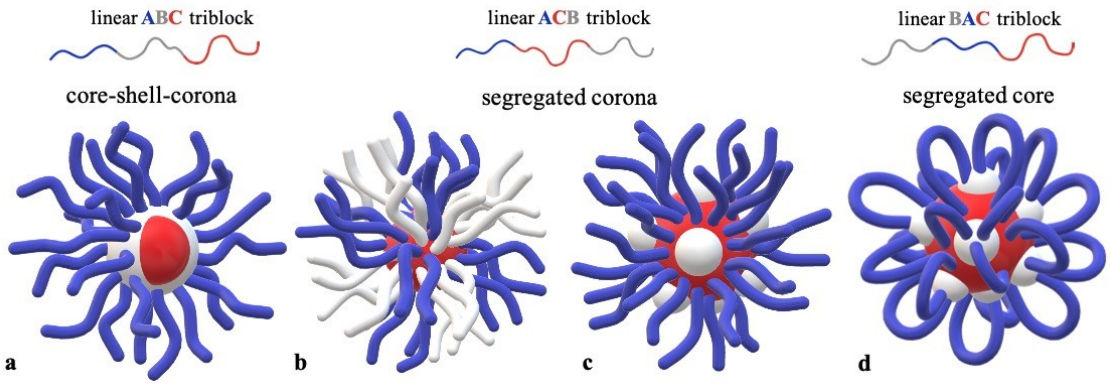

Figure 1:Micelles from linear triblock terpolymers with different order of block. ***Blue****-hydrophilic block A,* ***white****-less hydrophobic block B,* ***red****-hydrophobic block C.* ***a****-core-shell-corona micelle,* ***b****-corona-segregated micelle,* ***c****-corona-segregated micelle with collapsed block B,* ***d****-core-segregated flowerlike micelle.*

ABC triblock terpolymers with the least soluble block C at the one side of the chain and the solvophilic block A at the other side can self-assemble in structure types depicted in Figure 1 and Figure 2. The most common self-assembly in A selective solvent yields concentric core-shell-corona micelle (Figure 1, **a**).[6, 7, 8, 10] Even though three domains of nanoparticle, these are A block corona, B block shell and C block core, miss independent access to the exterior of micelles, this polymer is often used for drug delivery systems. The solvent isolated C core effectively protects solubilized cargo and prolongs the circulation time of transported drug in the body.[8, 9]

However, triblocks can also self-assemble into corona-segregated nanoparticles. The approach to obtain this type of nanoparticles is based on the play with selection of the selective solvent. ABC triblock needs to be dissolved in non-solvent for B block that is at the same time a good solvent for blocks A and C.[11, 12] Also, ACB triblocks yield this type of nanoparticles with segregated corona when dissolved in A and B selective solvent. Example of corona-segregated nanoparticle is in Figure 1, micelle type **b**. Corona segregated nanoparticles can be further tuned by changing of the solvent to the non-solvent for one of the corona forming block, most frequently the B block. This solvent change leads to the collapse of a solvophobic B block and formation of separate micellar compartments on the surface of the C block core. These multicompartment core segregated nanoparticles issued from corona segregated micelles shown as micelle type **c** in Figure 1. They attract attention thanks to the separate access of C and B domains of micelles to the surface of the nanoparticle that is highly effective for dual solubilization of compatible and mainly incompatible drugs for drug delivery.[13, 14, 15, 16]

In comparison, the BAC triblock terpolymer self-assemble in a very similar structure type that are core segregated nanoparticles also called as flowerlike micelles. In more detailed, the BAC triblock is dissolved in a selective solvent for only the middle A block. The incompatibility favors the formation of an A block polymer loop between B block at one side and the C block at the other side of the loop. Following the loop formation, the incompatibility between B and C block favors the microphase separation at a core level yielding two types of separate core subdomains represented in Figure 1, in micelle type **d**. The figure represents mainly the C core with protruding B compartments that are located mainly in the C core. These core-segregated nanoparticles with solvophilic block loops are also very attractive for dual drug delivery for the same reasons why ABC corona segregated nanoparticles are. Both of the core domains have individual access to the nanoparticle surface and can serve as a good environment to dissolve incompatible drugs or different types of cargo.[17, 18]

Non-linear triblock terpolymers and polymer blends

Three types of domains within one nanostructure can also self-organize after blending two diblock copolymers with one identical block, AB and BC respectively. Although this method of using two diblocks over more polymerization demanding triblocks brings more opportunities to control and tune the system, this approach generally faces struggles with

a likelihood aggregation or formation of two separate nanoparticles instead of one. Literature presents examples of concentric core-shell-corona nanoparticles of spherical or cylindrical shape.[19, 20, 21] When using AB and CD diblocks with electrostatic interaction between B and C blocks, the self-assembly of these two diblocks can yield higher order core-shell-corona nanoparticles, Figure 2, micelle type **a**. In addition, the blend of AB and BC diblocks can self-assemble into hamburger-like nanoparticles, that can turn to segregated rod-like nanoparticles as can be seen in the Figure 2, micelle type **f** and **g**, respectively.

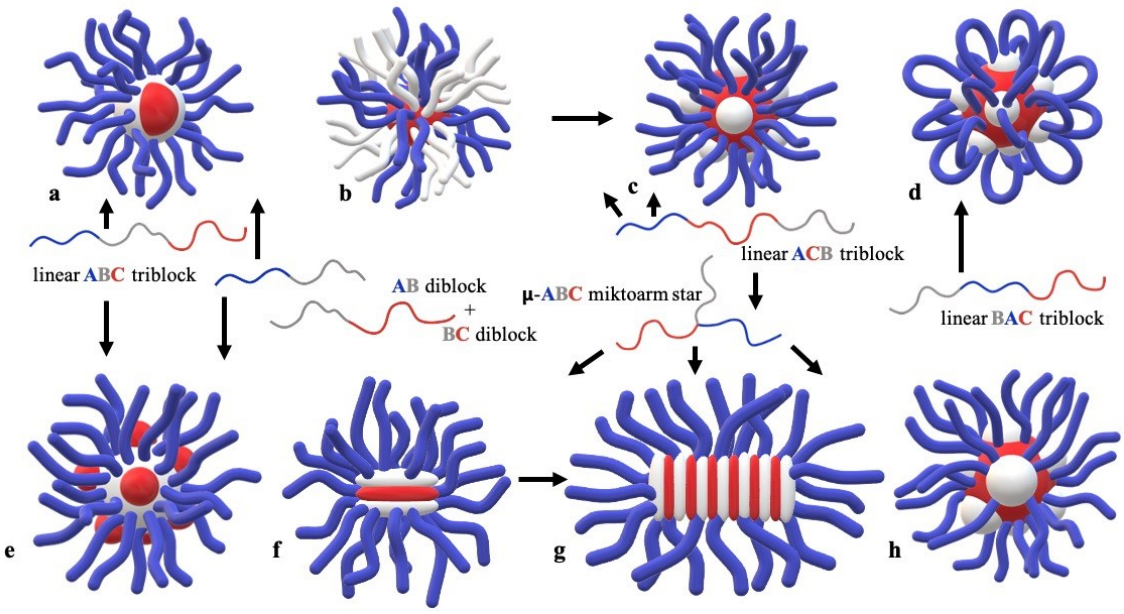

Figure 2:Micelles form linear, non-linear triblock terpolymers and from polymer blends (arrows assign polymers to allowed nanoparticle shapes based on polymer architecture). ***Blue****-hydrophilic block A,* ***white****-less hydrophobic block B,* ***red****-hydrophobic block C.* ***a****-core-shell-corona micelle,* ***b****-corona segregated micelle,* ***c****-corona segregated micelle with collapsed block B,* ***d****-core segregated flowerlike micelle,* ***e****-core segregated micelle,* ***f****-hamburgerlike micelle,* ***g****-wormlike core segregated micelle with B and C alternating discs,* ***h****-core segregated micelle.*

Three ABC blocks can be organized into ABC miktoarm stars terpolymer architecture. The convergence of three blocks at common point in hand forbid the concentric core-shell-corona nanoparticle formation adopted by linear ABC triblocks but at other hand this block organization give rise to a number of elaborate multicompartment nanoparticles. In the same way as linear ABC triblocks, miktoarm polymers consist of three incompatible blocks A, B and C.[15, 22] First, the A block typically stands for a solvophilic block while B and C blocks stand for incompatible solvophobic block ensuring microphase separation during self-assembly into three discrete nanoparticle

domains. Self-assembly of these polymers can adopt spherical micelles with segregated core consisting of C block, B block compartments in touch with core block and A block corona pointing from the interphase points between C and B block, Figure 2, micelle type **h**. These nanoparticles can appear similar to core segregated structures from linear ABC, ACB and BAC triblocks, shown as micelle types **e**, **c** and **d**, respectively. Comparing core segregated micelles issued from ABC, ACB and CAB to miktoarm star triblocks core segregated micelles, A block corona in ABC triblocks is issued from entire surface of B block, in ACB triblocks from C block surface and finally, in BAC nanoparticles is connected to both of the remaining blocks B and C by forming a solvophilic loop. Then, ABC miktoarm polymers can form also hamburger like nanoparticles with alternating flat B and C discs forming core compartments surrounded by solvophilic A corona, micelle type **f** in Figure 2. When changing the block length of one of the blocks resulting in the change of ratio between solvophobic and solvophilic polymer part, the self-assembly can yield worm-like particles with alternating B and C discs forming core surrounded by A corona, micelle type **g**.[22, 23, 24, 25, 26] The influence of the ratio between solvophobic and solvophilic blocks will be the topic of following section.

Given these points, the organization of blocks in polymeric chain highly influences the self-assembly of triblock terpolymers. Apart of core-shell-corona nanoparticles, core segregated or corona segregated nanoparticles, hamburger-like and worm-like micelles described above, triblock terpolymers offer even more structures that can self-assemble by varying the block organization. As has been noted, the careful selection of blocks in polymer and their placement can tune the macroscopic shape of particles and can influence the polymer application.

2.1.2. Length of blocks in triblock terpolymers

Variety of presented nanostructures including concentric core-shell-corona micelles, core or corona-segregated micelles can be further modified by varying the blocks length. In one hand, the overall length of the polymer and the compatibility between blocks affect the microphase separation of micelles, in other hand the ratio of solvophobic and solvophilic block strongly influences the macroscopic shape of nanoparticles. These factors play an important role in formation of nanoparticles and should be considered while planning the synthesis of the polymer.

Phase diagram of block copolymers in bulk and solution

The connecting of three chemically independent polymer blocks in one structure naturally brings some degree of incompatibility. Moreover, the incompatibility between blocks in triblock terpolymers for drug delivery is even desired. When transferred to a selective solvent, the polymer system tries to reach the minimum-energy state favoring the microphase separation. Microphase separation is a two components equilibrium process between the enthalpy and entropy forces. The enthalpy force relates to the mixing and de-mixing of the polymer chains with solvent and the entropy force represents the conformation of polymer chains.[1, 2, 3] In case of homopolymer in solution, the explicit formula for the enthalpy and entropy increment associated to the mixing of polymer with solvent is the Flory-Huggins equation,

$$\Delta G_m = RT\,[n_1 \ln \emptyset_1 + n_2 \ln \emptyset_2 + n_1 \emptyset_2 \chi_{12}] \quad (1)$$

where ΔG_m is the change in Gibbs molar energy of mixing of the polymer with solvent, R is the gas constant, T is the absolute temperature, n_1 is the number of moles and $\emptyset_1$ is the volume fraction of the solvent (component 1), n_2 is the number of moles and $\emptyset_2$ is the volume fraction of the polymer (component 2) and finally, χ_{12} is the interaction parameter of interdispersing polymer and solvent molecules. When the system contains a diblock copolymer with two blocks A and B, we can express the interaction parameter χ_{AB}, between these blocks as follows

$$\chi_{AB} = z\Delta w\,/kT \quad (2)$$

where Δw stands for the energy change or the free energy cost per A-B interaction compared to A-A and B-B interactions, and where z stands for the number of nearest neighbor monomers for a lattice site.[27, 28] The equation shows, that the Flory-Huggins segment-segment interaction parameter, χ_{AB} is inversely proportional to the temperature T, and is also proportional to the enthalpy term of Flory-Huggins equation. In addition, in self-assembly of block copolymers, the entropy term of Flory-Huggins equation is given by χN, where N is the degree of polymerization or in other words the number of

monomers in the polymer chain. With this in mind, the self-assembly structure of a diblock block copolymer depends on following controllable parameters: 1. the Flory-Huggins interaction parameter χ; 2. the degree of polymerization, N; 3. the volume fraction of the components blocks, f; and 4. the polymer architecture. Variation of the relation between χN and f described as a phase diagram of block copolymers results in various structure types, among them disorganized chains, lamellae, cylinders, close-packed spheres, gyroids, etc. (Figure 3, **a**).[1, 3, 27] In case of triblock terpolymers, one interaction parameter increases to three and one composition variable also increases to two. As a result of a higher number of variables, triblock terpolymers grant the formation of a higher number of self-assembled structure types.[1, 3, 27] The example of a diblock and triblock phase diagram is in the Figure 3.

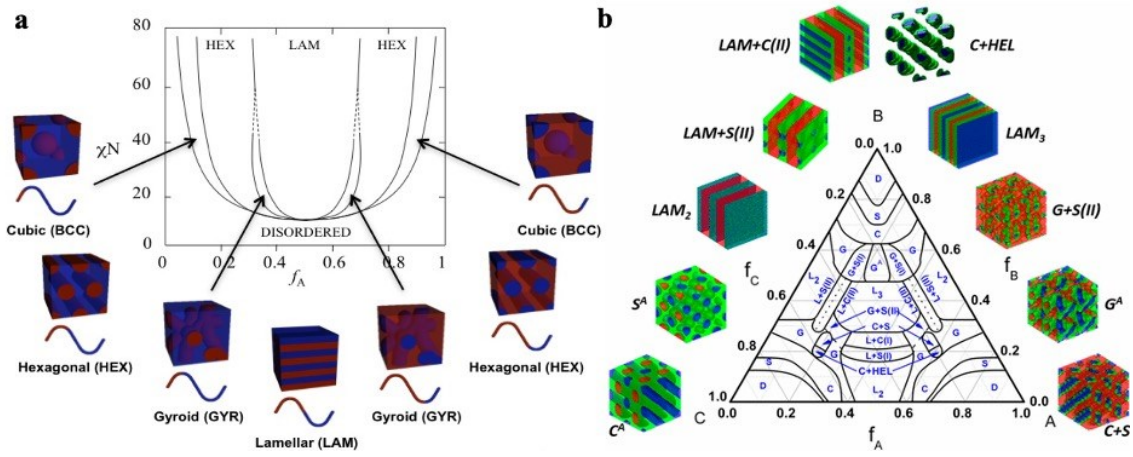

*Figure 3:Phase diagram for **a**-diblock copolymers[27] and **b**-triblock terpolymers in bulk.[3]*

Packing parameter

Predictions of nanoparticle shapes from polymers can be made in simpler way than these based on taking into account the entropy term and enthalpy term from Flory-Huggins theory. When describing the microphase separation system beyond the segregation limit, the interaction of segments of individual blocks and solvent are neglected. Then, the morphology of the self-assembled system is given by the volume ratio of solvophobic and solvophilic blocks called as packing parameter, P.[2, 29, 30, 31] Packing parameter equation is given by the theory of self-assembly of surfactants a phospholipids. Thus, the

simplified formula of dimensionless packing parameter for lipid vesicles and bilayers is as follows

$$P = V/a_0 \cdot l_c \tag{3}$$

where V is the volume of hydrophobic part, a_0 is the effective area of hydrophilic headgroup and l_c is the hydrophobic chain length, shown in Figure 4, **a**. In block copolymers, the packing parameter is expressed by the volume ratio of solvophobic and solvophilic blocks.[2, 30] The volume ratios are usually replaced by molar mass of the blocks and the packing parameter is estimated in following manner

$$P = {M_{hydrophobic\ block}}\Big/{M_{hydrophobic\ block} + M_{hydrophilic\ block}} \tag{4}$$

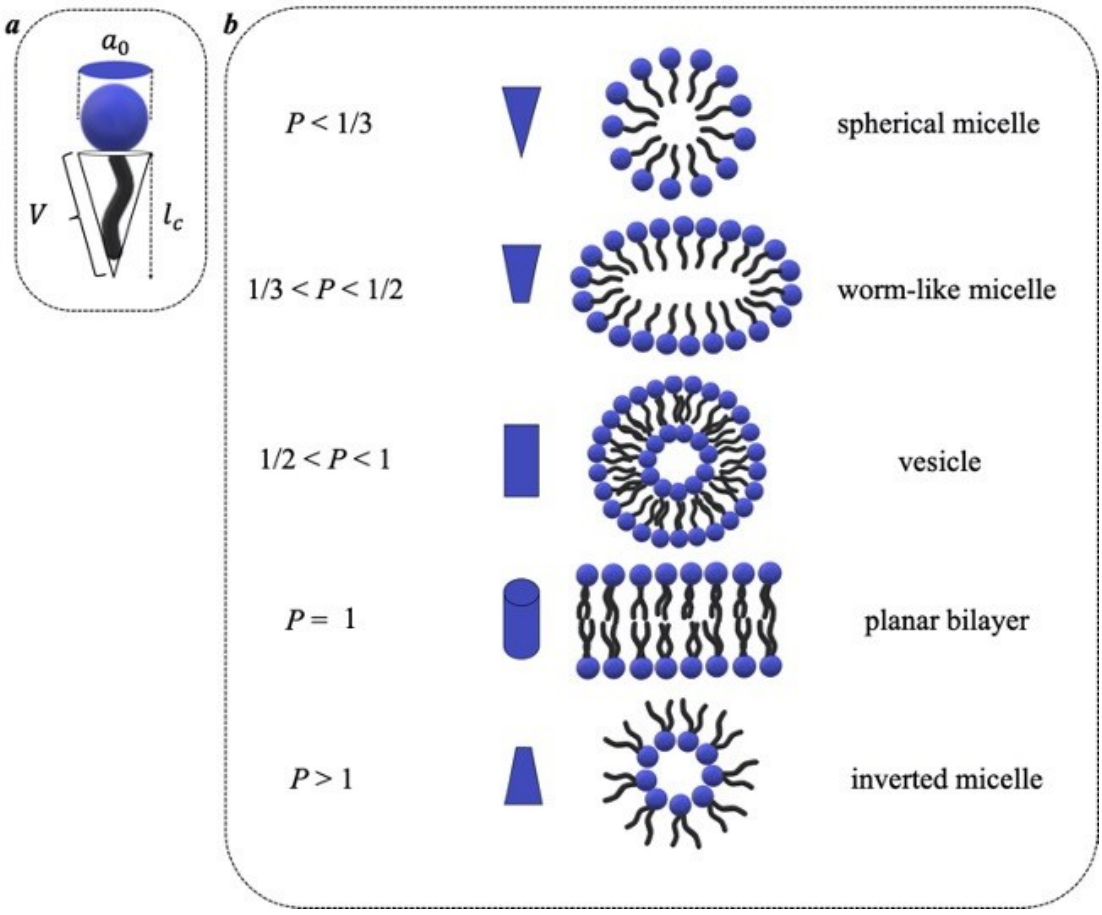

*Figure 4: Representation of packing parameter: **a**-packing parameter unit, **b**-nanoparticle shapes based on packing parameter value. **Blue**-hydrophilic part, **black**-hydrophobic part of chain.*

Equally, to the vesicles and bilayers structures based on P, triblocks show the same structures based on this ratio. For example, while P lower than 1/3 represents spherical micelles, $1/3 < P < 1/2$ is typical for wormlike micelles. More examples are show in Figure 4, **b**.[2, 30, 32]

To conclude, structural, macroscopic and microscopic properties of triblocks terpolymer nanoparticles are influenced mainly by the order of blocks, then by the block length, by the compatibility between blocks and also by the ratio between solvophilic and solvophobic polymer blocks. In addition, the structure and function of triblock terpolymer nanoparticles can vary once self-assembled, in function of the response of polymer functional groups to the outer stimuli. These stimuli-responsive blocks and functional groups will be described in following chapter.

2.2. Stimuli-responsive blocks and functional groups

The control over the self-assembly structure of triblock terpolymers can be obtained by a smart design of triblock terpolymer composition. Apart of above described influence of order, length and compatibility between blocks in the triblock structure, the inclusion of functional groups and stimuli-responsive blocks can vary the structure of nanoparticles even after the self-assembly. Stimuli-responsive blocks and functional groups can change properties upon being exposed to external stimuli. These external stimuli are for example the exposition to light, temperature change, or pH change.[4, 10, 22, 24] The response of these groups and bocks to the specific stimuli can change the polymer solubility, change binding selectivity towards a class of compounds or streamline some reactions pathways as for example the drug release from nanoparticles.

2.2.1. Photo-sensitive blocks and groups

Polymer blocks containing functional groups sensitive to light irritation[4, 35] can undergo for example photodimerization or in contrary photocleavage reactions. Both reactions can improve encapsulation and release of cargo to and from polymeric nanoparticles in a required time and place. In more detailed about photodimerization reactions, this

photochemical process between electronically excited unsaturated molecule and the unexcited molecule of the same species yield addition product. Photodimerization allows a fast change of the molecular and thus, also micellar size and function. An example of such a molecule is coumarin. Coumarin can be brought to the polymer by click reaction between azide functionalized moieties of the polymer and coumarin molecules forming an ester bond.[4, 33] This photodimerization molecule can reversibly form dimers undergoing a [2+2] photodimerization where cycloaddition involves carbon-carbon double bonds formation between two neighboring coumarin molecules resulting in a cyclobutene dimer. The light >310 nm induces the photodimerization reaction and in contrary, the excitation of a coumarin dimer with light of 250 nm induces its decomposition. When applying this molecule to the drug delivery system, the photodimerization can serve for the entrapment of a transported cargo in the newly formed pore, while the photodecomposition of the complex induces the release of the cargo at its target place.[33] An example is shown in Figure 5.

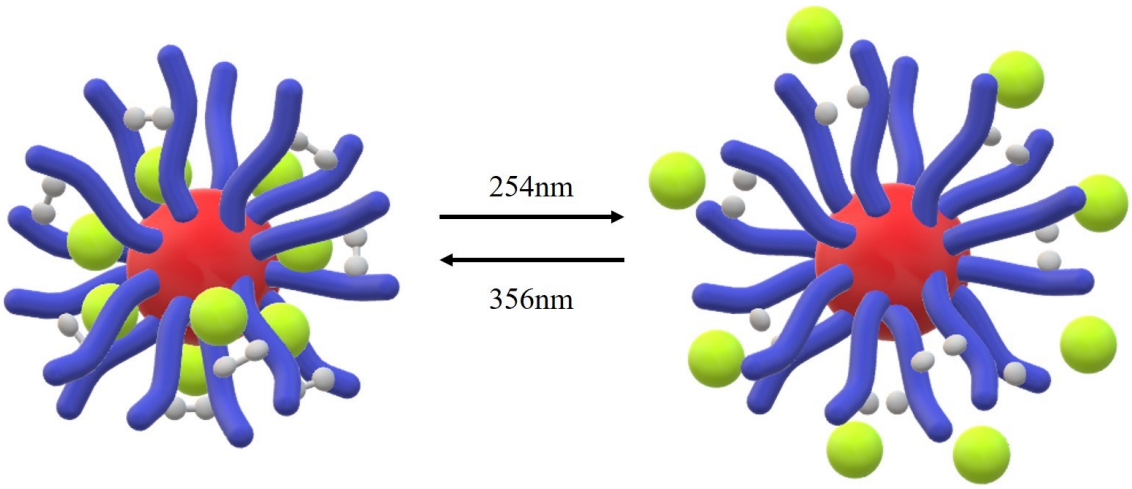

Figure 5:Nanoparticles with photo-sensitive coumarin gates. **Red**-*hydrophobic core,* **blue**-*hydrophilic corona,* **white**-*coumarin molecules,* **green**-*transported drug.* **Left image**-*closed coumarin-dimer gate,* **right image**-*opened gate with coumarin single molecules.*

However, UV wavelengths region is not considered as the most effective in the field of drug delivery due to the low penetration depth through the tissues. More convenient for the induction of photosensitive reaction in drug delivery field is the near infrared, NIR, radiation. Also, at these wavelengths coumarin is one of the molecules showing promises in photosensitive reactions. For example, Li et al. shows the mesoporous silica nanoparticles with coumarin-containing photoresponsive amphiphilic polymer.[35] In

there, when the nanoparticle is excited with 800 nm light, the ester bond cleavage of the coumarin conjugated methacrylic acid block destabilized the polymer. This destabilization of whole polymer continuously increases the release of doxorubicin drug from the nanoparticle.

2.2.2. Thermo-responsive blocks and groups

Thermo responsive polymers commonly show a phase transition from a solvent swollen hydrated state to a dehydrated polymer state with a large part of a reduced volume of the polymer when changing the temperature.[4, 22, 24, 37, 38, 39] An example of such a polymer extensively used in drug delivery is poly(*N*-isopropylacrylamide), PNIPAAm. This polymer and its derivatives in most of the studies show a lower critical solution temperature, LCST close to human body temperature. When the temperature of the system containing PNIPAAm is in a temperature below LCST, the polymer is in its hydrated and swollen form making the drug encapsulation the most effective. Once system reaches human body temperature which is above the LCST of PNIPAAm, the encapsulated cargo is released thanks to the dehydration and contraction of the polymer chain as shown in Figure 6.[35]

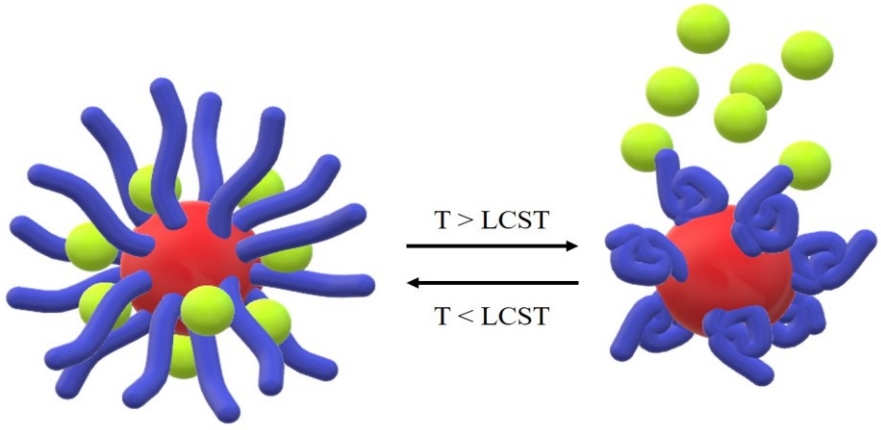

Figure 6:Nanoparticle with thermo-responsive PNIPAAm block. **Red**-*hydrophobic core,* **blue**-*thermo-responsive PNIPAAm corona,* **green**-*transported drug.* **Left image**-*hydrated and extended corona chains transporting the cargo,* **right image**-*dehydrated corona chains releasing the cargo.*

This polymer was used for example in a study Zhou and co-workers concerning a drug delivery copolymer system composed of poly(*N*-isopropylacrylamide) and poly(2-hydroxyethyl methacrylate). In this system, hybrid nanoparticles were used as a drug delivery vehicle for aspirin transport that can be released above the LCST of 36.9°C.[36]

2.2.3. pH-Responsive blocks and groups

The pH-sensitive systems are the most popular among the delivery system in biomedicine. Naturally, the pH of the extracellular environment (pH 7) differs from the pH of the endosome and lysosome environment (pH 4). Also, the tumor microenvironment caused by the production of lactic acid and hydrolysis of ATP can act as a target delivery area for pH sensitive drug delivery systems.[40, 41] Groups and polymer blocks sensitive to pH usually rely on changes of the solubility, size, shape or binding properties, and a number of pH sensitive groups and polymers can be hydrolyzed or dissolved with decreasing pH. This advantage in structural and chemical changes upon the pH stimulus offers an advantage to these systems to work autonomous from a complicated release mechanisms and reactions while these mechanisms are in the most cases reversible.[40, 41, 42, 43, 44] An example of a pH sensitive polymer that changes solubility, attraction to other molecules and also that can be further modified with additional functional groups is poly(vinyl pyridine).

Poly(vinyl pyridine) as a stimuli responsive block

Poly(vinyl pyridine) can be categorized in stimuli-responsive polymers based on two types of parameters. The first concerns its natural inherent properties relied to the chemical properties and position of nitrogen atom in the phenyl ring. The second is relied to the properties that poly(vinyl pyridine) may acquire upon modification of the nitrogen atom.

To begin with the structure factors, poly(vinyl pyridine) exists in two isomers, these are poly(2-vinyl pyridine), (P2VP) and poly(4-vinyl pyridine), (P4VP). These two isomers act as weak poly-base that can be soluble or insoluble in water, depending on the pH of the solution. Above the pH 4.8, both of the polymers are water insoluble, and in contrary the polymer gets protonated and water soluble when crossing the pK_A of the nitrogen on the phenyl ring to the lower pH values.[45, 46, 47] Relied to the protonation of the

nitrogen atom, when P2VP and P4VP are present in its insoluble non-protonated form, two and more vinyl pyridine units can form nitrogen-metal complexes with metals as for example copper, iron or cobalt. The lone electron pair of the neighboring nitrogen atoms can chelate metal ions. The effect of geometry of vinyl pyridine molecules on the metal complexation shows P4VP to be more geometrically accessible for formation of metal complexes over the P2VP.[48, 49, 50, 51, 52, 53] In other hand, there are examples of nanoparticles from triblock terpolymer containing P2VP block, that can self-assemble in manner permitting to fuse multiple P2VP blocks of individual micelles. When P2VP is present in a segregated-corona micellar system acting as a collapsed corona block, P2VP compartments of two and more near micelles can stick together thanks to the hydrophobic effect at certain concentration and can form long patchy micelles. This type of micelles with P2VP block is shown in article of See A. H. Gröschel et al.[15, 54, 55]

In addition to intrinsic properties of poly(2-vinyl pyridine) and poly(4-vinyl pyridine), P2VP and P4VP can become a suitable host for implementation of a new polymeric property. Nitrogen atom on the phenyl ring can be quaternized by a halogenated compound with pendant functional groups. This halogenated compound acting as a quaternization agent can bring new stimuli responsive properties, based on its chemical properties even after the polymerization reaction. In more detailed, the quaternization reaction of a tertiary amine into quaternary salt by alkyl halides in a polar solvent, also called as Menshutkin reaction can be applied apart of a typical aliphatic amine also to aromatic compounds containing tertiary amines.[45, 56, 57, 58, 59, 92] The feasibility of halogenation of a broad number of chemical compounds as quaternization agents opens opportunities to tune the system in desired way. When designing a triblock terpolymer with a potential use in drug delivery, there is an option to halogenate already known biocompatible compounds that are for example able to sensitively bind drugs. An example of such a stimuli responsive molecule that offers to bind vicinal diol-containing drugs and that is responsive to pH and redox environment is phenylboronic acid.[45] Phenylboronic acid is used in a number of targeted delivery systems and the advantages of its use in triblock terpolymer systems will be described in a following chapter. Menshutkin reaction as a post-polymerization reaction shows a promise in a fast and not technically demanding functionalization of triblocks in desired manner that is mostly required in drug delivery field.

Given these points, incorporation of stimuli-responsive blocks to triblock terpolymer strongly affects polymer journey when applied to usage. Triblock with stimuli-sensitive blocks can change solubility and overall structure in response to outer stimuli and thus, can be controllable during its way to reaching its target. Moreover, when upgrading stimuli-responsive blocks with functional groups showing stimuli-responsive and reversible binding properties by post-polymerization reactions, we can gain a crucial control over the drug delivery system targeting for example cancerous cells.

2.3. Boronic acid as a stimuli-responsive functional group

Boronic acids may bring new functionality to the triblock terpolymers. In this section, let's focus on the derivatives of phenylboronic acid that are in one hand biocompatible and in other hand appropriate for drug delivery thank to the tuned pK_A by the presence of phenyl ring. In addition, phenylboronic acids are reversible in terms of structure related to pH, then reversibly reactive with diols, and also irreversibly sensitive to redox environment.

2.3.1. Structural reversibility

In the first place, boronic acids exists in two types of geometry depending on pH. At physiological and lower pH, boronic acid appears in its neutral trigonal form. Increase of pH over the pK_A of boronic acid turns the trigonal form to the negatively charged tetragonal form. This transition is reversible, so the tetragonal form of molecules can turn back to trigonal form. Moreover, in aprotic solvents two and more molecules of boronic acid in their trigonal form can reversibly associate in boroxine rings. Boroxines are clusters that appear spontaneously in non-aqueous solvents and dissociate spontaneously upon addition of water molecules into the system.[60, 61] Figure 7 shows all three structure types of boronic acid. We know situations, when boroxines and trigonal forms of boronic acid coexist; in block copolymer nanoparticles containing phenylboronic acid on the interface of the hydrophobic block and partially soluble or fully soluble neighbor polymer block. Molecules of phenylboronic acid situated in hydrophobic core are in form of boroxines and a portion of phenylboronic acids situated on the interface between the

hydrophobic core and water accessible shell is in trigonal form. Trigonal and tetragonal form of boronic acid strongly influences the diol binding.

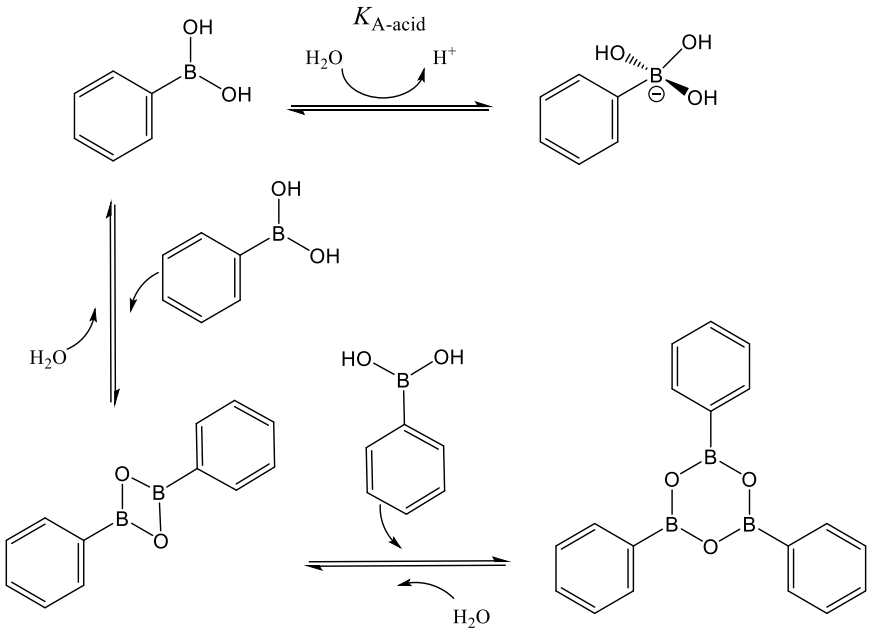

Figure 7: Reversible boronic acid transitions between: ***top****-trigonal form to tetragonal form,* ***bottom****-trigonal form and boroxine ring composed from two molecules(****bottom left****) and from three molecules (****bottom right****).*

2.3.2. Reversible diol binding

Boronic acid can reversibly bind to vicinal diols by forming boronate esters.[60, 61, 62] Binding typically takes place at physiological pH and the ester bond distracts in presence of acid. In more detailed, biding reaction is influenced by pH and thus, also by the geometry of phenyl boronic acid. In general, arylboronic acids bind more effectively to diols at a higher pH, when pH overcomes the pK_A of boronic acid causing the transition from trigonal to tetragonal form. The pK_A values of phenylboronic acid equal to 8.8 may change with substituents on phenyl ring. By functionalization of the phenyl ring we can tune the molecule for specific use either by lowering and also by increasing pH. Mono-, di- and tri-fluoro substitution causes pK_A decrease from 8.8 to 8.6, 7.0 and 6.8, respectively, because of its electron-withdrawing character. This type of functionalization is often used in case of molecules intended to be used in drug delivery, where binding of diols should take place at pH near to the physiological. In contrast, electron-donating groups like methoxy groups can raise the pK_A value of phenylboronic acid from 8.8 to

9.0. The pK_A of phenylboronic is important when choosing the reaction conditions for diol binding.[60, 61, 62, 63] The ester formation between phenylboronic acid and diol occurs the most effectively in a pH that corresponds to the half value of the sum of the pK_A of phenylboronic acid and of the pK_A of newly formed ester. This estimate of ideal pH for the reaction can be calculated from the equation

$$\mathrm{pH} = (\mathrm{p}K_A\,(1) + \mathrm{p}K_A\,(2))/2 \qquad (5)$$

In this equation, pK_A(1) corresponds to boronic acid and pK_A(2) to the newly formed ester.[62, 63] Although diol binding occurs the most effectively at boronic acid´s tetragonal form, the reaction can occur also at the trigonal form but at markedly slower rates. Particularly, Alizarin Red S is a molecule that preferably reacts with trigonal form of phenylboronic acid.[45, 63] Figure 8 shows diol binding at both geometric forms of boronic acid.

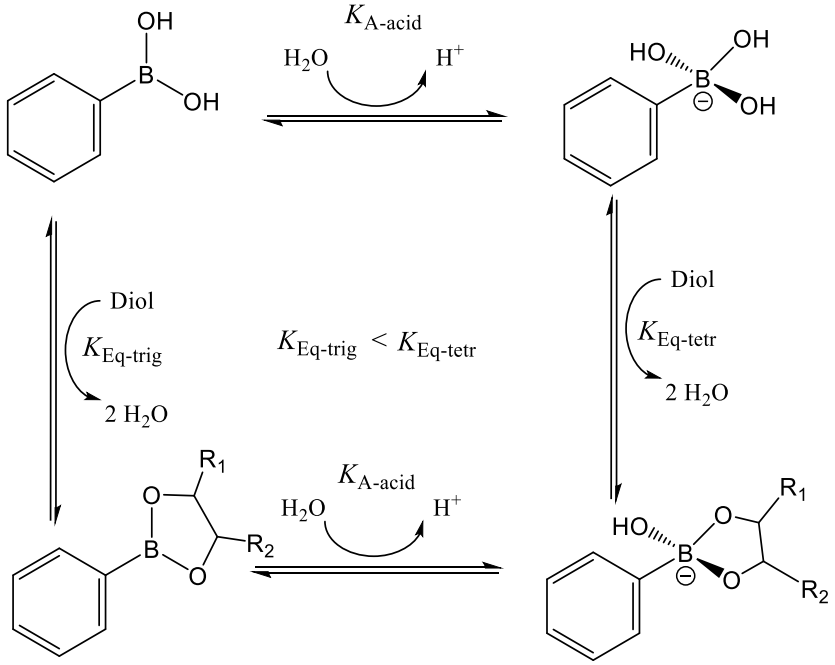

*Figure 8:Boronic acid-diol binding and ester hydrolysis with boronic acid in: **top**- trigonal form and **b**-tetragonal form.*

Binding and release of diols is attractive for the purposes of drug delivery, especially for cancer treatment. For this, phenylboronic acid can be an adequate molecule candidate to be included in nanoparticle systems for drug delivery. Boronic acid can bind to diols at physiological pH and can release the cargo in acidic environment that perfectly to the

environment of cancerous cells. Idea of boronic esters use for targeted delivery of drugs has already been discussed in scientific publications and proves promise provided that boronic acid group is for example grounded in the structure of a currently used anticancer drug Bortezomib (also called as Velcade).[64, 65, 66] Moreover, studies about boronic acid-containing-nanoparticles describe a wide range of approaches for boronic acid mediated sugar sensing.[67, 68, 69] Reversible binding of saccharides is often tied with the application of photosensitive molecules for visualization and better understanding of occurring events.

Alizarin Red S, ARS is an example of fluorophore that result in visible color, absorbance and fluorescence changes between their free forms and boron-dye complexes. Thus, this molecule is ideal for model studies of nanoparticles convenience for drug delivery and can be used for understanding of sugar binding via boronic ester linkages. In the first place, ARS can exist in three forms, shown in Figure 9. Those three forms are neutral, monoanionic and dianionic present in acidic, neutral and basic pH, respectively. The transition between the neutral to monoanionic form occurs when pH crosses the pK_A=4.5 and the transition between monoanionic and dianionic form occurs when pH crosses the pK_A = 11.[41, 53, 63, 70]

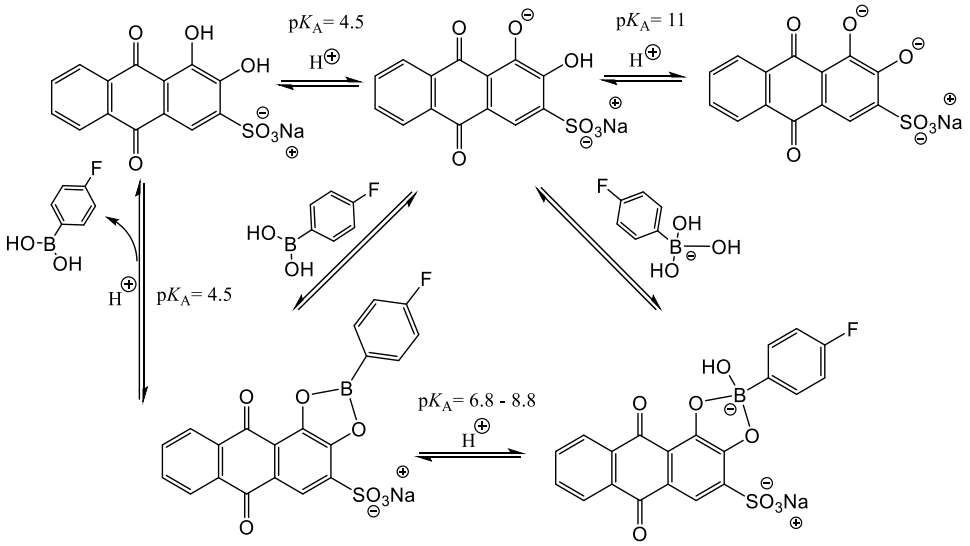

Figure 9: Alizarin Red S, ARS in: ***top left****-neutral form,* ***top middle****-monoanionic form,* ***top right****-dianionic form. ARS-boronic acid binding and release with boronic acid in:* ***bottom left****-trigonal form, (bottom left)* ***bottom right****-tetragonal form.*

The charge appears on the two hydroxyls of the anthracene that also give place to boronic ester formation and that charge of diols disappears with ester bond formation. The optimal pH for Alizarin Red S binding to phenylboronic acid is between 7 and 7.6 where can phenylboronic acid exist in trigonal or negatively charged tetragonal form. Thus, final ARS-phenylboronic acid complex can be neutral or charged, in case of trigonal or tetragonal form, respectively. Figure 9 shows two above mentioned ARS-boronic acid complexes types.[41, 45, 53, 63, 70]

The main advantage of using Alizarin Red S is that its non-ionic and monoanionic structure types differ in color and also in absorption and fluorescence spectra. As a result, ARS can easily help to map boron ester formation and hydrolysis reaction for model study of drug delivery systems. For further understanding of color, e.g., absorbance and fluorescence change, let's imagine three consecutive events where Alizarin Red S and boronic acid act as reagents in binding and release reactions. Individual events are summed up in the Figure 10.

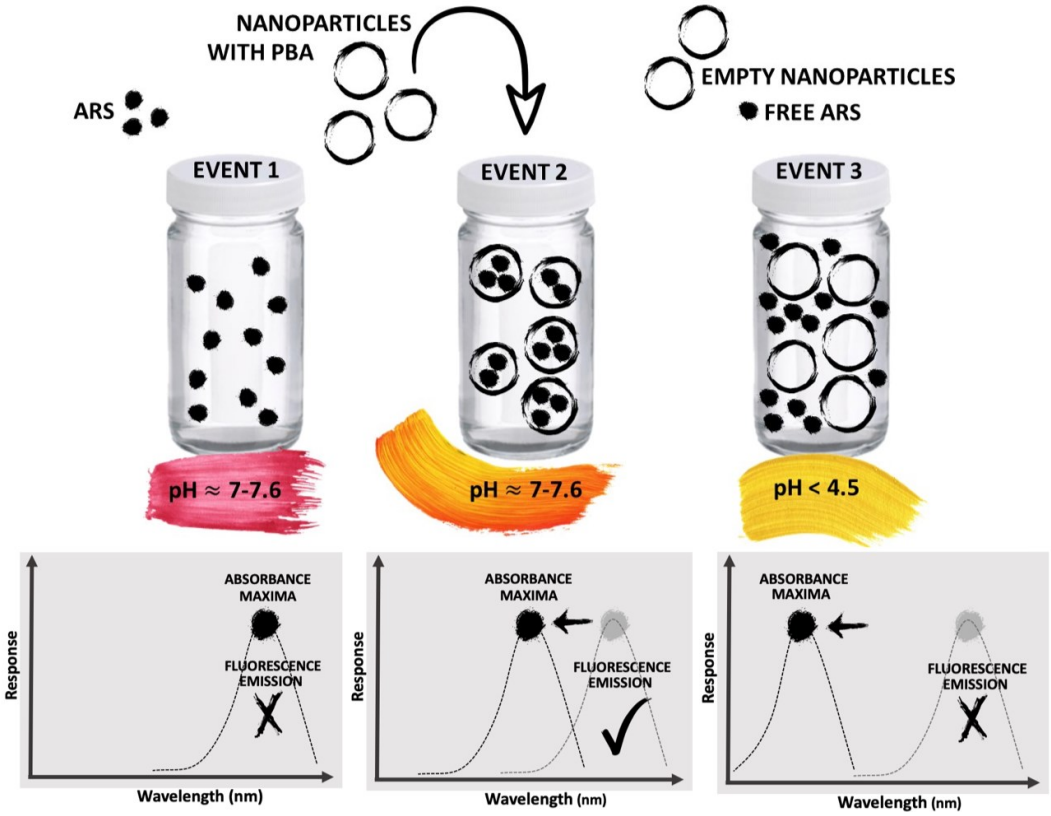

Figure 10: Three events of Alizarin Red S, ARS and nanoparticles containing boronic acid reaction ***Event 1****-physiological pH, free monoanionic ARS, pink color, absorbance maxima at high wavelength and no fluorescence emission.* ***Event 2****- physiological pH, formed ARS-phenylboronic acid ester in nanoparticles, orange color, blue shift of absorbance maxima and appearing fluorescence emission.* ***Event 3****-acidic pH, free ARS, yellow color, blue shift of absorbance, no fluorescence emission.*

In the first event, we have a solution of **free ARS** in **monoanionic form** at **physiological pH**. *In the second event*, a portion of nanoparticles containing phenylboronic acid is added to the solution of the event one while maintaining physiological pH. We suppose that ARS is quantitatively encapsulated into nanoparticles forming boronic acid-ARS ester. Thus, we have **bound ARS** in **non-ionic form** at **neutral pH**. *In the third event*, ARS-loaded nanoparticles reach acidic pH and the boronic-diol esters hydrolyze by releasing ARS to the solution. In this case, we suppose that all ARS molecules are released and that at the end of event three, there is a solution of nanoparticles in solution of **free ARS** in **non-ionic form** at **acidic pH**.

First of all, we can track the ester formation reaction thanks to Alizarin Red S color changes. In the first event, the color of free monoanionic ARS at physiological pH is **burgundy pink**. In the second event, ARS binds to boronic acid losing charge and yielding **non-ionic form** at physiological pH and its pink color changes to **yellow-orange**. In the third event, the ARS is free in **non-ionic form** at **acidic pH** and its color is **yellow**. Each of two anionic forms at different pH can be distinguished easily and the binding and release can be tracked by observation of color changes.

Secondly, we can distinguish between individual Alizarin Red S form in solution by absorbance maxima changes. The highest absorbance maxima between **515** and **530** nm belongs to **free monoanionic form** at **neutral pH** of event number one. Few tens of nanometers lower maxima at values approximately between **465** and **480** absorbance maxima shows **bound non-ionic form** at **neutral pH** corresponding to the event two. The lowest absorbance maxima between values **420** and **435** nm belongs to the **free non-ionic form** at the **acidic pH**.

Lastly, ARS results also in fluorescence changes. Only two possible situations can occur during biding and release of ARS by phenylboronic acid. **Free ARS does not emit** light while the **bound ARS shows strong fluorescence emission** with maxima between 560 and 575 nm.[41, 45, 53, 63, 70]

To sum up, phenylboronic acid can reversibly bind to functional vicinal diols. Alizarin Red S is an appropriate molecule for the study of competitive and fully reversible binding/release reactions between phenylboronic acids and sugars or diol-containing drugs. The color, absorbance and fluorescence change of this fluorophore may help to quantify the amount of encapsulated or sensed drug or sugar, respectively.

2.3.3. Irreversible hypoxic environment mapping

Moreover, reversible drug binding and sugar sensing property can be upgraded with a hypoxic environment mapping. Phenyl boronic acid is irreversibly sensitive towards red/ox environment. In particular, boronic acid undergo deboronation reaction in the presence of hydrogen peroxide that is highly present in tumorous environment. The boronic acid-containing molecule turns to an alcohol by releasing the boric acid as a side product of the reaction. The reaction is depicted in the Figure 11. Combined with fluorescence signaling molecules as for example Alizarin Red S, boronic acid exhibits ideal prepositions to be used as a hydrogen peroxide sensor for cancer treatment.[41, 71, 72]

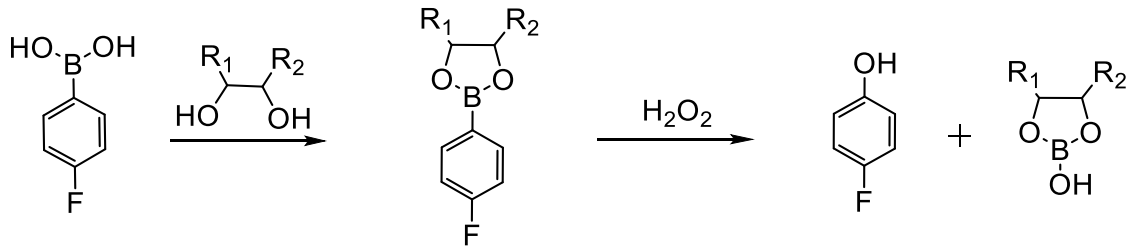

Figure 11:Irreversible deboronation of phenylboronic acid by hydrogen peroxide.

3. Characterization techniques

The analysis of triblock terpolymer involves a number of techniques for description of polymeric and micellar properties. Starting from the synthesis of the polymer, nuclear magnetic resonance is usually the first picked method for structural analysis of the polymer. When for example modifying the polymer by post-polymerization reaction, the comparison of infrared spectra of reactants and products can give us information on the efficiency of the reaction. When transferring the triblock terpolymer to the solution yielding micelles, very often used technique that become the "must-have" in nanoparticles solutions is the static and dynamic light scattering. Another completing method to the static and dynamic light scattering based on the similar principle of interaction of light with the matter is the measurement of zeta-potential by means of electrophoretic dynamic light scattering. Then, strongly arising in recent years is cryogenic transmission electron microscopy, giving the visual idea of *in situ* nanoparticles. When studying a micellar system focusing on its use in drug delivery, the

study typically involves encapsulation and release of fluorophores. For this reason, absorbance measurements together with fluorescence spectroscopy are the right methods to track the encapsulation and release thanks to the spectral changes of applied fluorophore. Following section will briefly sum-up the essential of the theoretical background of above-mentioned spectroscopy and scattering methods starting with method based on the interaction of matter with magnetic field, then following subchapters will describe the interaction of light with matter starting with scattering methods and followed by spectroscopy methods. The end of the chapter will be dedicated to the brief presentation of cryogenic microscopy of micelles.

3.1. Nuclear magnetic resonance spectroscopy

Nuclear magnetic resonance, NMR is an analytical technique for a quality control and molecular determining. This method works based on the interaction of matter with magnetic field and the principle usually consists of three steps. First, the magnetic nuclear spins of a nuclei align in a constant magnetic field B_0, in an equilibrium state. Second, the alignment of the nuclear spins is perturbed by a radiofrequency, (RF), pulse. Third, the RF pulse induces the Larmor precession of the nuclear spins around B_0, and the precession induces the voltage in a detection coil collected as NMR signal.[73, 74, 75] First to explain, an atomic nucleus has or does not have a spin, $\vec{I}$. When the number of neutrons and of the protons is both even, then the nucleus has no spin. When the number of neutrons plus the number of protons is odd, then the nucleus has half-integer spin (1/2, 3/2, 5/2). When the number of neutrons and the number of protons is both odd, then the nucleus has an integer spin (1, 2, 3). Each spin can oscillate around the center of atom in two states, $m = {}^{1}/_{2}$ and $m = -{}^{1}/_{2}$. These two states have the same energy, e.g. they are degenerate in absence of magnetic field. Atomic nucleus with non-zero spin $\vec{I}$, (entire or half number) has its non-zero magnetic dipole moment, $\vec{\mu}$ with following formula

$$\vec{\mu} = \gamma \cdot \vec{I} \tag{5}$$

where γ is gyromagnetic ratio, and $\vec{I}$ a non-zero spin. The gyromagnetic ratio, γ, is

$$\gamma = \frac{g_N \mu_N}{\hbar} \tag{6}$$

where ħ stands for the reduced Planck's constant, g_N is the g-factor and μ_N is the nuclear magneton. This relation corresponds to the ratio of a particle magnetic moment to its angular momentum. When the atom with non-zero spin as for example nuclides ^{1}H, ^{11}B, ^{13}C is exposed to an external magnetic field, B_0, its nuclear spins split between two levels, the higher and lower energy level, called as Zeeman effect. The population of spins is distributed in a manner that the antiparallel spins to the direction of $\overrightarrow{B_0}$ are situated in the high energy level, and the spins parallel to the direction of $\overrightarrow{B_0}$ are in the lower energy level. The energy difference between two states is

$$\Delta E = -\vec{\mu} \cdot \overrightarrow{B_0} . \tag{7}$$

If the nuclear spins would be distributed equally in the parallel and antiparallel orientation, the magnetic dipole moment of the atom would be zero.[73, 74, 75] However, the distribution of the spins in two directions is not equal, and the atom has a magnetic dipole moment, called magnetization. The energy of the magnetic dipole moment in magnetic field B_0 is

$$E = -\vec{\mu} \cdot \overrightarrow{B_0} . \tag{8}$$

The vector of magnetization exposed to external magnetic field, B_0 circle around the z axis which represents the direction of the external magnetic field. This circular movement of the magnetization in a cone around z axis is called Larmor precession, and its frequency, ω, is described as

$$\omega_0 = -\gamma \cdot B_0 \tag{9}$$

where ω_0 stands for the oscillation frequency in the magnetic field B_0. However, this precession in z axis is invisible for NMR detection.[73, 74, 75] The Larmor precession is measurable only when the direction of the $\vec{\mu}$ is not parallel to the B_0, so we have to add an additional magnetic field B_1 radio-frequency pulse of the frequency ω_{RF} to the system, that turns the magnetization usually 90° or 180° from the z axis (B_0) and that perturbates the spins from their equilibrium. The frequency of applied RF pulse has to fulfill the resonance condition

$$\Delta E = \gamma \cdot B_0 \cdot \hbar \tag{10}$$

meaning that the energy of the applied RF pulse has to be equal to the energy of the natural undamped frequency of the system. When applying the 90° pulse to the atom fulfilling this condition, the magnetization vectors is perpendicular to the axis of the vector of the magnetic field, $\overrightarrow{B_0}$ and the spins unify resulting in the precession in a phase. NMR measures the relaxation of the turned magnetization vector from the non-equilibrium perpendicular state after pulse until reaching the parallel equilibrium state.[73, 74, 75] The system can relax based on two types of relaxations, the T_1 relaxation that, also called longitudinal relaxation or spin-lattice relaxation, referring to the mean time for nucleus to return to its thermal equilibrium state of the spins including the interactions of the spin with surrounding molecules. T_1 is generally longer than the second type of the relaxation, the T_2 transverse or spin-spin relaxation. The T_2 relaxation refers to the interaction between the neighboring nuclei with identical precession frequencies but in different quantum states. In this situation the nuclei in a lower energy level can be excited, while the excited nucleus relaxes to the lower energy state. The T_2 relaxation results in a broadening of the signal in NMR spectra of molecules with slowed-down dynamics. Broad spectra signals are very typical for polymeric samples, where the interaction of molecules in a long chain with slow diffusion and dynamics prolongates the relaxation rates (it shortens the relaxation times).[73, 74, 75]

As explained in the introduction, the precession induces the voltage signal known as free induction decay, FID in a detection coil and contains the signal of all excited spins of the nuclei in thy system. The periodicity of the signal in a time is transformed to the frequency-domain by Fourier transformation. We obtain a spectrum of the NMR absorption intensity versus the NMR frequency. The peaks belonging to the atoms have a specific chemical shift,

$$\delta = \frac{\omega - \omega_{ref}}{\omega_{ref}} \tag{11}$$

where ω is a frequency of an analyte and ω_{ref} is a frequency of a reference, giving an NMR peak with units of parts per million, ppm. The shifts and their intensities are typically different for the atoms of the same type, which are chemically non-equivalent within the molecule. This is due to the chemical shielding of the analyzed nuclei by the

shell electrons, and also by the surrounding molecules electrons. The analysis of the NMR spectra consists of the logical assignment of the peaks to the atoms of a known or unknown molecule by integrating and by comparing the integration of all of the peaks in a spectrum. The typical chemical shifts of functional groups, of entire compounds can be found in NMR databases and can help to determine the exact molecular structure.[73, 74, 75]

3.2. Light scattering

Light scattering is a very important technique in analysis of colloids and dispersions of nanoparticles. Method is based on the elastic scattering of the wave component of the light on a particle. Elastic light scattering refers to the scattering while which the energy of the incident light is equal to the energy of the scattered light.[28, 75, 76] When a light interacts with a nanoparticle smaller than $\lambda/_{20}$ of the incident light, the intensity of the electromagnetic wave in this point harmonically oscillate and deform the electron shell of the molecule. This provokes the formation of an oscillating isolated dipole and the particles become a source of a secondary emission of light. The intensity of the light for small particles is independent on the scattering angle and in contrary is proportional to the intensity of the incident light and the square of the polarizability of the particle. The measured quantity of the scattering of small particles is the intensity of scattering

$$I = I_0 \frac{8\pi^4 N\alpha^4}{\lambda^4 r^2}(1 + cos^2\theta) \qquad (12)$$

where I_0 is the intensity of the incident light, N is the number of scatterers, α is the polarizability of the particle, λ is the wavelength of the incident light, r is the distance of scatterers, and θ is the angle between the incident light and the scattered light trajectory. [28, 75, 76, 77] When the light interacts with particles larger than $\lambda/_{20}$ of the incident light, the particles behave as a sum of individual dipoles. Polymeric chains in dilute solutions are in form of a statistical coil or in a dispersion of nanoparticles, and thus, the macromolecules act as isotropic particles with a number of distributed dipoles. For these larger particles, the scattering intensity is no longer independent of the scattering angle. We can analyze the particles with two principal measurement types, the static light scattering, SLS, and the dynamic light scattering, DLS. In both scattering methods we

analyze the scattering response as a function of so-called scattering vector, $\vec{q}$. The $\vec{q}$ is defined by the difference of the wave vectors of the scattered light $\vec{k}$ and the incident light $\overrightarrow{k_0}$ in different scattering angle θ,

$$\vec{q} = \vec{k} - \overrightarrow{k_0} \tag{13}$$

also represented in Figure 12.

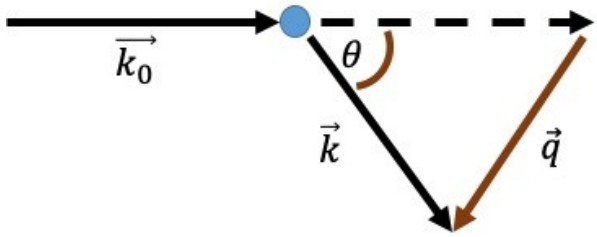

Figure 12: Representation of scattering vector $\vec{q}$ as a function of angle θ between incident light vector $\overrightarrow{k_0}$ and scattered light vector $\vec{k}$.

For an elastic scattering process, the magnitude of wave vector $|\overrightarrow{k_0}| = |\vec{k}| = {}^{2\pi}/_{\lambda}$ and the index of the solvent n_D has to be taken into account for including the changes of wavelength of incident light compared to its value in air, (n_D=1), and therefore the magnitude of scattering vector is

$$q = \frac{4\pi n_D \sin({}^{\theta}/_{2})}{\lambda}. \tag{14}$$

Starting with static light scattering, SLS, the objective of the measurement is to determine the weight average of the molar mass, M_w, the z-average of the radius of gyration, R_G, and also the z-average of the second virial coefficient, A_2, when measuring the q-dependent intensity of the scattered light, $I(q)$, described as

$$I(q) = \frac{(16\pi^4\alpha^2 I_O)}{\lambda^4 r^2} P(q) \tag{15}$$

where r is the distance of scatterers and $P(q)$ is the structure form factor. It can be shown that for small scatterers the form factor is a linear function of q^2 for any particle shape (so called Guinier region) as follows

$$P(q) = 1 - {}^{1}/_{3}\, R_G{}^2 q^2 \ldots, \tag{16}$$

which allows determination of the particle radius of gyration, R_G. As the intensity of the scattering by the larger particles depends on the scattering angle, θ, for determining M_W, R_G and A_2 we measure the sample at different scattering angles and also for different sample concentrations.[28, 75, 76, 77] The basis for analyzing the scattered intensity of particles from 10 nm to 50 nm radius is to treat the measured data of scattering intensity by the Zimm equation

$$ {}^{K_c}/_{R} = {}^{1}/_{M}\, P(q) + 2A_2 c \quad , \tag{17}$$

where R is the normalized scattered intensity, the Rayleigh ratio, and where A_2 is the second virial coefficient that describes the attractive and repulsive forces between particles, where c is the concentration of the analyte, and where K_c is

$$K_c = \frac{4\pi^2 n_0^2 (\mathrm{d}n/\mathrm{d}c)^2}{\lambda^4 N_A} \tag{18}$$

with refractive index increment, $\mathrm{d}n/\mathrm{d}c$, that refers to the contrast between the solvent and dissolved particles. Zimm equation provides the relation between the scattered intensity of the analyzed particles, their concentration and the amplitude of the scattering vector.[75, 76, 77]

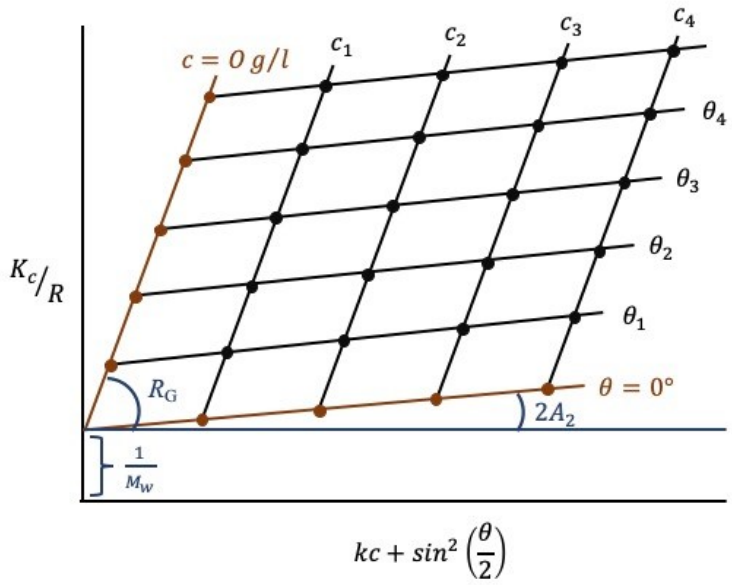

Figure 13:Zimm plot-extrapolation of scattering intensity to 0 concentration and 0 angle, θ, where M_W is absolute molecular weight of particle, R_G is absolute radius of gyration and A_2 stands for second virial coefficient .

When extrapolating the ratio $K_c/_R$ on $kc + sin^2\left(\frac{\theta}{2}\right)$ towards the angle $\theta = 0°$ and towards the concentration $c = 0$g/L shown in the Figure 13, the intersection of the curve with axis y gives us $\frac{1}{M_w}$. When dividing the mass of the polymer with M_W of polymer in sample, we can obtain the aggregation number, N_{agg}, in other words the number polymeric chains forming one micelle. Then, the slope of $K_c/_R\,(\theta = 0°, c)$ gives the doubled value of A_2. The R_G^2 value is given from the slope of $P(q)$ on q^2.[28, 75, 76]

The fundamental of DLS is based on the measurements of spatial and temporal fluctuation of the intensity of the scattered light from particles that undergo random Brownian motion.[28, 75, 76, 77] The fluctuation of scattering intensity due to particles mobility are expressed in autocorrelation function, $G(r,\tau)$ that for the Brownian motion only depends on the distance $r = |\vec{r}|$, and is given as

$$G(r,\tau) = \left[2\pi/_3\,\langle \Delta R(\tau)^2 \rangle\right]^{3/2} \exp\left(-\frac{3r(\tau)^2}{2\langle \Delta R(\tau)^2 \rangle}\right) \qquad (19)$$

where $\langle \Delta R(\tau)^2 \rangle$ refers to the mean-square displacement of the scattering particle that stands for the average distance squared it travels during time τ. The Brownian motion of the particles in solution is caused by the random thermal density fluctuations of the

solvent molecules. The particle in the scattering volume undergo a random walk, and the mean-square displacement is given

$$\langle \Delta R(\tau)^2 \rangle = 6D\tau \tag{20}$$

with D, the diffusion coefficient. The Fourier transform of the autocorrelation function (19) leads to the dynamic structure factor, which is proportional to ~exp(-q^2Dt), as a quantity that is measured in the DLS experiment.[28, 75, 76, 77] The Stokes-Einstein equation of diffusion coefficient, D relates the diffusion and the size of a spherical particle

$$D = \frac{k_B T}{6\pi\eta R_{\mathrm{H}}} \tag{21}$$

including k_B, the Boltzmann's constant, T, the absolute temperature of the suspension, η, the viscosity of the solvent and R_{H}, the hydrodynamic radius of the scatterer. Thus, the diffusion coefficient depends on the size and the shape of the particle and also on the viscosity of the system. Large value of diffusion coefficient, or small value of solvent viscosity stands for quickly moving small particles compared to the slow velocity of the movement of bigger particles with smaller value of diffusion coefficient, or to the slow velocity of particle movement in low viscous liquid. When measuring the dynamic light scattering at different angles and concentrations, similar to SLS, we can obtain the true hydrodynamic radius R_{H}, from experimentally found apparent diffusion coefficients by extrapolation to zero angle and concentration in dynamic Zimm plot adapting the Stokes-Einstein equation for diffusion coefficient.[28, 75, 76, 77]

Static and dynamic light scattering is considered as a key method for analysis of polymeric and colloid solutions. It is a non-destructive method that experimentally determines important quantities for nanoparticles characterization, and these quantities are M_{W}, N_{agg}, R_{G}, A_2, D and also R_{H}.

3.3. UV-VIS spectroscopy

The light from UV-VIS electromagnetic spectrum range can be absorbed by molecules with π electrons, or with electrons in non-bonding orbitals and lone pairs. UV refers to

ultraviolet light and is divided in two basic domains, the in near UV with wavelengths from 200 nm to 390 nm and the far UV with wavelengths from 10 nm to 200 nm. VIS stands for visible light ranging from 390 nm to 750 nm.[28, 73, 78] The UV-VIS absorption measurement can in one hand bring structural information about polymer containing for example a polymer block composed of phenyl molecules. In other hand it can serve as a quantitative method for chromophore compound quantification in case of system for targeted delivery and release. In more detailed, the absorptivity, A of a chromophore is sensitive to the polarity of the environment and it can also change between free form and bound to another molecule form. The chromophore can be a part of a polymeric backbone or can be attached as the functional pendant groups of the polymer. The absorptivity can give information about the chromophore thanks to the Lambert-Beer equation

$$A = \varepsilon \cdot l \cdot c \tag{22}$$

where ε is a molar absorption coefficient of analyte, l is the pathlength of the light and c, the concentration of analyte.[28, 73, 78] Absorptivity is linearly dependent on the length of the cuvette and concentration of the analyte only if the chromophore is uniformly distributed through the sample, if the concentration is not changing during the measurement and if the sample is not turbid. Absorptivity can be also expressed as

$$A = log \frac{I}{I_0} = -\log T \tag{23}$$

where I_0 is the intensity of incident light, I is the intensity of transmitted light and the relation $\frac{I_0}{I}$ is transmittance, T. The output data from the UV-VIS measurement can be shown by means of different functions of wavelength. The *x* axis of the spectra is usually representing the wavelength, while the *y* axis can show the absorbance, the intensity, the molar absorption coefficient, and in case of chiroptical spectroscopy the optical rotatory dispersion or the circular dichroism.[28, 73, 78] The absorbance measurements of polymers for drug delivery are usually tightly relied with fluorescence spectroscopy as a complementary technique.

3.4. Infrared spectroscopy

The absorption of a light of the wavelength from the range belonging to near infrared region by a molecule leads to its transition to higher vibrational levels. The wavelengths of infrared region of light ranges from approximately $7.5 \cdot 10^{-7}$ m that stands for a boundary of UV-VIS region, to approximately $1 \cdot 10^{-3}$ m that refers to the boundary with microwave region. The infrared spectroscopy uses the wavelength region of light from $2.5 \cdot 10^{-4}$ cm to $2.5 \cdot 10^{-4}$ cm.[28, 79, 80] Briefly, a non-linear molecule consisting of *N* atoms can be present in 3*N*-6 vibrational degrees of freedom, in other words normal vibrational modes. While each of the modes is characterized by three vibrational frequencies, some of the modes can be degenerated multiple times. When absorbing the light, the molecule's bonds start to vibrate in a specific frequency for each molecule type. Typical vibrations are for example the symmetric or antisymmetric valence vibration, or both, in plane and out of plane deformation vibration.[28, 79, 80]

A typical infrared spectrum can be organized as a dependence of the absorbance or transmittance on the frequency of vibration, transformed from Hz to the wavenumber, $\tilde{\nu}$, where $\tilde{\nu} = \frac{1}{\lambda}$. For both, there are two characteristic types of vibrational frequencies. First, the higher frequency vibration, in ν approximately from 800 cm^{-1} to 3600 cm^{-1}, that are typical for vibrations of functional groups, as for example -CH_3, -NH_2, -OH, -C=O, -CH=O. Second, there are slower vibrational frequencies in ν approximately from 200 cm^{-1} to 800 cm^{-1}, also called as fingerprint region.[79, 80] When analyzing a polymer with infrared spectroscopy, the number of atoms, *N* is very high, and the number of possible vibrational modes is very large as the vibrational frequency depends on nonbinding interactions of atoms with surrounding molecules.[28] However, there are usually some identical vibrations for functional groups, or for a close atom arrangement pattern, that can serve as a tool for identification even of a very complicated molecule. We can analyze for example the vibrational band typical for a double bond the most usually in the area from 1640 cm^{-1} to 1690 cm^{-1}, or the vibrational band of alcohols, with -OH vibration in the area from 3200 cm^{-1} to 3650 cm^{-1}.The infrared spectroscopy is mostly used in biochemistry and biophysical chemistry for analysis of the protein structure. For example, the vibrational frequency of amide group in α-helix, β-sheet and in a random chain differ and can serve for the structure determination.[28, 75, 79, 80]

3.5. Fluorescence spectroscopy

The absorption of photon in UV-VIS region by a molecule causes the transition of the molecule from its ground singlet state, S_0 to higher excited singlet levels S_1, S_2 and others.[75, 81, 82, 83] The absorption and excitation can be observed only when the selection rules are fulfilled. The transition dipole moment of the molecule, μ has to change upon the interaction of the electromagnetic wave and its value has to be non-zero. The most probable transition is when $\vec{\mu}$ is parallel with the plane of the polarized light. Also, the probability of the transition is the highest for the vertical transitions with the largest overlap of vibrational functions. Then, the precondition for excitation described by Franck-Condon principle explains that the internuclear distances of the molecules have to stay unchanged.[28, 75, 81, 82] When the conditions are fulfilled and the atom absorbs a photon in a timescale lower than 10^{-15} s, the molecule persist a moment in some of vibrational levels of excited state and then returns to some of the vibrational levels of the ground state. Molecules are the most usually excited from the ground singlet state to the excited state of the same multiplicity (S_1, S_2 etc.), also called singlet state. The excitation of the molecule with transition to the excited state with different multiplicity (T_1, T_2 etc.), e.g. from singlet state to triplet state is forbidden, but the triplet state can be reached from singlet excited state. The return to the ground state can follow different pathways, that differ by the time scale of the return process, as shown in Jablonski diagram in Figure 14. Jablonski diagram describes the electronic states of a molecule and the transitions between corresponding vibrational and rotational states.[28, 75, 81]

There are basically two types of relaxation processes of the molecule to the ground state, the non-radiative processes (indicated by curved arrows) and radiative relaxation (indicated by straight arrows).[28, 75, 81] First, there are three types of non-radiative processes. The vibrational relaxation, which is the mechanism of relaxation of the molecule to the lowest vibrational level of the excited state by dissipating the kinetical energy to the surrounding in form of thermal energy. Molecule also can relax by vibrational energy until reaching the ground state. Another two radiation-less deexcitation of molecule that prolongate the lifetime of the molecule in excited state are the internal conversion and the intersystem crossing. The process of internal conversion is the dissipation of energy within two states with the same spin multiplicity with time frame from 10^{-11} s to 10^{-9} s in between electronic levels higher than the S_1. If the spin multiplicity

while the process of dissipation changes for example from singlet state S_1 to triplet state T_1, it refers to the intersystem crossing. This process is more slowly than internal conversion and is important in molecules with large spin-orbit coupling. After both radiation-less processes, the internal conversion and the intersystem crossing, the molecule returns to the ground state by radiative relaxation. First, when the molecule reaches the ground state S_0 from excited state of the same multiplicity, this molecule undergoes radiative transition that is called fluorescence. Fluorescence occurs in time scale from 10^{-9} s to 10^{-7} s. Second, the intersystem crossing of excited molecule from singlet to triplet state prolongates the excitation time of the molecule. The delayed radiative process of relaxation from the excited triplet state to the ground singlet state is called phosphorescence. Phosphorescence occurs in time scale ranging from 10^{-3} s to seconds.[28, 75, 82, 83]

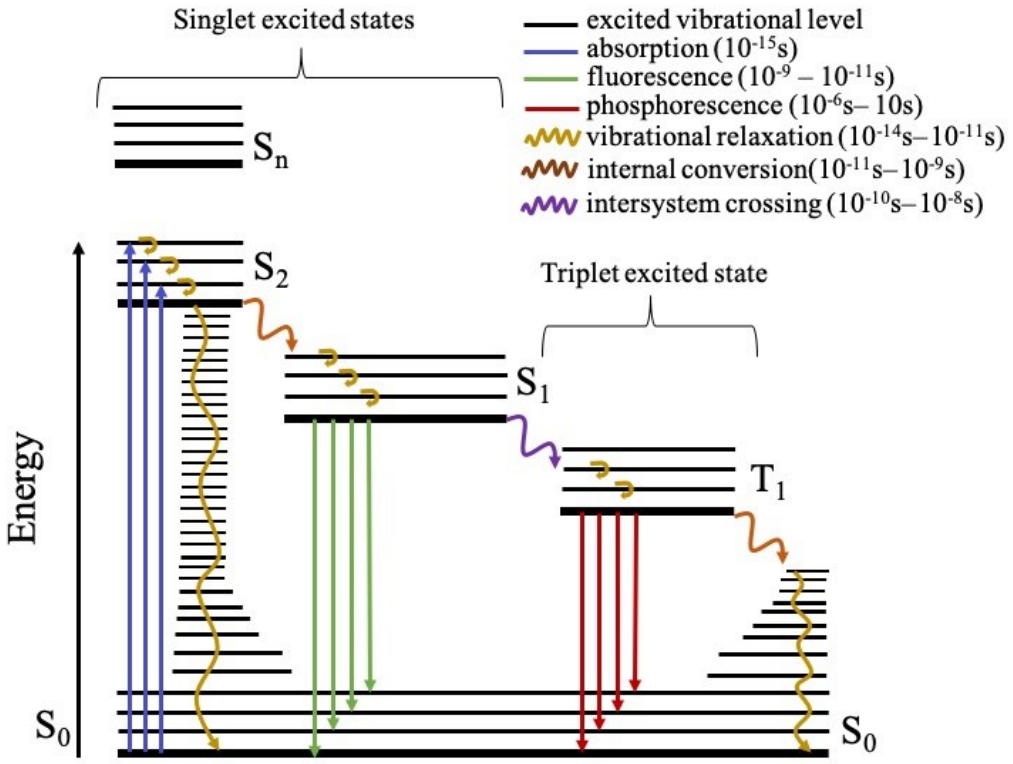

Figure 14:Jablonski diagram. Schematic representation of the electron transitions between the moment of its excitation until the relaxation. ***Curved arrows****-non-radiative processes,* ***straight arrows****-radiative processes.*

Substances capable of emitting light are called fluorophores. These are typically aromatic compounds as for example conjugates of coumarins, anthracenes and pyrenes

with a typical fluorescence lifetime, τ, describing the time of relaxation to the ground state. Each of fluorophores shows a different capability of light emission, called the fluorescence quantum yield, ϕ_F. Fluorescence quantum yield relates the number of emitting photons, n_F to the number of absorbed photons, n_A. This variable is usually expressed by use of rate constants of individual radiative and radiation-less events as follows

$$\phi_F = n_F/n_A = k_F/\sum_i k_i \quad (24)$$

where k_F is rate constant of fluorescence and the denominator relates to the sum of the rate constants of all the processes (radiative and radiation-less).[28, 81, 82] The quantum yield of a fluorophore is decreased by radiation-less processes occurring after molecule's excitation (for example quenching or energy transfer). The fluorophore excitation and radiative relaxation can be analyzed by measuring the dependence of fluorescence intensity on the varying excitation wavelength when excited by a light source of a constant wavelength, called as fluorescence emission spectrum measurement. When exciting the fluorophore with a light source of a variable wavelength and when analyzing the intensity of fluorescence emission at constant wavelength, we talk about excitation spectrum measurement. Excitation spectrum of a fluorophore should give information about the absorption maxima of the molecule, and it is closely related to the UV-VIS spectrum. The emission spectra measurement is usually organized in way to excite the molecule with the wavelength corresponding to its absorption maxima. The intensity of a fluorescence emission can be proportionally affected by a concentration of fluorophore. The shape and wavelength range of fluorophore's emission spectra can be affected also by its environment in solution, more exactly the polarity of the solvent. Polar solvents shift the emission to the red area (longer wavelengths) due to the solvation of the molecule causing the change of a dipole moment of a fluorophore. Similar to fluorophore environment effect on emission, also reactions of binding or release of the fluorophore to or from a molecule can shift emission spectra to lower or higher wavelengths.[28, 81, 82]

Fluorescence spectroscopy can be used in a polymer chemistry as an analyzing tool for systems as for example nanoparticles for drug delivery. The encapsulation and release of a fluorophore as s model drug usually cause the changes of fluorophore's microenvironment. The fluorescence emission spectrum of a fluorophore in polar solution usually differs from the fluorescence emission spectrum of fluorophore in non-polar

micellar core. Drug delivery systems often consist of functional groups that may reversibly bind to fluorophore to ensure the effectivity of the system. Studying of biding and release reactions with fluorescence emission measurements may help to determine the quantity of the fluorophore in the drug delivery system.[28, 82, 83]

3.6. Cryogenic transmission electron microscopy

The cryogenic transmission electron microscopy, the cryo-TEM is a microscopy technique that permits to study a soft matter it means the biological sample or polymeric materials at a high-resolution level.[75, 84]

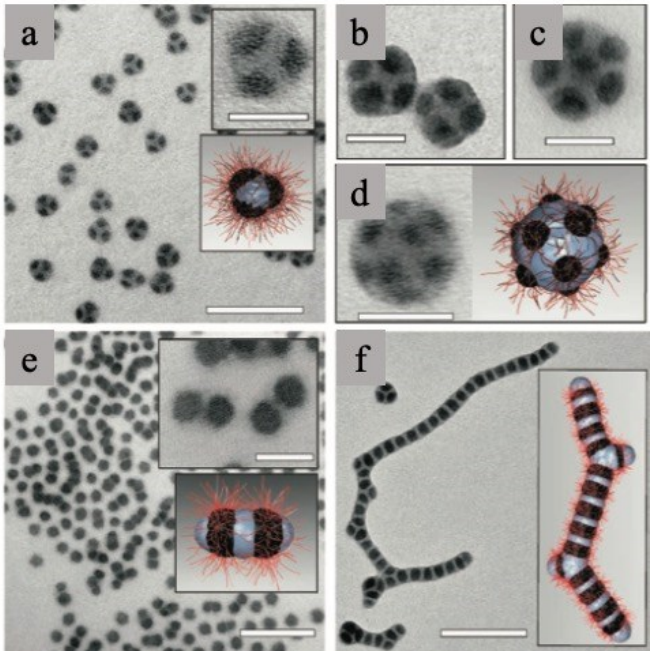

Figure 15:Cryo-TEM image of spherical and linear multicompartment nanoparticles formed by poly(styrene)-b-poly(butadiene)-b-poly(methyl methacrylate), PS-b-PB-b-PMMA with various core volume ratios (V_{PS}/V_{PB}). Micelles staining with OsO_4 results in black PB block, grey PS block and PMMA solvophilic block is invisible. Images show: ***a****- "clovers" micelles,* ***b****-"Maltese crosses" nanoparticles,* ***c****,* ***d****- football like micelles,* ***e****-"double burgers" nanoparticles,* ***f****-linear multicompartment rods. The scale bars are 200 nm and 50 nm in the insets.*[15]

The method is based on the transmission of accelerated electrons with high kinetical energy (100-400 kV) through a thin layer of sample in vitreous ice. Electron beam is focused on the sample by the magnetic field and the transmitted electrons are focused by the electromagnetic lenses of the microscope. The formation of an image is based on the modification of electron waves transmitted through the sample. The phase of electrons

that do not interact with analyte remain identical while the phase of electron interacting with sample changes. The waves may then constructively interfere resulting in increased detected intensity, also called as a phase object. The sample preparation for cryo-TEM is advantageous aspect of whole measurement. The liquid sample is applied on a copper grid usually covered with lacey carbon film. The grid with sample is plunge-frozen in liquid ethane or mixture of ethane and propane to ensure the formation of vitreous ice avoiding the crystallization of the sample. The analyzed specimen can be observed in its native environment, *in situ* in contrast to X-ray crystallography where the sample usually undergo conformational changes upon monocrystal formation.[75, 84]

The cryo-TEM is mainly used for biological samples of viruses, ribosomes or mitochondria. However, this method is gaining interest in field of macromolecular chemistry as a completing method for nanoparticles analysis to light scattering methods (SLS, SAXS and SANS). The changes in electron density between incompatible polymer blocks usually accompanied with selective staining can show multicompartment architecture of block copolymer nanoparticles. The example of multicompartment micelles visualization by cryo-TEM is in the Figure 15 from publication of Gröschel et al.[15]

4. Aims of the thesis

This thesis is a contribution to the study of stimuli-responsive triblock terpolymer micelles in the Soft Matter group, Department of Physical and Macromolecular Chemistry, CU. The aims of this diploma thesis are following:

1. To functionalize the poly(styrene)-*b*-poly(4-vinyl pyridine)-*b*-poly(ethylene oxide), PS-*b*-P4VP-*b*-PEO with 2-bromomethyl-4-fluorophenylboronic acid and separately with 2-bromomethyl phenylboronic acid, by post-polymerization quaternization reaction yielding a stimuli-responsive phenylboronic acid-containing triblock terpolymer.
2. To characterize and quantify the post-polymerization quaternization reaction efficiency.
3. To prepare in a controlled manner micellar solution of newly modified triblock terpolymers and to characterize the micelles in term of size and molar mass.
4. To study the encapsulation, stimuli-induced release and sugar sensing using model drugs Alizarin and ARS, and to analyze the reactions by means of UV-VIS spectroscopy and fluorescence spectroscopy.

The obtained knowledge will allow for a reproducible preparation of stable stimuli-responsive boronic acid-containing nanoparticles in aqueous solution and for the understanding of the influence of outer stimuli on the drug encapsulation and release by block copolymer nanoparticles.

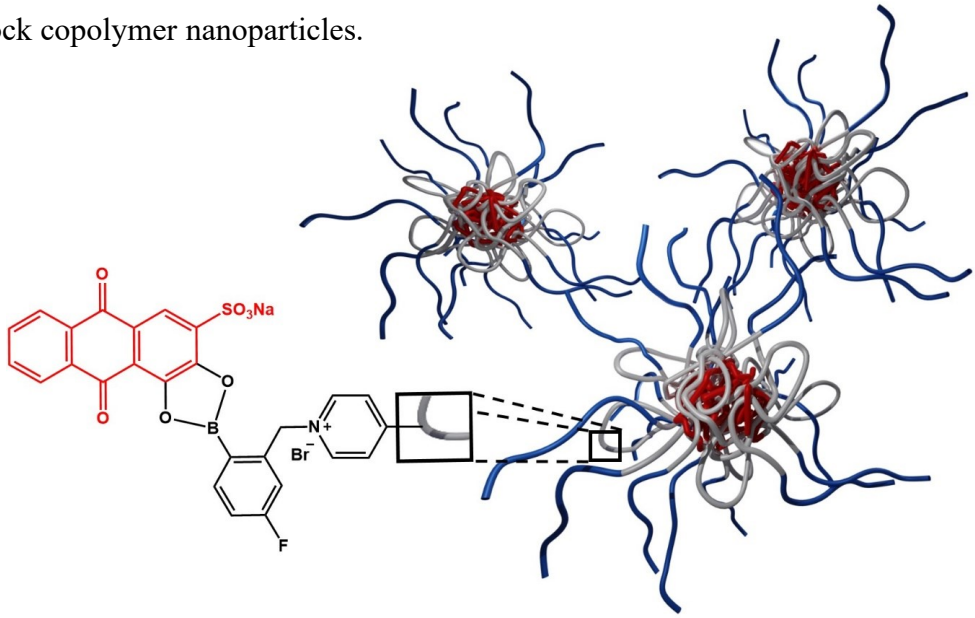

Figure 16:Representation of studied stimuli responsive system containing phenylboronic acid bound to model drug Alizarin Red S.

5. Materials and methods

5.1. Reagents

Poly(styrene)-*b*-poly(4-vinyl pyridine)-*b*-poly(ethylene oxide), PS-*b*-P4VP-*b*-PEO, structure in Figure 17, was purchased from Polymer Source, Inc. (Dorval, Quebec, Canada).

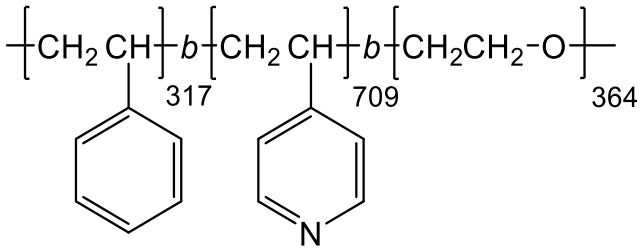

Figure 17:Structure of used PS-b-P4VP-b-PEO triblock terpolymer.

The triblock terpolymer was synthesized by living anionic polymerization by successive addition of monomer using cumyl potassium as initiator. Further information on the synthesis protocol is from supplier Polymer Source under sample #P10212-S4VPEO. Briefly, the molar mass of individual polymer blocks, M_n, of PS-*b*-P4VP-*b*-PEO is (33.0-*b*-83.0-*b*-16.0) · 10^3 g/mol and the dispersity of the polymer, $Đ$ is 1.15. Both results are based on size exclusion chromatography. Poly(4-vinyl pyridine) (M_n = 6000 g/mol, $Đ$ = 1.2), PVP, was purchased from Polymer Source, Inc. (Dorval, Quebec, Canada).

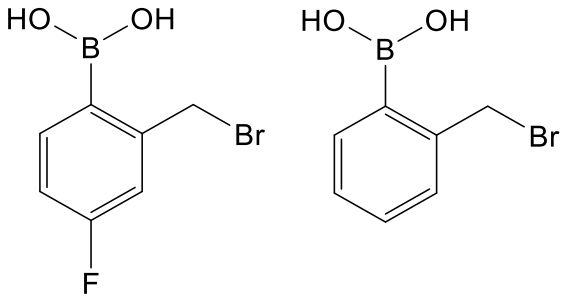

Figure 18:Structure of quaternization agents: ***left*** *- 2-bromomethyl-4-fluorophenylboronic acid, FPBA,* ***right****- 2-bromomethyl phenylboronic acid, PBA.*

Quaternization agents, 2-bromomethyl-4-fluorophenylboronic acid, (95 %, M.W. = 232.8 g/mol), FPBA, and 2-bromomethyl phenylboronic acid (95 %, M.W. = 214.85 g/mol), PBA were purchased from Combi-Blocks, structures shown in Figure 18.

Spectra/Por® dialysis membrane with a nominal MWCO of 6000–8000 was used for dialysis. In addition, we used Alizarin Red S, ARS (Acros Organics), Alizarin, (Sigma Aldrich, USA), Galactose, (Sigma Aldrich, USA), Fructose (Sigma Aldrich, USA), Ascorbic acid, (Sigma Aldrich, USA).

Solvents that were used for the quaternization of the polymer, for the self-assembly: *N,N*-dimethyl formamide (DMF), (for HPLC, ≥ 99.9 %, Sigma Aldrich, USA), methanol, (for HPLC ≥ 99.9 %, Sigma Aldrich, USA), 0.01 M NaOH and 0.01 M HCl were prepared by dissolving of NaOH beads and by diluting 37 % HCl, (Sigma Aldrich, USA), respectively, both using MiliQ water prepared by reverse osmosis.

NMR measurement were carried out using deuterated solvents: CD_3OD, (Sigma Aldrich, USA), *N,N*-dimethyl formamide-d7, (Sigma Aldrich, USA), THD-d8, (Sigma Aldrich, USA), D_2O, (99.8 atom %D, ARMER Chemicals).

5.2. Quaternization of SVE triblock terpolymer with FPBA and PBA

In this study, we aimed to quaternize PS-*b*-P4VP-*b*-PEO, SVE (S – PS block; V – P4VP block; E – PEO block), with 2-bromomethyl-4-fluorophenylboronic acid, FPBA, and 2-bromomethyl-phenylboronic acid, PBA, yielding SVE-FPBA and SVE-PBA samples respectively, to bring the diol binding and hypoxic environment mapping properties. Previous results of Soft Matter research group, specifically, the study performed by Dr. Ďorďovič shown that percentage of the quaternized P4VP units in SVE triblock terpolymer strongly influences the solubility and stability of the polymer. When comparing the solubility and stability of 25 % quaternized, 50 % quaternized and 100 % quaternized PS-*b*-P4VP-*b*-PEO, the 50 % quaternized analogue shown the most appropriate solubility and stability for the purposes of drug delivery. The solubility of the polymer in methanol makes the self-assembly into nanoparticles easier to handle in comparison to DMF or DMSO, which are good solvents for 25 % and 100 % quaternized SVE. For this reason, we chose to quaternize the poly(4-vinyl pyridine) block by 50 % with FPBA and PBA, and the exact degree of quaternization was checked by NMR after each reaction. Thus, following study is directed towards the analysis of fifty percent quaternized P4VP in PS-*b*-P4VP-*b*-PEO with 2-bromomethyl-4-fluorophenylboronic

acid, FPBA denoted as SVE-FPBA and with 2-bromomethyl-phenylboronic acid, PBA denoted as SVE-PBA. Quaternization reaction equations and images of solutions and products are in Figure 19.

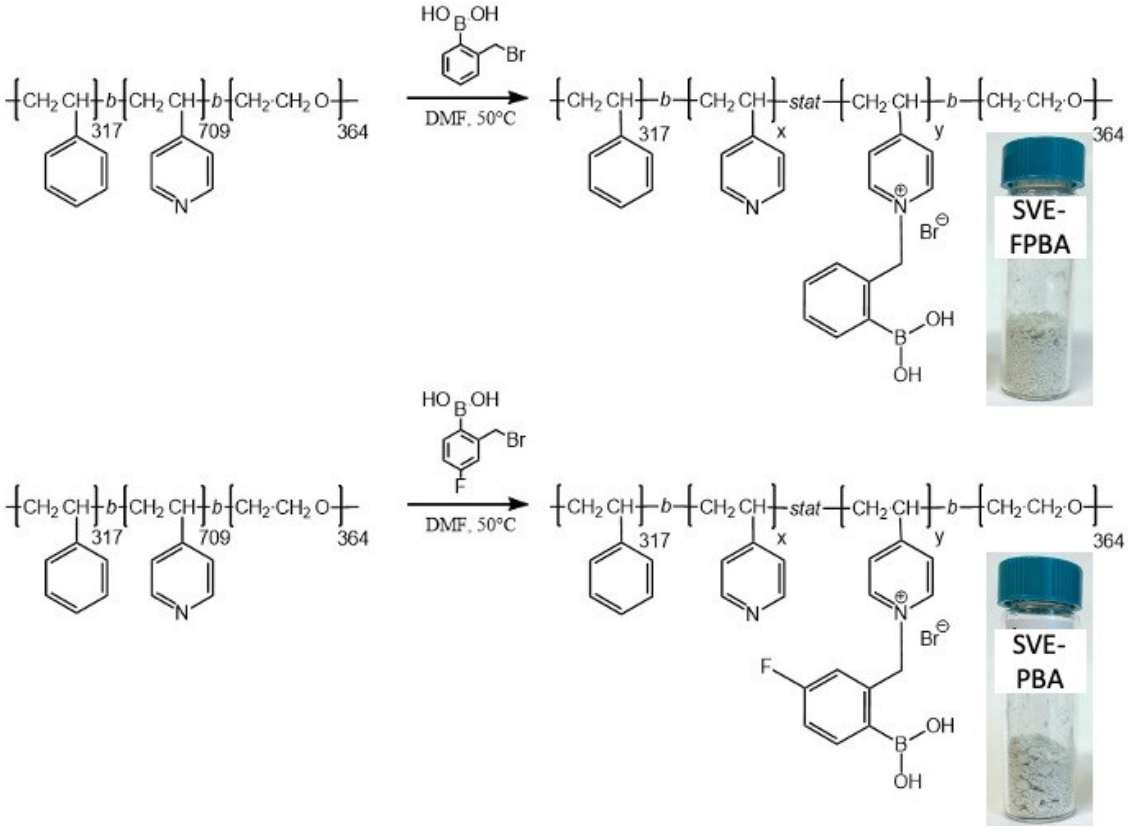

Figure 19:Reaction mechanism and pictures of solid products of PS-b-*P4VP*-b-*PEO quaternization with FPBA and PBA, yielding:* ***top****-SVE-FPBA,* ***bottom****-SVE-PBA triblock terpolymer.*

Typical quaternization reaction occurred as following. In two separate round-bottom flasks was dissolved 200 mg of PS-*b*-P4VP-*b*-PEO in 12 mL of DMF. Both flasks contained a magnetic stir, and both were heated at 60 °C to enhance the solubility of the polymer. In parallel, 0.5 molar equivalent of quaternization agent FPBA or PBA, 132 mg and 122 mg respectively, was dissolved in 3 mL of DMF. When all reagents dissolved, FPBA solution was added dropwise into one of the round-bottom flasks with SVE by giving the reaction mixture SVE-FPBA. In the same manner, the solution of PBA was injected into remaining SVE solution giving rise to the SVE-PBA mixture. Reaction mixtures were kept at 60 °C while stirring for 5 days. The visible color change from slightly yellowish solution to dark brown green solution was observed for SVE-FPBA sample and a slightly lighter brown green color was observed for the solution SVE-PBA.

After five days of quaternization, both samples were separately transferred into dialysis cellulose tubes with the 6-8 kDa cut-off and were dialyzed against 1 liter of deionized water. The dialysis bath was changed three times in manner that the samples were dialyzed twice for 4 hours and once for 12 hours to ensure the complete removal of DMF. The color of both samples became lighter green when changing the solution solvent from DMF to water. Dialyzed solutions of SVE-FPBA and SVE-PBA were subsequently lyophilized yielding light green fluffy solid. The product of both reactions was analyzed with NMR and IR spectroscopy.

SVE-FPBA: **^{1}H NMR (400 MHz, CD_3OD) δ (ppm):** 8.87-8.49 (s), 8.43-8.08 (s), 7.94-7.72 (s), 7.70-6.58 (broad triplet), 6.10-5.55 (d), 6.11-5.84 (d), 3.71-3.51 (s), 2.17-1.23 (broad multiplet). **^{11}B NMR (400 MHz, CD_3OD) δ (ppm):** 18.54 (s).

SVE-PBA: **^{1}H NMR (400 MHz, CD_3OD) δ (ppm):** 8.84-8.44 (s), 8.39-7.96 (s), 7.93-7.72 (s), 7.66-7.26 (s), 7.16-6.56 (doublet), 6.06-5.55 (d), 3.72-3.52 (s), 2.17-1.23 (broad multiplet). **^{11}B NMR (400 MHz, CD_3OD) δ (ppm):** 18.60 (s).

Quaternization of pyridine with FPBA for pK_A *determination*

Pyridine, Pyr, quaternized with 2-bromomethyl-4-fluorophenylboronic acid, FPBA was used for determination of the pK_A of the FPBA moieties attached to the pyridine ring instead of SVE-FPBA sample. The pK_A determination was performed by Dr. Somdeb Jana from Soft Matter research team. Briefly, an adduct of pyridine and 2-bromomethyl-4-fluorophenylboronic acid, Pyr-FPBA, was synthesized as follows. In total, 500 mg of FPBA was dissolved in a round bottom flask with a magnetic stir in 5 mL of dried THF. Then, 0.188 mL of pyridine (density 0.982 g/mL; 2.33 mmol) was added. The reaction mixture was stirred at temperature 60 °C for 2 days under argon atmosphere. Pyr-FPBA as a product partly precipitated, and the liquid phase was decanted and poured into cold diethyl ether to precipitate. Both precipitates were dissolved in methanol to remove reagents, and then, methanol was evaporated on a rotatory evaporator. 0.555 mg (81 % yield) of product was isolated as a white powder and analyzed with NMR and IR spectroscopy. Pyr-FPBA: **^{1}H NMR (400 MHz, CD_3OD) δ (ppm):** 9.03-8.91 (d), 8.69-8.56 (t), 8.21-8.07 (t), 7.70-7.60 (m), 7.55 (m), 6.11-5.84 (d).

5.3. Self-assembly of SVE-FPBA and SVE-PBA

pH dependent self-assembly of SVE-FPBA

The self-assembly protocol of quaternized PS-*b*-P4VP-*b*-PEO, (denoted in the further text as SVE-FPBA or SVE-PBA) was as first performed with aim to determine the influence of the solvent on the nanoparticle size and stability. Three parallel self-assembly processes were performed in acidic, neutral and basic aqueous media. These self-assembly reactions were noted as A, N and B, respectively, and were organized as follows. In three separate flasks labeled as A, N and B was dissolved 10 mg of SVE-FPBA in 1 mL of methanol. Each of three green solutions was separately drop by drop quenched into 3 mL of water while constant stirring. The rate of addition was one droplet every 3 seconds. The transfer of SVE-FPBA from methanol as a good solvent for PEO and P4VP blocks into a prevalent amount of water, that is a good solvent only for PEO block and part of the quaternized P4VP block gave rise to stable kinetically frozen nanoparticles. For further stabilization of nanoparticles and methanol removal, the micellar solutions were dialyzed against three different aqueous solutions from 5 mL dialysis capsule with 6-8 kDa cellulose membrane. The sample labelled as A was dialyzed against 0.01 M HCl, the sample N against pure deionized water and sample B against 0.01 M NaOH. The polymer in dialysis capsule buffered the A and B solutions to pH approximately 4 and 9 respectively. Within several minutes, the sample B shown precipitation thus, the dialysis bath was changed to 0.01 M HCl as was used in case of the sample A. The precipitate of sample B partially dissolved within first hour of dialysis. The dialysis bath was changed with 4 hours intervals and then the dialysis continued overnight for 12 hours. At the end of dialysis, the samples A and N were stable while the sample B shown traces of precipitates. These precipitates were eventually dissolved after stronger agitation of dialysis capsule. The solutions A and B turned into light yellowish green color and the solution N was light green. The volume of all three samples after dialysis increased identically to 4.7 mL with final concentration 2.27 mg/mL.

Samples were analyzed by dynamic and static light scattering, more exactly they underwent in one hand static measurement, e.g. Zimm plot, for determination of weight-averaged molecular weight of nanoparticles, M_W, and their radius of gyration, R_G, and in other hand dynamic measurements for determination of absolute diffusion coefficient, D, and hydrodynamic radius, R_H of nanoparticles. For each solution type (A SVE-FPBA, N

SVE-FPBA and B SVE-FPBA), a series of four concentrations was prepared as follows: 700, 600, 500 and 400 μl of polymeric solution in vials with labels 7, 6, 5 and 4 was filled with stock solutions of sample type corresponding dialysis baths to the final volume 1.2 mL yielding concentrations 1.324 mg/mL, 1.135 mg/mL, 0.946 mg/mL and 0,757 mg/mL, respectively.

Samples with the highest concentration from each set of nanoparticles (A, N and B) were also used for measurements of zeta potential and also a small volume of each sample type was used for Cryo-TEM measurements.

Solutions of nanoparticles A SVE-FPBA, N SVE-FPBA and B SVE-FPBA were stable for more than one month without any traces of precipitates.

SVE-PBA self-assembly

In line with SVE-FPBA systems, SVE-PBA nanoparticles were prepared by the quenching as described in the previous sub-chapter followed by the dialysis against deionized water with no pH adjusting leading to N SVE-PBA sample.

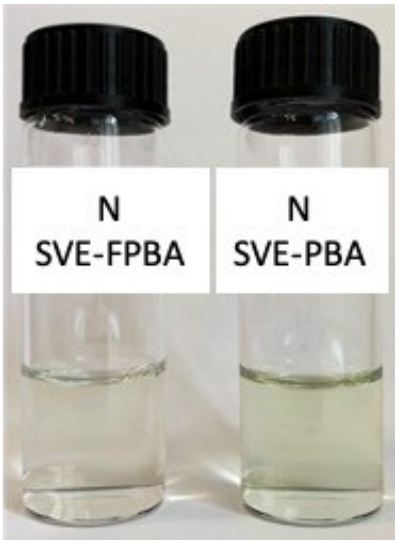

*Figure 20:Micellar solutions of: **left**-N SVE-FPBA, **right**-N SVE PBA, both prepared in physiological pH*

More exactly, 10 mg of polymer was dissolved in 1 mL of methanol and then quenched into 3 mL of water. In total 4 mL of 2.5 mg/mL concentrated solution were dialyzed in dialysis capsules against water through cellulose membrane with 6-8 kDa cut-off. The dialysis bath was changed three times as in previous experiment and the solution

of final concentration 2.0 mg/mL was analyzed in the same manner by means of dynamic and static light scattering, followed by zeta potential measurements and Cryo-TEM imaging. The comparison of N SVE-FPBA and N SVE-PBA solutions are shown in Figure 20.

5.4. Encapsulation and release of fluorescent probe

Encapsulation and release of a fluorophore molecules as a model drug was performed using only nanoparticles prepared in neutral water solution, N SVE-FPBA due to the potential use of the nanoparticles for drug delivery. Nanoparticles prepared in neutral solution with pH approximately 7.5 show the suitable pH for the boron ester formation between the boronic acid and model drug.

Encapsulation of Alizarin Red S in SVE-FPBA micelles

Encapsulation of Alizarin Red S, ARS in N SVE-FPBA by the boron ester formation was performed following two different protocols.

First, the boron-ester formation occurred after the above described quenching process of N SVE-FPBA, when the nanoparticles were already created and formed stable solution. Briefly, 10 mg of SVE-FPBA was dissolved in 1 mL of methanol and subsequently quenched to 1.5 mL of water. Simultaneously, 1 mg of ARS was dissolved in 1.5 mL of water that is a 35 % molar equivalent to FPBA molecules present in quaternized polymer. The pH of ARS solution was adjusted from initial pH 4.50 to pH 7.79 by addition of 0.1 M NaOH to ensure the transition of ARS to the monoanionic reactive form. This transition was accompanied with a typical color change of ARS from yellow to burgundy pink. Then, the ARS solution was added dropwise to the stable N SVE-FPBA nanoparticles at pH approximately 7.3. The final pH of SVE-FPBA with ARS was 7.45 that is an ideal pH for the formation of FPBA-ARS boronic ester. The solution was then dialyzed against water of pH approximately 7.5 with 3 times changed dialysis bath to ensure the removal of unbound ARS molecules. The volume SVE-FPBA-ARS after dialysis was 5 mL and the concentration of ARS was supposed to be measured by absorbance measurements, more exactly, from an ARS calibration curve. However, the solution precipitated next day due to the destabilization of already quenched

nanoparticles by an additional charge disbalance brought by ARS molecules in ionic form.

Second, the encapsulation procedure including of the boronic acid-ester formation was carried out at the very beginning of the SVE-FPBA self-assembly procedure. 10mg of SVE-FPBA was dissolved in 1 mL of methanol, and 1mg of ARS was dissolved overnight in 1.5 mL of separate methanol solution. Then, two droplets of 0.1 M NaOH were added to ARS solution accompanied with color change from yellow to pink that stands for the transition of ARS from non-ionic to reactive monoanionic form. The solution of ARS was added dropwise to the SVE-FPBA in methanol where both PEO and P4VP blocks are soluble. The color of polymeric solution was changing from greenish color (typical for solutions of pure polymer) to orange color while adding the ARS solution what is characteristic for bound ARS. Polymeric solution with bound ARS was then quenched to 2 mL of water to ensure the self-assembly and stabilization of the micelles loaded with ARS, in order to ensure the kinetical freezing of the non-quaternized part of P4VP block. Micellar solution was visibly opalescent but did not show any traces of precipitates. The methanol from SVE-FPBA-ARS solution and also the unbound ARS molecules were then removed by dialysis against three times changed water bath. During the dialysis, no coloration of the dialysis bath was observed, thus we expect that the reaction occurred quantitatively what stands for all of ARS molecules in FPBA-ARS ester. The total volume of the micellar solution after dialysis was 4.7 mL and as in previous experiment, the dialyzed sample had turbid appearance, and small precipitates were observed within a few minutes. Nevertheless, 0.27 mL of SVE-FPBA-ARS was diluted with 1.73 mL of water to the volume 2 mL with concentration of ARS $8 \cdot 10^{-5}$ M. Two absorbance spectroscopy experiments with SVE-FPBA-ARS sample were done in the range from 300 nm to 700 nm for determining the ARS absorbance maxima when encapsulated and after subsequent release of ARS from nanoparticles. The first absorbance measurement was done when the pH of the solution was 6.38, mimicking the physiological pH. Then, 20 μl of 0.1 M HCl was added to decrease the pH to 3.5 to mimic cancerous environment where the FPBA-ARS ester should be hydrolyzed, accompanied by ARS release. However, the lowering of the pH did not cause any changes in absorbance maxima. The SVE-FPBA-ARS sample precipitated, and the experiment was stopped at this stage.

Encapsulation of Alizarin in SVE-FPBA micelles

Due to the poor stability of the nanoparticles with Alizarin Red S due to the unexpected impact of ARS charge to the nanoparticle stability, we decided to use non substituted analog of ARS, the Alizarin, AL, with aim to avoid the presence of an additional ion pairing in the system. The encapsulation procedure begun as previously, 10mg of polymer was dissolved in 1 mL of methanol. Simultaneously, 2.14 mg of Alizarin was dissolved in 1 mL of methanol at 60 °C yielding deep orange transparent solution. This AL solution that stands for 75 % molar equivalent of phenylboronic acid groups in SVE-FPBA was then added dropwise while stirring the polymeric solution without observing any precipitates. SVE-FPBA-AL was then quenched to 2 mL of water to ensure the methanol removal from the micellar core and the kinetical freezing of non-quaternized part of P4VP block. After a classical overnight 3 cycle dialysis, the sample stayed transparent and deep orange with no traces of precipitates for more than 3 months. The volume of SVE-FPBA-AL after dialysis was 5.4 mL. The structure of AL and solution of SVE-FPBA-AL are shown in Figure 21.

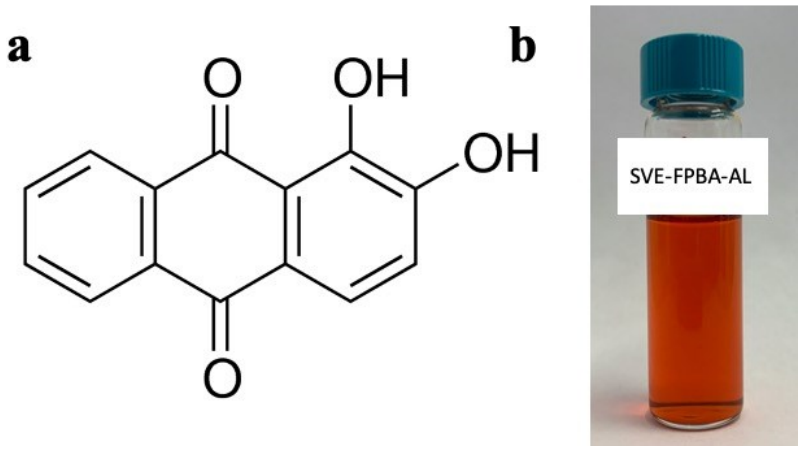

*Figure 21:**a**-strcture of Alizarin, AL, **b**-micellar solution of SVE-FPBA with Alizarin bound by ester bond.*

SVE-FPBA-AL micelles – AL encapsulation and pH induced release

This experiment was performed in manner to mimic physiological conditions of drug distribution to target place and also acidic conditions typical for drug release by monitoring absorbance maxima shifts of Alizarin. For this purpose, the solution of SVE-

FPBA-AL was diluted with dialysis bath solution to the volume of 2 mL with final concentration of Alizarin of $2 \cdot 10^{-4}$ M. The solution was visibly light orange and the pH was 7.96. First, the absorbance of the solution was measured in the wavelength range from 300 nm to 700 nm at the pH 7.96 and then 0.1 M HCl was added to the solution until reaching the pH to 2.79 and the solution was remeasured with same experimental setup to analyze the release of the Alizarin from SVE-FPBA micelles. Even though the pH of the solution crossed the pK_A value of FPBA-AL ester above which the ester should undergo hydrolysis, the orange color did not change to yellow color. This indicates that the hydrolysis did not occur and thus, there are no separate molecules of SVE-FPBA and Alizarin in the solution. The absorbance measurements with no shifts of AL absorbance maxima also confirmed that the reaction did not occur. The vials with SVE-FPBA-AL in neutral and acidic solutions with no color change are to be seen in Figure 22.

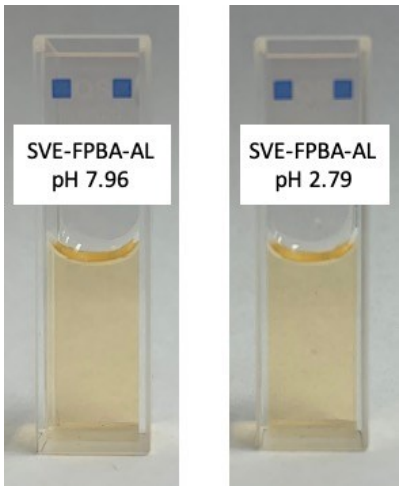

*Figure 22:Micellar solutions: **left**-encapsulation, **right**-release of AL from N SVE-FPBA-AL micelles.*

Competitive binding of sugars in SVE-FPBA-AL micelles

In this part of study, we studied the release of Alizarin from SVE-FFPBA-AL micelles induced by preferential binding of sugar molecules containing vicinal diols. Chosen saccharides should preferentially bind to phenyl boronic acid molecules in SVE-FPBA and should release bound AL from the nanoparticle in physiological pH. This reaction was tracked by measuring absorbance of SVE-FPBA-AL before and after the addition of sugars to the micellar solution. When sugar molecules preferentially bind to FPBA and release AL molecules, the absorbance maxima of SVE-FPBA-AL with bound AL in neutral conditions should shift to the higher wavelengths, typical for free monoanionic

AL form. In parallel, this reaction can be tracked by fluorescence emission changes. The intensity of fluorescence emission typical only for bound AL molecule should decrease when substituted by sugars and when released from nanoparticle as a single molecule. Also, the release of AL from SVE-FPBA-AL in pH above the pK_A of AL should be visible by naked eye thanks to color change of the solution from orange (bound AL) to pink, typical for free AL in monoanionic form. For the purpose of above described reaction of sugar competitive binding, we decided to analyze the SVE-FPBA-AL micelles when interacting with three different sugars, fructose, F, galactose, G and ascorbic acid, C, also known as vitamin C. Similar to previous absorbance measurement protocol, four samples of SVE-FPBA-AL micelles with concentration $2 \cdot 10^{-4}$ M in vials were prepared for absorbance measurements from 300 nm to 700 nm as follows. In detailed, 21.4 mg of fructose, 21.4 mg galactose and 21 mg ascorbic acid was added separately to three vials with SVE-FPBA micelles and these were labeled as F, G and C, respectively. The molar ratio sugar:phenylboronic acid in these samples was 10:1. The pH of the solutions was controlled during the experiment to avoid the transition of Alizarin molecules to its non-reactive form. Before the addition of sugars, the pH of SVE-FPBA-AL micelles was 7.96, and after addition of sugars the pH was 6.88 for sample F, 7.82 for sample G and surprisingly 2.98 for sample C.

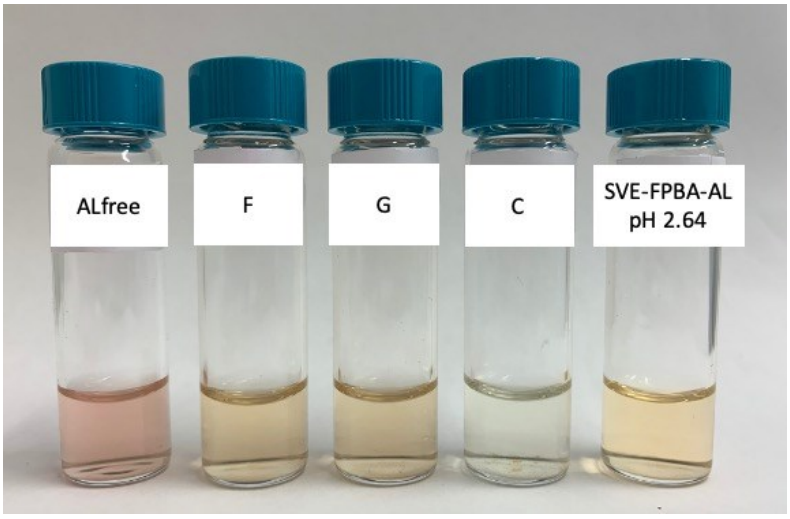

Figure 23:Solutions for competitive-binding analysis. From left. ALfree-free solution of Alizarin in physiological pH, micellar solutions of SVE-FPBA-AL with F, fructose in physiological pH, G-galactose in physiological pH, C, ascorbic acid with naturally acidic pH and micellar SVE-FPBA-AL with decreased pH by use of 0.1 M HCl.

The color of individual samples is shown in Figure 23, showing unexpected transition of color for sample C, from orange to yellow, that is typical for AL released from micelles induced by pH decrease. Such a transition due to the pH decrease was expected and not found in previous experiment of *SVE-FPBA-AL micelles – AL encapsulation and pH induced release.* In parallel, two remaining samples F and G did not show expected color transition from orange to pink.

Thus, we prepared the solution of free Alizarin in water in its monoanionic form labeled as ALfree shown in Figure 23, that should be identical in terms of color and absorbance maxima to the samples F, G and C after the AL release from micelles upon the competitive binding of sugars. However, samples F and G remained unchanged, showing the orange color typical for SVE-FPBA-AL esters instead of pink, typical for free AL. Due to the pH change after vitamin C addition (from pH≈8 to pH≈3) and color change (from orange to yellow) of the sample C, we prepared one sample of SVE-FPBA-AL micelles with pH 2.64 labeled as SVE-FPBA-AL pH 2.64. This sample with AL release induced by pH decrease identical to previous experiment served as a comparison of the to the release induced by addition of ascorbic acid that naturally decreased pH to the value 2.98. For additional information, we analyzed the effect of ascorbic acid on AL molecule resulting in color and ionic form change in a separate sample containing only free Alizarin molecules, ALfree with the same amount of ascorbic acid that was added to the micelles in sample C. The color changed directly from pink to clear yellow and the absorbance maxima was shifted to lower wavelengths as shown in *Results and Discussion* chapter together with SVE-FPBA-AL and sugars results.

The molecular complex of SVE-FPBA-AL in pH 7.69 should show fluorescence emission according to the literature that was previously explained in the chapter *2.3. Boronic acid as a stimuli-responsive functional group*. For this reason, we diced to measure the steady state fluorescence spectra of the sample SVE-FPBA-AL in pH 7.69 and to compare these results to the samples containing sugars, where we expected AL release, thus also the fluorescence intensity decrease. In more detailed, we analyzed 5 different samples with volume of 2 mL that were prepared identically to the samples in previous paragraph. The sample number one was the referent sample SVE-FPBA-AL in pH 7.6, (SVE-FPBA-AL pH 7.96). The second sample was a freshly prepared SVE-FPBA-AL sample containing Fructose, (F day 1). The third sample was a three days old SVE-FPBA-AL sample containing Fructose, (F day 3) with aim to compare the decrease of the fluorescence of FPBA-AL in time between the sample two and three. The fourth

sample was the sample SVE-FPBA-AL with ascorbic acid with its natural pH 2.3, (C). This sample was compared to the fifth sample, that was the SVE-FPBA-AL in pH lowered to the value 2.21 with addition of 0.1M HCl, (SVE-FPBA-AL pH 2.21). All the data of fluorescence emission measurement are listed in the chapter of *Results and Discussion* and the samples are shown in Figure 24.

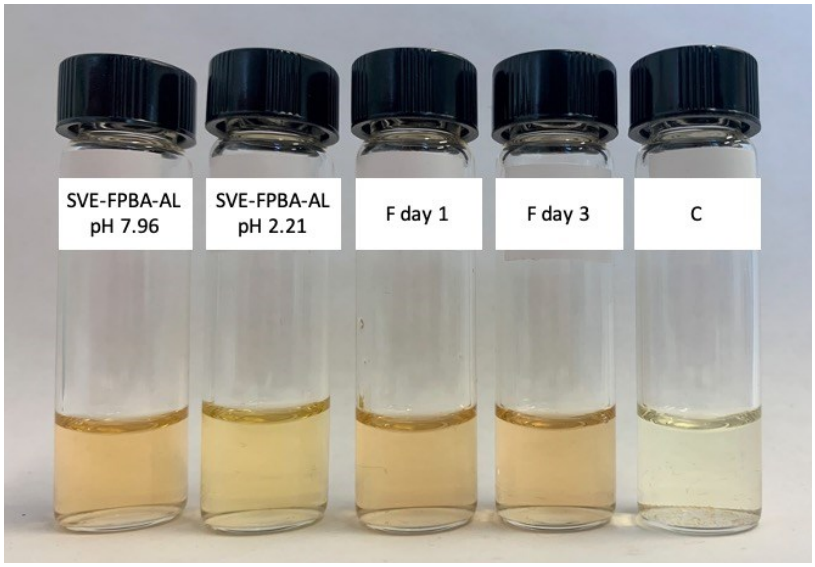

Figure 24:Micellar solutions for fluorescence emission measurements. Micellar solution of SVE-FPBA-AL, (from left) first, in pH of encapsulation, second, in acidic pH of release, third, fresh sample with addition of fructose, F, in physiological pH, fourth, 3 days old sample with addition of fructose, F, in physiological pH, fifth, with addition of ascorbic acid, C, in its naturally decreased pH to 2.21.

5.5. Sample preparation for NMR, LS, IR, Cryo-TEM measurements

Nuclear magnetic resonance measurements

^{1}H and ^{11}B NMR spectra were measured on a Varian UNITYINOVA 400 spectrometer in D_2O and CD_3OD (Chemotrade, Leipzig, Germany) at 25 °C. All of the experiments were measured in quartz cuvettes. For analysis of SVE-FPBA and SVE-PBA we used the concentration of 16.7 g/L and for Pyr-FPBA pK_A experiments 10 g/L. For the pK_A experiments, the pH of the solution was calculated from the pD using the relation pH = pD + 0.4.[85] The pK_A values were determined using relation

$$PPM_{calc} = (PPM_{min} + PPM_{max}10^{\,pK_A}[H^+])(1 + 10^{\,pK_A}[H^+]) \qquad (25)$$

where PPM_{calc} is the calculated chemical shift in parts per million, PPM_{min} is the initial chemical shift, PPM_{max} is the final chemical shift, and $[H^+]$ is the concentration of hydrogen ions (Cooper, & James, 2000). The pK_A measurements and calculations were performed by Dr. Somdeb Jana, the member of Soft Matter research team.

Light scattering measurements

The light scattering measurements (dynamic and static) were performed with light scattering setup (ALV, Germany) consisting of an ALV CGS-3 goniometer, ALV 7004 autocorrelator, two APD detectors operated in the pseudo-cross correlation mode and a 100mW diode-pumped solid state laser with the wavelength lambda = 660 nm (Cobolt AB, Sweden). The samples were measured in cleaned vials at 25°C for the scattering angles ranging from 30 ° to 150 °, with an angular step of 10 °. Vials with samples were measured in water and the standard solution was toluene. The static light scattering analysis was treated by standard Zimm method. The dynamic measurements analysis was performed by the ALV software based on fitting of experimentally normalized autocorrelation function of intensities.

Zeta potential measurements.

ζ-Potential measurements were performed using a Nano-ZS Zetasizer (Malvern Instruments, UK). ζ-Potential values were calculated from electrophoretic mobilities (average of three subsequent measurements, each consisting of 15 runs) using the Henry equation in the Smoluchowski approximation, $\mu = \varepsilon\zeta/\eta$, where μ is the electrophoretic mobility, η is the solvent viscosity, and ε is the dielectric constant of the solvent.

Cryo-TEM measurements

The cryo-TEM measurements were performed by Dr. Sami Kereïche from Institute of Cellular Biology and Pathology, First Faculty of Medicine, Charles University, Prague. A volume of 3 μL of the sample solution was applied to an electron microscopy gird with carbon-covered polymer supporting a film (lacey-carbon girds LC200-CuC, Electron Microscopy Sciences), glow discharged for 40 s with a 5 mA current. The gird was

immediately plunged into liquid ethane held at -183 °C. The sample was then transferred without rewarming into a Technical Sphera G20 electron microscope (FEI, Hillsboro, OR). Images were recorded 120 kV accelerating voltage and microscope magnifications ranging from 5000x to 14500x using a Gatan UltraScan 1000 slow scan CCD camera.

The size distribution of nanoparticles was done analysing population of 50 nanoparticles for samples A, N and B SVE-FPBA all together and 50 nanoparticles for sample N SVE-PBA, both using manual diameter measurement in ImageJ software. Micellar diameter values were processed in Origin.

Absorbance measurements

The absorbance measurements were performed on Shimadzu UV-VIS spectrophotometer. Samples were measured in 1cm pathway quartz cuvettes at a slow speed rate in wavelength range from 300 nm to 700 nm. Spectra of individual samples were collected at laboratory temperature. The standard solution of the sample was water.

Fluorescence measurements

Fluorescence emission measurements were carried out in 1cm pathway quartz cuvette using Fluorolog FL 3-22 fluorometer (Horiba Jobin Yvon, France) equipped with double-grating excitation and emission monochromators, a FluoroHub time-correlated single photon counting module and a TBX single photon counting detector. Steady-state fluorescence measurements were performed using a 450 W high-pressure xenon arc lamp as a light source. The excitation wavelength of the measurement was 470 nm that is equal to the absorbance maxima wavelength of the used samples. The emission wavelength range was from 520 nm to 750 nm. The slit of excitation light was open to 1 nm and the slit of emission to 0.5 nm. The integration time was set to 0.5 nm/s.

6. Results and Discussion

The main intention of modifying the poly(4-vinyl pyridine) block in PS-*b*-P4VP-*b*-PEO triblock terpolymer with fluorinated phenylboronic acid molecules is to introduce a stimuli responsive and drug delivery attractive compounds to triblock at desired amount independently on its polymerization process. We have shown, that the post polymerization modification of PS-*b*-P4VP-*b*-PEO with 2-bromomethyl-4-fluorophenylboronic acid, FPBA is a suitable method for designing a made to measure multi-functional stimuli responsive triblock terpolymer for a potential use in drug delivery. The quaternization reaction was confirmed with ^{1}H NMR, ^{11}B NMR and FT-IR spectroscopy. Then the self-assembly of the polymer was analyzed with dynamic and static light scattering measurements, together with zeta-potential measurements and cryo-TEM imaging. The model drug Alizarin Red S was after several unsuccessful attempts replaced with its analogue Alizarin. The encapsulation and release and the test of sensitivity to sugars of a model drug Alizarin was analyzed with absorbance measurements and fluorescence emission measurements.

6.1. Quaternization SVE triblock terpolymer with FPBA and PBA

The quaternization, also known as Menshutkin reaction,[73, 92] of PS-*b*-P4VP-*b*-PEO with 2-bromomethyl-4-fluorophenylboronic acid, FPBA and also with 2-bromomethyl-phenylboronic acid, PBA was carried out, and the desired product formation confirmed and quantified with the ^{1}H NMR and with ^{11}B spectra in deuterated methanol. Also, the quaternization reaction of pyridine, Pyr with 2-bromomethyl-4-fluorophenylboronic acid, FPBA, was studied for the pK_A determination with ^{11}B NMR. In addition, Fourier-transform infrared spectra served also as an evidence of occurred post polymerization reaction.

Nuclear magnetic resonance spectroscopy

The ^{1}H NMR measurements of quaternized pyridine, Pyr-FPBA, then homopolymer, P4VP-FPBA previously analyzed in Soft Matter research group together with newly analyzed triblock terpolymer in this study, PS-*b*-P4VP-*b*-PEO point out a repetitive pattern that confirms the quaternization reaction. First, comparing unmodified PS-*b*-P4VP-*b*-PEO with quaternized SVE-FPBA and SVE-PBA in Figure 25, modified polymer shows increased number of overlapping peaks in aromatic area. ^{1}H NMR of unmodified triblock shows only three peaks in aromatic area. One of the peaks belong to 5 protons of polystyrene, (peak **4**) and two remaining peaks, (peaks **3**) correspond to two sets of two protons of pyridine ring. Ones of the new appearing peaks in quaternized SVE-FPBA belong to the 4 protons of the phenyl ring of the quaternization agent FPBA/PBA, (peak **1**, clearly visible only in spectra **I.** and **II.**). Then other peaks belong to protons of P4VP phenyl ring which are influenced by near presence of phenyl ring of the quaternization agent FPBA/PBA. Although the integration of these peaks could possibly give the quaternization percentage of the reaction, the resolution of broad polymer peaks did not allow to separate the overlapping signals. Moreover, deuterated methanol is not a good solvent for the PS block and potentially for non-quaternized part of P4VP block what can cause that a part of PS and P4VP units can remain undissolved. Thus, the signals intensity could potentially be non-exact. For this reason, two well-defined signals were chosen to determine the quaternization reaction yield. One of these is the new appearing signal belonging to two protons of the methylene linker between phenylboronic acid and P4VP, (peak **2**) which is present in all of the quaternized analogues and the second signal belongs to completely dissolved PEO, (peak **4**) that serves as a reference for quaternization determination in case of SVE-FPBA and SVE-PBA. To sum up, the degree of quaternization determined by the comparison of the integrated signals **2** and **4** shown, that there have been modified approximately 30 % of P4VP units in SVE-FPBA and approximately 45 % of P4VP units SVE-PBA.

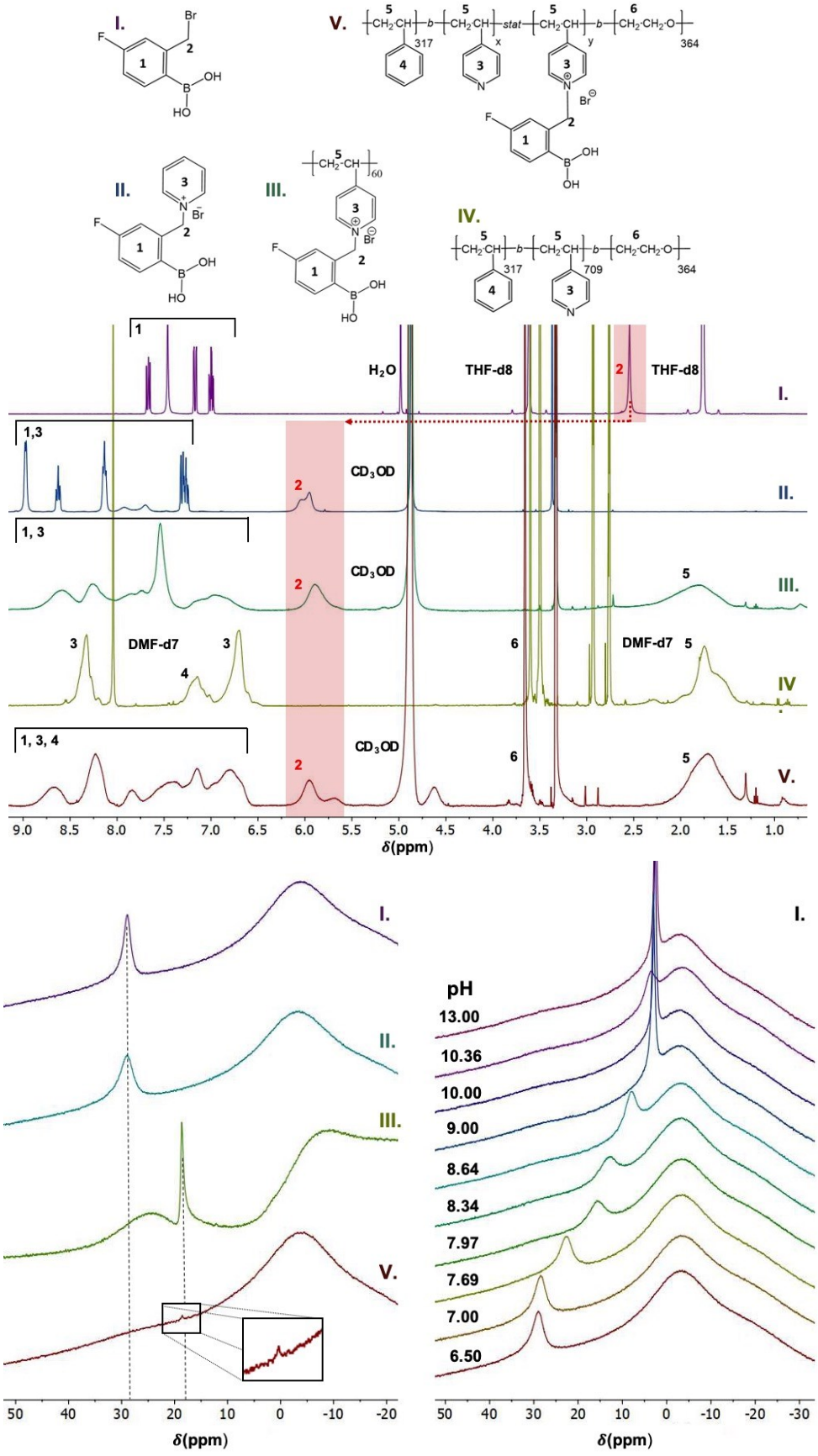

Figure 25:NMR figures of I. FPBA, II. Pyr-FPBA, III. PVP-FPBA, IV. SVE, V. SVE-FPBA. ***Top****-*^{1}*H NMR with methylene linker shift after quaternization,* ***bottom****-*^{11}*B NMR with boron shift after quaternization.*

Second, ^{11}B NMR confirms the modification of polymer with boronic unit by appearance of a typical boron ester peak that is shifted ~ 20 ppm to the high field in compared to the boronic acid signal at 28 ppm. However, polymeric spectra show only a very low intensity signal in comparison with pure compound because of the lower concentration of boron atoms in the polymer. Low intensity is also caused by high background of the used boron-containing NMR instrument probe. Both NMR spectra types before and after post polymerization reaction can be seen in the Figure 25. In addition, the influence of the pH change on the boron ester peak shift in monomeric analogue Pyr-FPBA performed in our group served to determine an approximate pK_A of FPBA on quaternized pyridine ring. The determined pK_A of monomeric analogue is pK_A≈ 7.75. However, we have to take in account a possible deviation of pK_A of phenylboronic units bound to triblock terpolymer system from this value, and we can use this value only as an estimate.

Fourier-transform infrared spectroscopy

Furthermore, FT-IR also confirm the quaternization reaction. The main element indicating the SVE-FPBA and SVE-PBA quaternization is the vibration at 1633 cm^{-1}. (black and red spectra Figure 26).[45, 92]

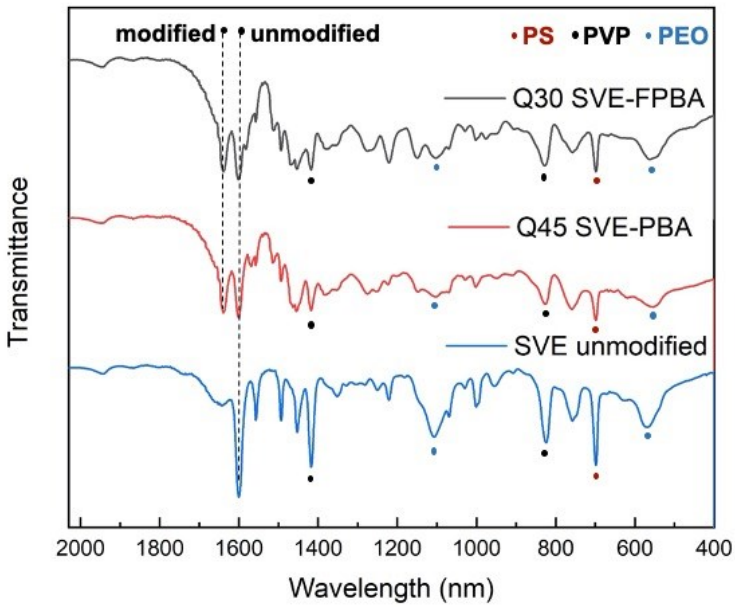

*Figure 26:Infrared spectra: **black**-N SVE-FPBA, **red**-N SVE-PBA, **blue**-SVE unmodified. Peaks marked with dots: **red**- PS signal, **black**-PVP signal, **blue**-PEO signal. Dashed line: **left**- modified PVP, **right**-unmodified PVP.*

This pattern is showing in all quaternized analogues and is compared to reactants of the Menshutkin reaction. This vibration band corresponds to the shifted C=N ring stretching towards higher frequencies comparing to the identical stretching type typical for unmodified pyridine at 1586 cm^{-1} (blue spectra Figure 26).[45, 92] In case of our samples, the polymer shows both vibration types, the unmodified and modified pyridine C=N ring stretching, because only about 30 % and 45 % of all P4VP units are modified in SVE-FPBA and SVE-PBA, respectively. We can also see, that the percentage of the quaternization reflects on the unmodified/modified P4VP peak ratio. For the sample SVE-PBA, we can see two similarly intense vibration peaks corresponding to quaternized (45 %) and unmodified P4VP (55 %). When the percentage of the quaternization is lower as in SVE-FPBA (30 %), there is a small change in unmodified/modified ratio, where the intensity of unmodified peak dominates (70 % over the modified one (30 %). As a comparison, the FT-IR spectra of unmodified PS-*b*-P4VP-*b*-PEO are shown in Figure 26 showing only one vibration peak of unmodified P4VP at 1586 cm^{-1}. To conclude, the reaction of P4VP quaternization by FPBA and PBA can be confirmed also by means of FT-IR spectroscopy. However, we have to take in account that the peak intensity change is not proportional, and that FT-IR spectroscopy does not serve for quantitative determination.

6.2. Self-assembly of SVE-FPBA and SVE-PBA

Static and dynamic light scattering

pH dependent self-assembly of SVE-FPBA and SVE-PBA self-assembly

Three sample types of SVE-FPBA and one sample of SVE-PBA nanoparticles prepared by quenching protocol followed by dialysis in acidic, neutral and basic aqueous baths (denoted as A, N and B, respectively) were analyzed by dynamic and static light scattering.

Static and dynamic light scattering measurements evaluation of data requires the value of sample's refractive index increment, $\frac{\mathrm{d}n}{\mathrm{d}c}$ that was calculated for SVE-FPBA triblock terpolymer from the values for individual blocks according to following equation

$$\left(\frac{\mathrm{d}n}{\mathrm{d}c}\right)_{\mathrm{SVE-FPBA}} = \left(\frac{\mathrm{d}n}{\mathrm{d}c}\right)_{\mathrm{PS}} \cdot w_{\mathrm{PS}} + \left(\frac{\mathrm{d}n}{\mathrm{d}c}\right)_{\mathrm{PVP}} \cdot w_{\mathrm{PVP}} + \left(\frac{\mathrm{d}n}{\mathrm{d}c}\right)_{\mathrm{PVPQ}} \cdot w_{\mathrm{PVPQ}} \quad (26)$$

$$+ \left(\frac{\mathrm{d}n}{\mathrm{d}c}\right)_{\mathrm{PEO}} \cdot w_{\mathrm{PEO}}$$

where $\left(\frac{\mathrm{d}n}{\mathrm{d}c}\right)_{\mathrm{X}}$ stands for refractive index increment of individual blocks in water multiplied by their weight fraction in polymer with value 0.257 mL/g for PS block, 0.170 mL/g for PVP block and 0.130 mL/g for PEO block (available from literature[93]). PVPQ stands for quaternized PVP block of which refractive index increment with value of 0.165 mL/g was measured previously in Soft Matter research team using PVP-FPBA quaternized homopolymer in 0.01 M NaOH. Estimated value of refractive index increment of SVE-FPBA triblock terpolymer micelles is 0.1808 mL/g.

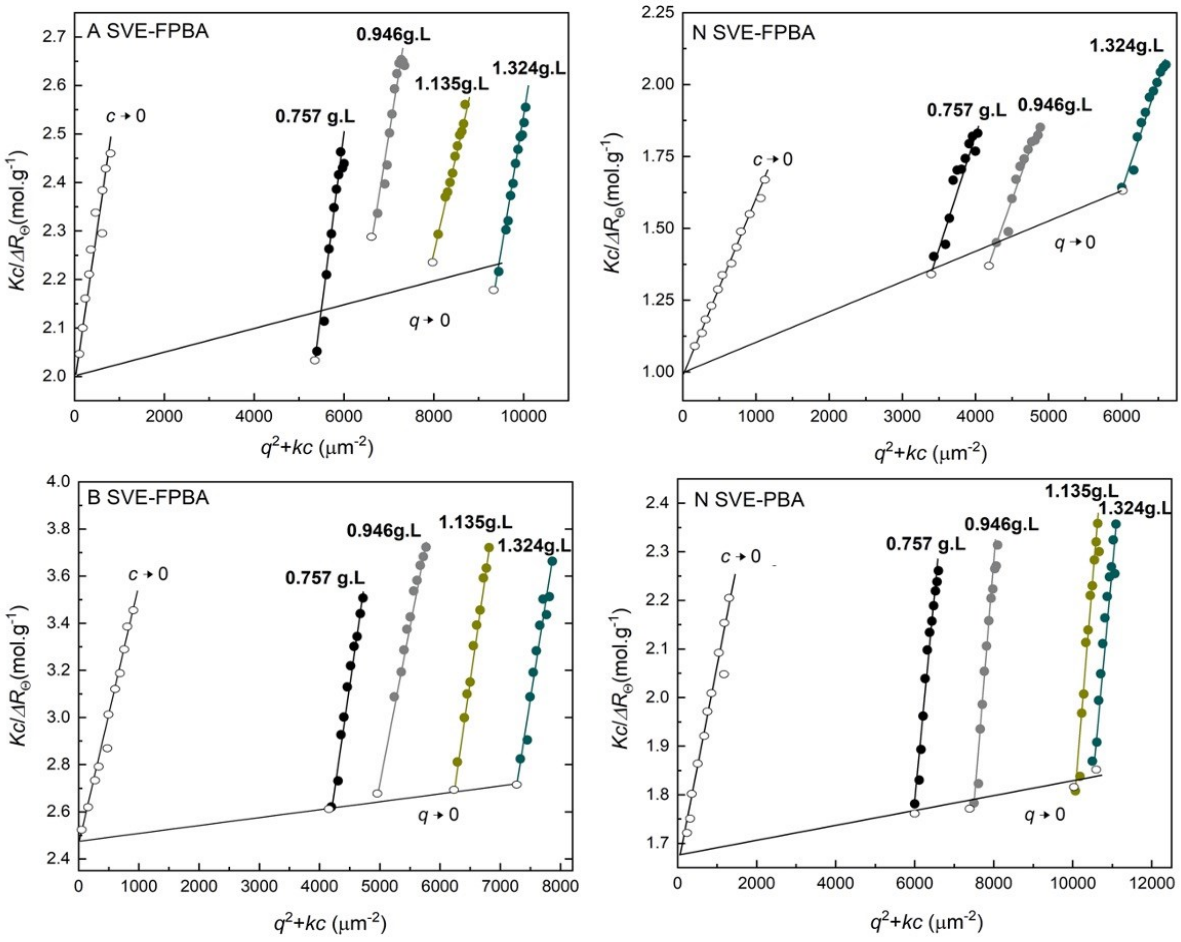

Figure 27: Zimm plot of A SVE-FPBA, N SVE-FPBA, B SVE-FPBA and N SVE-PBA.

Once calculated the refractive index increment, the concentration and angular dependence can be treated with Zimm equation. All the static light scattering graphs are to be seen in Figure 27.

The curvature of individual scattering curves and fluctuations of data points can be due to the usage of non-filtered samples with aim of obtaining very precise sample concentration. The extrapolation of data to zero angle and concentration, both treated with Zimm equation can give the values of absolute weight averaged molecular weight of micelles, M_W, and the radius of gyration, R_G. When dividing the M_W of nanoparticle by the molecular weight of the polymeric chain, we can obtain the number of chains assembling one nanoparticle, in other words the aggregation number, N_{agg}. All these variable´s values are collected in Table 1.

Table 1: Static light scattering data. R_G-absolute radius of gyration, M_W-absolute weight averaged molecular weight, N_{agg}-aggregation number.

Sample	R_G (nm)	$M_w \cdot 10^6$ (g/mol)	N_{agg}
A SVE-FPBA pH 5.10	38 (± 10 %)	5.10 (± 3 %)	29
A SVE-FPBA pH 2.50	36 ***	4.80 ***	25 ***
N SVE-FPBA pH 7.20	50 (± 10 %)	9.80 (± 7 %)	56
B SVE-FPBA pH 5.10	42 (± 4 %)	3.80 (± 2 %)	21
N SVE-PBA pH 7.10	40 (± 4%)	6.10 (± 2 %)	31

*** apparent value

Firstly, the apparent weight averaged molecular weight, M_W of self-assembled polymer under acidic and neutral conditions differs markedly. The sample A and B prepared in acidic dialysis bath show approximately 50 % lower M_W than neutral samples, N of both fluorinated and non-fluorinated phenylboronic acid-modified polymer, SVE-FPBA and SVE-PBA, respectively. This decrease in value of M_W for nanoparticles prepared in acidic solution is the most likely caused by the difference in solubility of P4VP block in acidic and neutral solvent. As was explained in the overview of the literature, at condition of pH higher than 4.8-5, the poly(4-vinyl pyridine) is not soluble in water. Once the pH of the solvent decreases under pH approximately 5, a small portion of P4VP units get protonated. The positive charge on P4VP units brings in one hand solvent swelling of P4VP corona and in other hand repulsion between two positively

charged chains in near proximity. Both, the swelling and the repulsion cause that a fewer number of polymer chains self-assemble in one loosened nanoparticle. Thus, we could suppose the number of chains per micelle vary with the force of chain repulsion and the repulsion force is affected with the percentage of P4VP protonation. The effect of pH on poly(2-vinyl pyridine) with similar properties is described in both articles of Štěpánek et al. from 2005.[86] Also, the influence of pH on protonation degree of PVP is described in recently published article of Fernandez-Alvarez et al. with results sustained by the simulation experiments.[87] Considering our system in pH 5 that is the pH close to P4VP pK_A, we could conclude, that only a small portion of P4VP in our triblock is protonated and that the change in M_W should not be so important. Although this may be true, we have to point out that in our system, there are constantly positively charged P4VP units (quaternized ones) at any pH that raise the overall number of positive charges on polymeric chain. These positively charged units belong to the quaternized nitrogen atom in P4VP. When adding this permanent charge effect to the newly protonated nitrogen caused by only a small decrease of the pH near to the to the P4VP pK_A, we can suppose that the repulsion effect reflected in M_W will be more important, as in case of our sample. To conclude, the self-assembly protocol in acidic pH give rise to looser nanoparticles, constituted of a lower number of polymeric chains. Conversely, N SVE-FPBA and N SVE-PBA nanoparticles prepared in pure water with pH=7.20 yields more compact micelles able to assemble more polymeric chains in one nanoparticle. The neutral system behaves in way to maximally avoid the solvent molecules access in the non-soluble and partially glassy shell. This theory is further extended in following section to explain the influence of the solvent on the aggregation number.

The radius of gyration (Table 1) of individual A, N and B SVE-FPBA samples changes according to the solution type that was used for their dialysis. The nanoparticles prepared in acidic dialysis bath show smaller nanoparticles with approximately 20% lower R_G values than for sample type N. The restriction of R_G of A and B SVE-FPBA micelles can be due to the increased ionic strength of the solution A and B in comparison to the solution N what is also explained in article of Štěpánek et al,[86] presented in the section of dynamic light scattering measurements.

In addition to M_W, N_{agg} and R_G, dynamic light scattering measurements permit to obtain absolute value of z-averaged diffusion coefficient, D_Z, and thus, also to obtain the value of hydrodynamic radius, R_H, from Stokes-Einstein equation. We can estimate an approximate shape of micelles from the R_G /R_H ratio. All of relied variables assist to

further describe the micellar system, and these are listed in Table 2. Also, the dynamic Zimm plots of concentration and angular dependence are to be seen below, in Figure 28.

Table 2: Dynamic light scattering data. R_H-absolute hydrodynamic radius, D_Z-z-averaged diffusion coefficient, R_G /R_H- radii ratio for estimation of nanoparticle's shape.

Sample	R_H (nm)	D_Z ($\mu m^2/s$)	R_G/R_H
A SVE-FPBA pH 5.10	44	5.40 (± 4 %)	0.860
A SVE-FPBA pH 2.50	46 ***	5.80 ***	0.782 ***
N SVE-FPBA pH 7.20	31	7.40 (± 7 %)	1.610
B SVE-FPBA pH 5.10	51	4.60 (± 4 %)	0.820
N SVE-PBA pH 7.10	30	8.00 (± 2 %)	1.330

*** apparent value

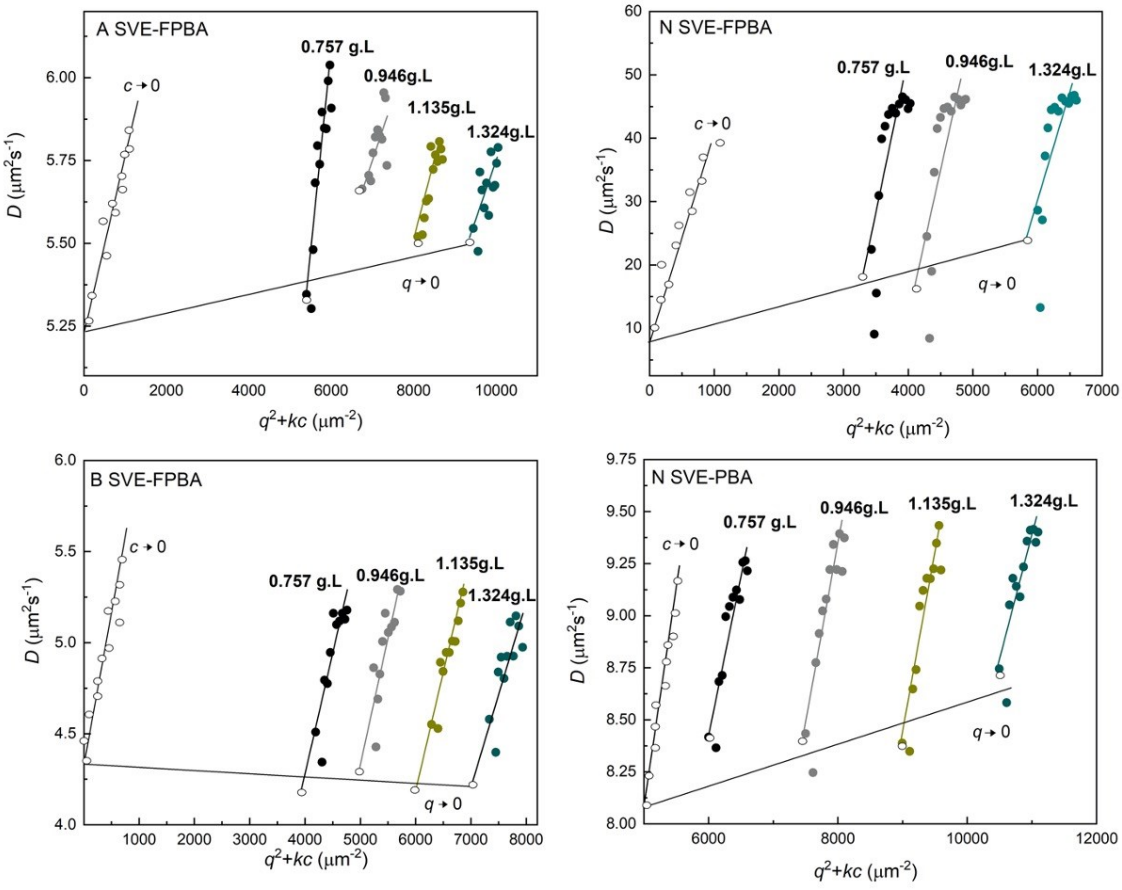

Figure 28: Dynamic Zimm plot of A SVE-FPBA, N SVE-FPBA, B SVE-FPBA and N SVE-PBA.

The size of the solvation shell and of the overall nanoparticle affects reciprocally the velocity of the diffusion motion of analyzed nanoparticles in solution. In other words,

small nanoparticles with small solvation shell move fast in the solution, thus exhibit higher value of diffusion coefficient and large nanoparticles with a large solvation shell move slowly and thus, show lower diffusion coefficient. Dynamic Zimm plot shows the highest diffusion coefficient value for nanoparticles in the neutral water solution. This means that N SVE-FPBA nanoparticles have a smaller solvation shell and thus they move faster comparing to A and B SVE-FPBA nanoparticles with larger hydration sphere that move more slowly.

The size of hydration sphere together with the radius of the polymeric nanoparticle, R, is described by the value of hydrodynamic radius, R_H. Dynamic light scattering data from nanoparticle solutions A, N and B SVE-FPBA support previously explained theory of chains repulsion and solvent swelling of P4VP. The R_H of nanoparticles prepared in acidic dialysis bath, A SVE-FPBA and B SVE-FPBA show more than 15 nm larger nanoparticles that in case of micelles prepared in neutral solution, N SVE-FPBA. This change is also the result of the repulsive interactions between polymeric chains and of the solvent swelling of P4VP. These looser nanoparticles in pH=5.10 with rougher solvation shell are apparently larger even if they consist of a lower molecular mass compared to nanoparticles prepared in water of pH=7.20. According to the publications concerning P4VP in micellar systems, further lower pH should enhance the protonation of P4VP and thus, its water solubility. For this reason, we decided to decrease the pH of A SVE-FPBA with pH=5.10 to lower values. However, when decreasing the pH with 0.1 M HCl to the very acidic pH=2.5, we can see that the further drastic decrease of pH does not affect the hydrodynamic radius (apparent value for pH=2.5) anymore as we expected based on the article of Štěpánek et al. and also the one of Fernandez et al. The R_H^{app} of A SVE-FPBA in pH=2.5 increases only by 2 nm as can be seen in Table 2. We suggest the theory, that the water molecules struggle to penetrate the very dense system with very long P4VP block consisting of 709 units, and that the dependence of the R_H on the pH and ionic strength of the solution does not influence our system below some threshold protonation percentage of P4VP units. In more detailed, we expect that when decreasing the pH below the pK_A of P4VP, only the P4VP units near to the P4VP-PEO interface get protonated, thus the chains partially reorganize only at the P4VP-PEO interphase level, what can cause the increase in R_H of about 15 nm. However, the P4VP units in the deeper frozen P4VP shell close to PS frozen core does not permit to penetrate the H^+ molecules deeper to the corona due to the extensive hydrogen bonds between the nitrogen electron pair and hydrogen-containing backbone. Thus, we suppose that the decrease of the pH affects only

the portion of solvent accessible P4VP units in the P4VP-PEO interface and causes small reorganizations in the shell-corona level. We also suppose, that our system starts to deviate from behavior of similar systems in published studies when the pH crosses the value approximately 4. Below this value the pH does not further influence the frozen part of the P4VP shell together with PS core.

Considering the R_H values from other point of view, the micelles shown in the dynamic measurements performed at 90° angle treated with constrained inverse Laplace transform routine, CONTIN in the Figure 29 shows monomodal nanoparticles for each of the sample types. More exactly, these size distributions show that the micellar solutions of A, N and B SVE-FPBA consist of only one population of micelles. The R_H of micelles in acidic solution is visibly larger, than the R_H of micelles in pH 7.2. When comparing the SVE-FPBA micelles to SVE-PBA micelles we can conclude that the fluorination of the phenylboronic acid almost does not influence the overall structure of the micelles. These monomodal distributions for all four SVE-FPBA samples and also for SVE-PBA sample are completely in agreement with the cryo-TME images shown in following section.

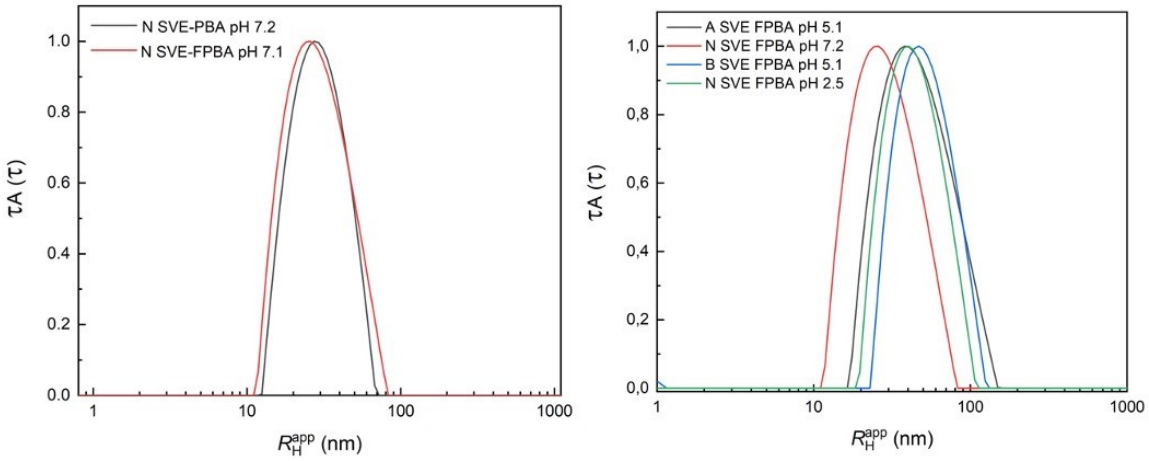

*Figure 29: CONTIN analysis of samples: **left-** comparison of R_H^{app} of N SVE-FPBA and N SVE-PBA micelles, **right-** comparison of R_H^{app} of SVE-FPBA micelles in A, N, B solutions with different pH.*

When comparing the R_H values to R_G values, R_H change reciprocally to R_G based on the used solvent of the micellar solution. This reciprocity in R_H and R_G values is explained in the article of Štěpánek et al.[86] In there, the authors show that pH, polymer concentration and also ionic strength have an impact on micellar size in case of very similar PS-*b*-P2VP-*b*-PEO triblock polymer. The article shows increasing R_G of nanoparticles with increasing

concentration of HCl against decreasing R_H. In more detailed, this study shows a reciprocal correlation between the radius of gyration and hydrodynamic radius of nanoparticles in a solution with decreasing pH, that underlines our theory of P4VP solvent swelling and chains repulsion.

Combining the results of static and dynamic measurements in the form of R_G/R_H ratio also known as ρ-ratio we can estimate approximate vision of the nanoparticles shape.[76] According to the book of Scattering from Polymers written by Wolfgang Schartl we can conclude that values near to 0.8 belong to spherical micelles and these values belong to samples A and B. Light scattering data of nanoparticles prepared in neutral water solution yield the R_G/R_H value of 1.5 what fit to the interval of an ellipsoid micelle or better said non-spherical micelle. To explain, in our system we work with a partially quaternized P4VP polymer block which is also partially soluble in water. We suppose that in neutral solution, the portion of quaternized P4VP units tend to be exposed to the solvent while the non-quaternized parts of P4VP block tend to be hidden in the PS-P4VP interface, forming kind of compact entanglements with PS block. We expect, that individual P4VP segments form a sort of loops within the very long P4VP block. These positively charged P4VP loops interfere with PEO corona in way to reach stable nanoparticles. This polymer organization in neutral solution is represented in Figure 30.

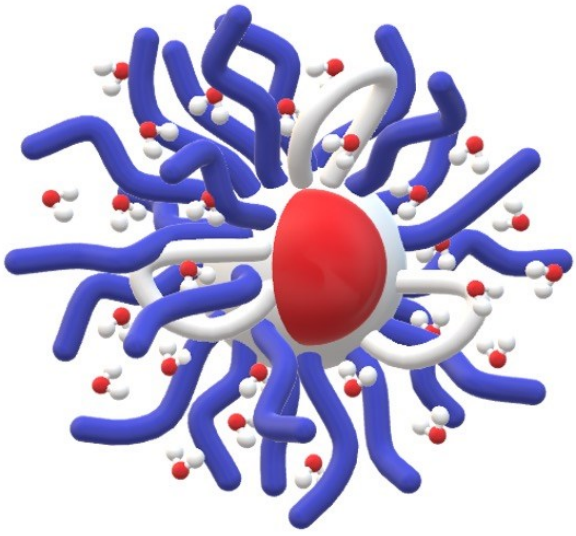

Figure 30: Visual representation of estimate micellar morphology of SVE-FPBA micelles. ***Red sphere****-frozen PS core,* ***white sphere****-frozen P4VP (non-quaternized) shell,* ***white loops****-solvent swelled quaternized P4VP shell,* ***blue chains****-solvent swelled PEO corona. Water molecules present in PEO corona and in surrounding of mobile quaternized P4VP shell segments.*

Red chain segments represent the hydrophobic and kinetically frozen PS block, white sphere on the top of the PS core represent the frozen part of P4VP shell and the partially soluble quaternized P4VP block segments are shown as the loops interfering with blue solvent swelled PEO block. For more accurate interpretation of data, we performed cryo-TEM measurements, that completely fit to our hypothesis.

Cryo-TEM

Three types of SVE-FPBA samples (A, N and B) and one SVE-PBA sample (N) were visualized with cryogenic transmission electron microscopy, cryo-TEM. Generally, when no staining is applied to the micellar samples, cryo-TEM analysis shows only highly solvophobic and kinetically frozen parts of the analyte, or alternatively crystalline and highly ordered domains (not applicable for our system). In case of our sample, only the PS block and a part of frozen hydrophobic P4VP may be visualized on cryo-TEM images, while the solvophilic P4VP shell part and PEO corona are no visible. Taking into account that all of the samples A, N and B SVE-FPBA are prepared by an identical quenching process of SVE-FPBA from methanol to water we could expect that the solvent change induced P4VP swelling at the P4VP-PEO interphase and that these small changes in solvophobic corona are hardly to be distinguished on cryo-TEM images. For this reason, we have performed one common size distribution of nanoparticles for all the samples A, N and B SVE-FPBA and one separate size distribution for non-fluorinated analogue SVE-PBA micelles in Figure 31.

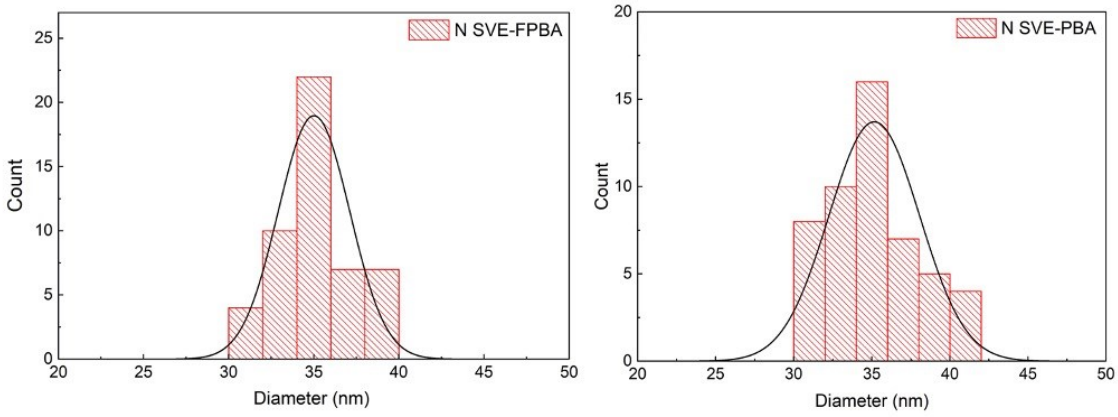

Figure 31: Size distribution of: ***left****-A, N and B SVE-FPBA micelles,* ***right****-N SVE FPBA micelles.*

The size distribution of three samples A, N and B SVE-FPBA systems show that there are nanoparticles ranging from 30 nm to 40 nm diameter, what stands for 15 nm and 20 nm radius. Based on our light scattering results, the R_G ranges from 40 nm to 50 nm and the R_H ranges from 30 nm to 50 nm. We could admit that as we previewed in above described light scattering section, in our nanoparticles, there is a PS frozen core, part of the non-quaternized P4VP shell is in frozen state and the other part of quaternized P4VP together with hydrophilic PEO form a mobile corona. Based on the structure of the polymer PS-*b*-P4VP-*b*-PEO, that consists of 317 solvophobic PS units, of 709 P4VP units from which ≈460 units are solvophobic ≈250 units are solvophilic (quaternized ones) and of 364 solvophilic PEO units, we suppose that a bigger half of the polymeric chains are frozen (≈ 780 units) and less than half of polymeric chain is mobile and soluble (≈610). Also, our estimation of micelles with hydrophilic P4VP loops on issued from frozen P4VP shell (Figure 30, above), are sustained by a few cryo-TEM images, showing a sort of "arms" pointing from the visible micellar PS and P4VP core and shell, respectively. From the other point of view, when comparing the micelles with fluorinated phenylboronic acid SVE-FPBA to the micelles with non-fluorinated analogue SVE-PBA, we can suppose that using fluorinated analogue does not affect the frozen micellar core, visible on cryo-TEM. The size-distribution diagrams and cryo-TEM images are to be seen in the Figure 32.

We have equally performed the calculation of estimate micellar core radius of PS, $R_{C(PS)}$ using formula

$$R_{C(PS)} = \left(\frac{3 \cdot N_{agg} \cdot M_{W,PS}}{4 \cdot \pi \cdot N_A \cdot \rho_{PS}}\right)^{1/3} \quad (27)$$

where $M_{W,PS}$ stands for absolute weight averaged molecular weight of PS block calculated from light scattering data, N_A is Avogadro constant and ρ_{PS} is the density of PS block. The calculated values of $R_{C(PS)}$ for N, A and B SVE-FPBA and also of N SVE-PBA micelles are listed in Table 3 and compared to averaged radius found from cryo-TEM size distributions.

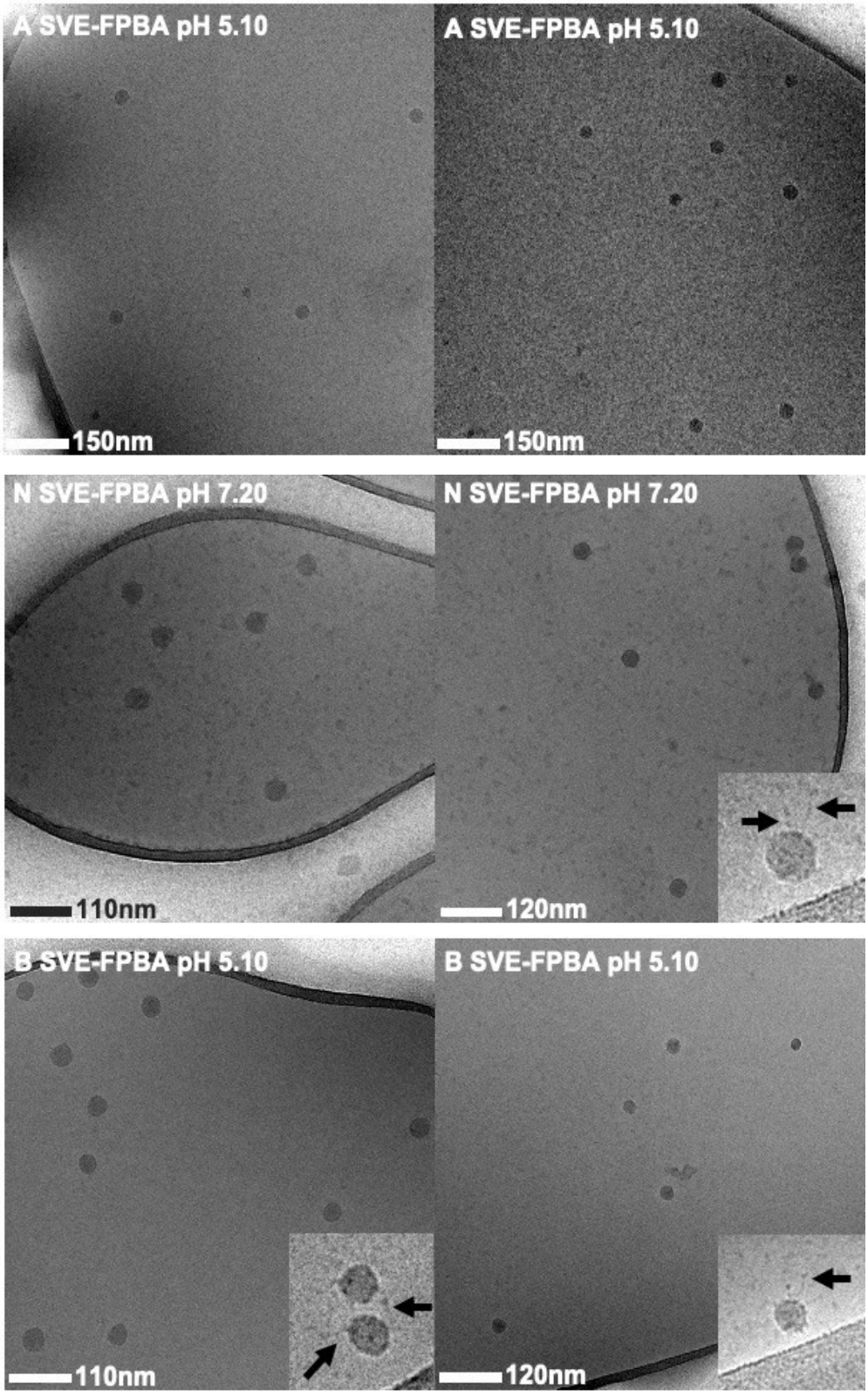

Figure 32: Cryo-TEM images of: ***top****-A SVE-FPBA micelles,* ***middle****-N SVE-FPBA micelles, input image with quaternized P4VP loops,* ***bottom****- B SVE-FPBA micelles, input image with quaternized P4VP loops.*

Table 3: Comparison of PS core radius to the radius of frozen part of micelle from cryo-TEM.

Sample	A SVE-FPBA	N SVE-FPBA	B SVE-FPBA	N SVE-PBA
$R_{C(PS)}$ (nm)	7.00	8.70	5.90	7.20
$R_{cryo\text{-}TEM}$ (nm)	18	18	18	18

The calculations of PS core radius show that the frozen micellar core as observed by cryo-TEM consists not only of PS blocks, but it is much larger. These calculations sustain our hypothesis considering the formation of micelles consisting from frozen PS and non-quaternized P4VP core, then from solvent swelled quaternized P4VP loops and from solvent swelled PEO corona.

Zeta potential

Zeta potential measurements of A, N and B samples of micelles showed positive zeta potential values for all the samples. The value of +40 mV for samples A and N shows very stable nanoparticles in acidic and neutral solution. In contrary, precipitated polymer sample B prepared in basic conditions that was subsequently transferred and dissolved in acidic dialysis bath was destabilized during the preparation. The sample B shows a lower zeta potential of +25 mV what exhibits decreased stability of particles in comparison to sample A and N. Particles with lower zeta potential show lower effective electric charge on the surface and thus, lower electrostatic repulsion between these nanoparticles.

In this work we aim to study the potential use of PS-*b*-P4VP-*b*-PEO in drug delivery. For this reason, we decided to perform following encapsulation and release experiments using SVE modified with fluorinated analogue of phenylboronic acid, FPBA. Based on previous studies of our group, FPBA molecule showed lower pK_A value than non-fluorinated parent molecule PBA, which has a biological aspect in reaction efficiency of the diol binding. Then, from three studied micellar systems, A SVE-FPBA, N SVE-FPBA and B SVE-FPVA, we chose to perform the encapsulation and release experiment using N SVE-FPBA nanoparticles prepared in neutral aqueous solution with the pH the nearest to the physiological conditions.

6.3. Encapsulation and release of fluorescent probe

The 2-bromomethyl-4-fluorophenylboronic acid, FPBA as a quaternization agent of PS-*b*-P4VP-*b*-PEO, SVE, shows promise in sugar sensing, diol binding and drug delivery of diol containing drugs. The advantage of using of fluorinated phenylboronic molecule in drug delivery system is its lower pK_A in comparison to its parent non-substituted molecule. The lower pK_A of FPBA shifts the window of effective diol binding from higher pH to physiological conditions. In this study, we aimed to analyze the diol binding and release by ester formation and hydrolysis of FPBA modified SVE triblock terpolymer mimicking physiological conditions. For this purpose, we used fluorophore Alizarin Red S, ARS, that was later changed to the more suitable parent molecule Alizarin, AL. Also, we aimed to study the competitive binding between AL and sugars containing vicinal diols to FPBA molecules. This part of the work is divided in four subchapters, among these the chapter concerning the difficulties with encapsulation of Alizarin Red S molecule, following chapter concerning the successful encapsulation of Alizarin molecules in SVE-FPBA micelles. Then, two remaining chapters consider the properties of only Alizarin, AL. Third chapter compare and analyzes the absorbance properties of Alizarin in physiological and acidic pH mimicking drug distribution and release at the target place. The last chapter describes the competitive binding and encapsulation of various saccharides with Alizarin tracked by measuring absorbance and fluorescence changes.

Encapsulation of Alizarin Red S in SVE-FPBA micelles

The encapsulation of water-soluble charged Alizarin Red S caused the destabilization of the stable micellar system as described in detail in experimental part, *Encapsulation of Alizarin Red S in SVE-FPBA micelles*. In principle, Alizarin Red S molecule is a sulfonic acid sodium salt of Alizarin. This substitution of Alizarin by -SO_3Na group brings the water-solubility to the fluorophore and makes it more applicable in systems similar to ours compared the parent Alizarin molecule. However, addition of an extra ion pair to the micellar solution probably caused the destabilization of our system within interval of hours. For this reason, we decided to return to use the parent Alizarin molecule soluble in methanol to avoid this destabilization and precipitation of our polymeric micelles.

Encapsulation of Alizarin in SVE-FPBA micelles

The quaternization of PS-*b*-P4VP-*b*-PEO, SVE with 2-bromomethyl-4-fluorophenylboronic acid, FPBA, dramatically changed its solubility. Before the post polymerization reaction, PS-*b*-P4VP-*b*-PEO was soluble only in DMF. The introduction of FPBA to this triblock yielding SVE-FPBA turned the polymer to be soluble in methanol. Methanol is also a good solvent for Alizarin molecule when heating the solution to 65 °C. With this in mind, we provided the encapsulation of the fluorophore Alizarin in a very first step of SVE-FPBA self-assembly, when methanol solubilizes the P4VP block and the PEO block, as is further described in detail in experimental part, *Encapsulation of Alizarin in SVE-FPBA micelles*. In this state, the entire polymer block P4VP is more accessible to the solvent molecules than when self-assembled in micelles in water, where the non quaternized P4VP is in frozen state. Slow introduction of monoanionic Alizarin solution in methanol caused color transition of the initially pink Alizarin solution to strong orange micellar solution. This color change is a first sign of boron-ester formation between FPBA and Alizarin molecules. Bound Alizarin to the SVE-FPBA triblock terpolymer yielding SVE-FPBA-AL micelles was quenched to a prevalent amount of water, and then purified by dialysis from unbound Alizarin molecules.

Final solution was analyzed by cryo-TEM imaging showing formation of spherical micelles, visible in Figure 33. These micelles do not show any differences in a frozen core compared to SVE-FPBA micelles without AL. In addition, we have found that a small 1nm aggregates present also in solution previously probably fused to larger aggregates and become more contrasted after adding the Alizarin to the solution as can be visible on cryo-TEM images and also on the size distribution in Figure 33. An aliquot of the same SVE-FPBA-AL solution shown shifted absorbance maxima to lower wavelengths, typical for FPBA-Alizarin ester that will be shown and explained in next section.

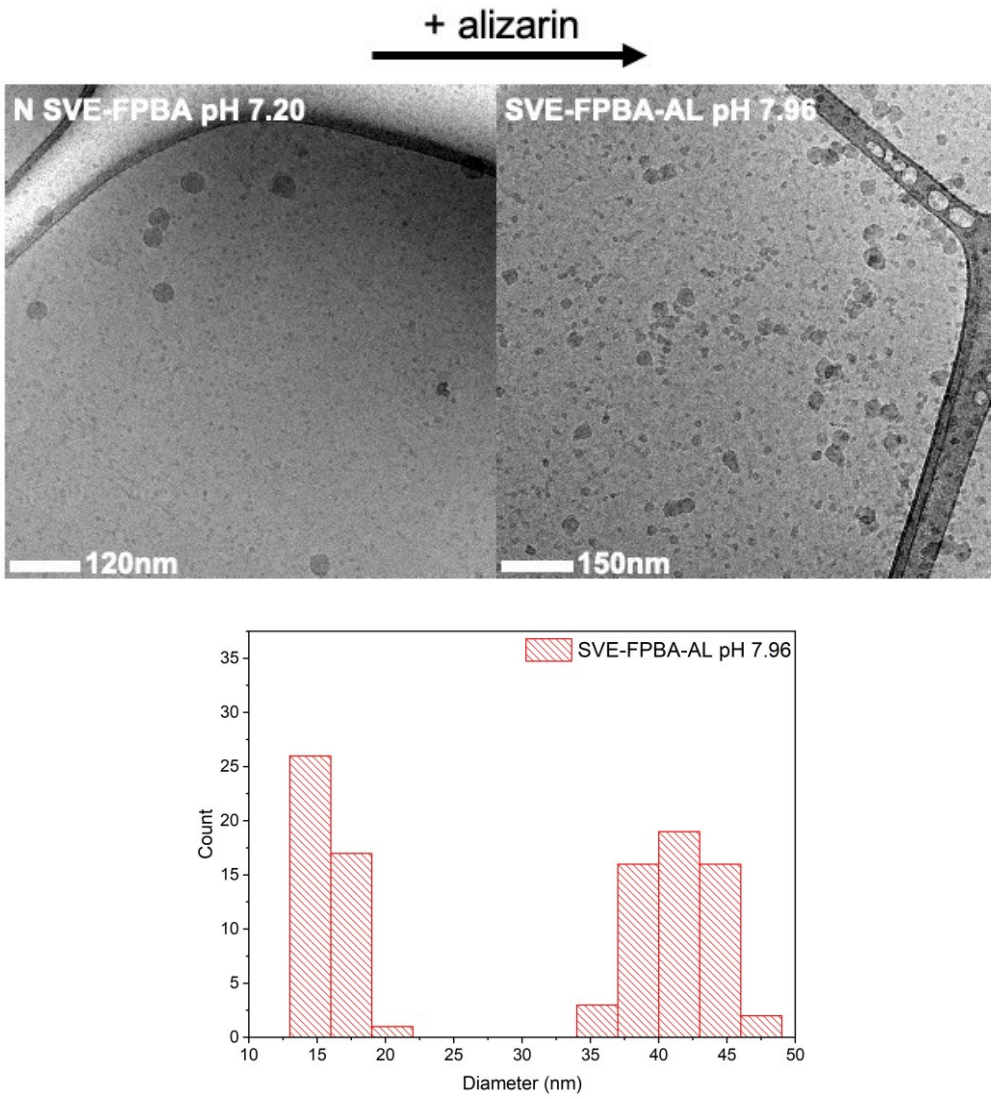

*Figure 33:On the **top-**Cryo-TEM images of N SVE-FPBA micelles **left**-before Alizarin, AL addition, **right**-after AL addition. On the **bottom**- size distribution of N SVE-FPBA-AL micelles corresponding to N SVE-FPBA micelles with encapsulated AL.*

SVE-FPBA-AL micelles – AL encapsulation and pH induced release

The absorbance of SVE-FPBA-Alizarin, denoted as SVE-FPBA-AL solution was analyzed in physiological and acidic conditions mimicking drug encapsulation and distribution, and to the drug release conditions. The absorbance maxima of SVE-FPBA-AL in physiological condition of pH approximately 7.5 was found at 475 nm that corresponds to monoanionic AL that is bound the FPBA-AL boron ester (SVE-FPBA-AL pH 7.96). [41, 88] This absorbance maxima should shift to lower wavelengths near to 425 nm when crossing the pK_A of boron ester and pK_A of AL (transition from monoanionic

from to non-ionic form) which matches to the pH lower than 4.5. In solution of this pH, the hydrolysis of boron ester should be tracked with color change from orange to yellow, that is typical for free AL molecule. For this purpose, we changed the pH of the SVE-FPBA-AL solution first to 3.50 and then to 2.79, (SVE-FPBA-AL pH 2.79). However, none of the conditions gave place to the hydrolysis of the SVE-FPBA-AL ester. The absorbance maxima of the SVE-FPBA-AL micelles in pH 2.79 did not shift to the lower wavelength visible in Figure 34 and also the color of the solution remained unchanged. The decrease of the intensity of the SVE-FPBA-AL pH 2.79 solution is caused by the dilution of the solution with 0.1 M HCl while decreasing pH of the solution.

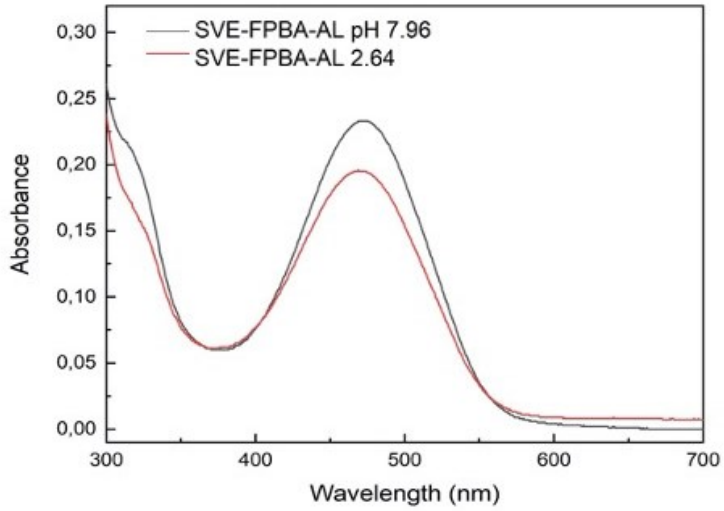

Figure 34: Absorbance measurement of N SVE-FPBA-AL micelles in pH=7.69 and in pH=2.79.

We suppose, that the protons from the solution struggle to affect the micellar properties due to the boron-nitrogen interaction, forming a complex between P4VP and FPBA molecules.[53, 89] Moreover, the lower pH than the pK_A of the P4VP causes the protonation of a small portion of the P4VP units in addition to the permanently charged quaternized P4VP units, that may form hydrogen bonds with hydroxyl groups of released Alizarin when released due to the lower pH. For this reason, the molecule may stay entrapped and solubilized within even in a low pH condition. Also, studies concerning AL analogue, the Alizarin Red S show, that Alizarin molecule in monoanionic form could be potentially entrapped on positively charged nitrogen of P4VP units by ion-pair interaction. In order to release the encapsulated Alizarin molecules form SVE-FPBA-AL micelles, we decided to analyze the system with various sugars with higher binding

affinity to FPBA, than the AL affinity is. The preferential binding of sugars to FPBA in physiological pH should provoke the release of monoanionic AL molecules from micelles with avoiding the transition of the system to acidic pH, which enhances the protonation and positive charge increase on P4VP units.

Competitive binding of sugars in SVE-FPBA-AL micelles

Alizarin binds to the FPBA through two hydroxyls. When adding another compound containing diols with higher affinity to FPBA molecule to the system in physiological solution, this compound can displace the Alizarin from FPBA-AL molecular complex and preferentially form new boronic ester. In this study, we decided to analyze the SVE-FPBA-AL system after addition of different saccharides, these are fructose, F, galactose, G, and ascorbic acid, C, also known as vitamin C. These sugars should preferably bind to boronic acid over the Alizarin molecules. Thus, we expected that after adding amount corresponding to a molar ratio 10:1 sugar:Alizarin to the system at physiological conditions, we should observe the release of Alizarin from the system accompanied with a color change from orange to pink and with an absorbance maxima shift to higher wavelengths, typical for free A. We analyzed SVE-FPBA-AL micelles with all of above-mentioned sugars, F, G and C by measuring the absorbance.

We found out, that when fructose, F and galactose, G, to SVE-FPBA-AL micelles, no changes in color nor absorbance are visible even after 72 hours. This means, that these sugar molecules struggle to penetrate the very compact micellar structure which is probably highly interlaced with hydrogen bonds. The intact absorbance spectra after sugars addition can be seen in Figure 35. However, when adding ascorbic acid, C, to the system, SVE-FPBA-AL nanoparticles showed a color change from orange to clear yellow, typical for non-ionic Alizarin under acidic conditions. In addition, the pH of the solution changed naturally after adding vitamin C to the system to the value 2.98 and the absorbance maxima shifted to 425 nm what corresponds to free Alizarin in acidic pH. We suppose, that the addition of ascorbic acid, C, to the system caused the reduction of the Alizarin causing the disintegration of the boron ester and the release of Alizarin molecules from the SVE-FPBA-AL nanoparticles. To confirm that the red/ox reaction affects only alizarin and does not cause the FPBA deboronation, we added the same amount of ascorbic acid, C to the saturated solution of AL in water at pH 7, (ALfree), yielding ALfree + C solution in Figure 35. We observed the same color and pH change and also

the absorbance maxima shift from the highest maxima corresponding to the unbound monoanionic form to the lowest absorbance maxima ≈425 nm that is characteristic for the non-ionic free molecule in acidic environment.

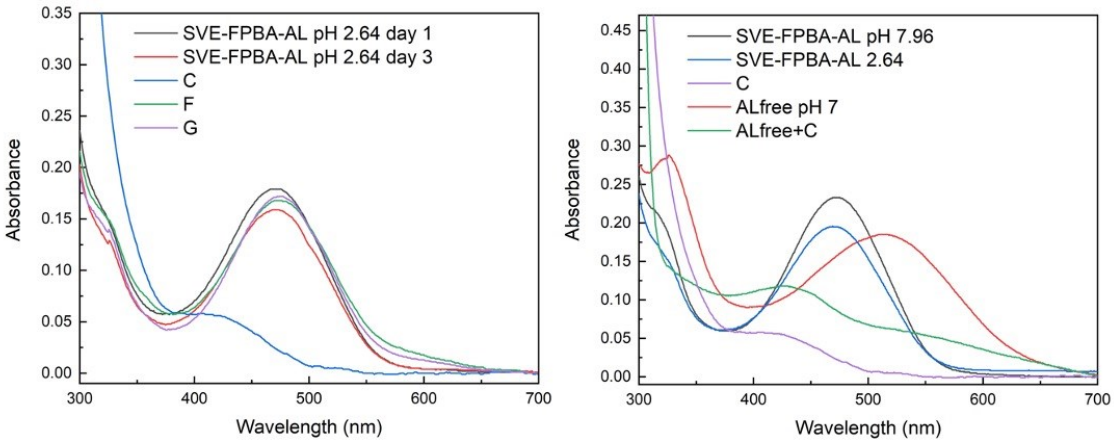

*Figure 35:Absorbance measurements: **left**- N SVE-FPBA-AL micelles with addition of sugars-ascorbic acid, C, fructose, F, and galactose, G, then N SVE-FPBA-AL micelles in acidic pH, **right**- comparison of N SVE-FPBA-AL micelles in physiological pH, in acidic pH, in solution with ascorbic acid, C, to the solution of free AL and free AL after addition of ascorbic acid.*

Thus, we can conclude, that the release of Alizarin from SVE-FPBA-AL nanoparticles is hindered by the hydrogen bonds between protonated P4VP in acidic pH and boron atoms and also that a portion of AL molecules can be entrapped in form of ion pairs between Alizarin's negatively charged hydroxyls and positively charged nitrogen atoms of P4VP units. [53, 90] When introducing a reductive agent, that is in our case the vitamin C, red/ox reaction between Alizarin and vitamin C yield in one hand dehydroascorbic acid that probably binds to boronic acid via hydroxyls on two terminal carbons and in other hand quinonoid form of Alizarin that gives neither the possibility to form boron ester with FPBA molecule, nor the ion pair with quaternized nitrogen. The schematic representation of the red/ox reactions is in the Figure 36. [91]

The cryo-TEM images in the Figure 37 show no differences in micellar size induced by the red/ox reaction. We could only see the loss of the contrasted aggregated from the small 1 nm aggregates in the solution, that were contrasted after the AL addition, caused by the disintegration of the FPBA-AL ester and release of AL from the aggregates.

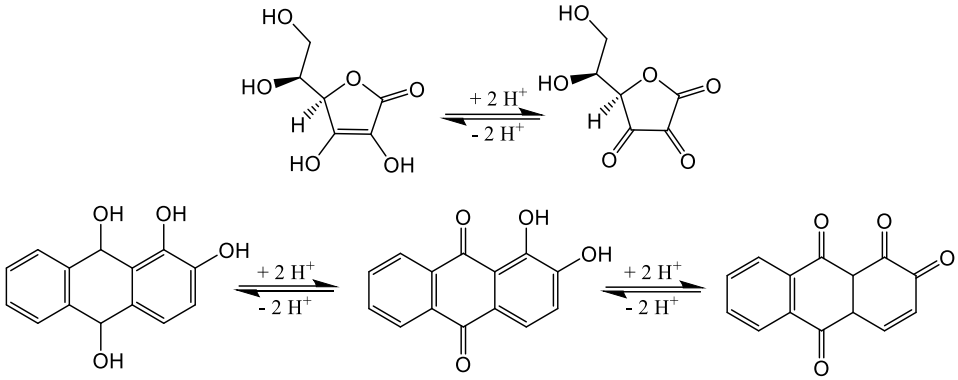

Figure 36: Red/ox reaction of: ***top****-ascorbic acid, C,* ***bottom****-alizarin, AL*

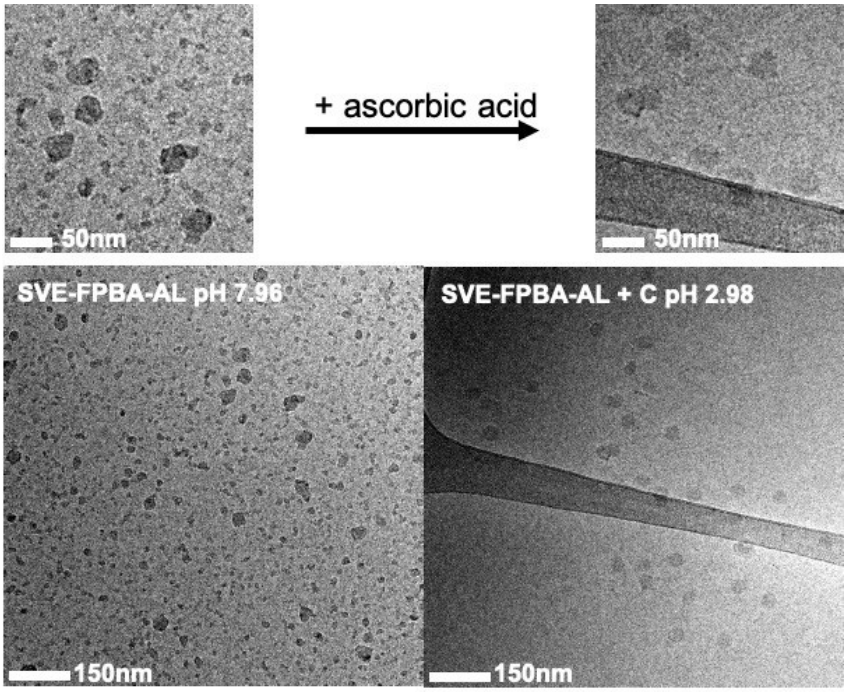

Figure 37:Cryo-TEM images of SVE-FPBA-AL micelles: ***left****-before ascorbic acid, C, addition,* ***right****-after ascorbic acid addition.*

We have also confirmed the release of Alizarin induced by the red/ox reaction with fluorescence emission measurements. We have compared SVE-FPBA-AL micelles in pH 7.96, (AL pH 7.96) to micelles with sugars. We have analyzed SVE-FPBA-AL nanoparticles after addition of fructose, F after three days, (AL+F day 3), then the same but freshly prepared SVE-FPBA-AL with F, (AL+F day 1) as a study of Alizarine release in time. We have also studied the fluorescence emission of SVE-FPBA-AL nanoparticles without adding sugars but by mimicking acidic conditions of drug release. We have changed the pH of the solution to pH 2.2 by addition of HCl (AL pH 2.2) and we have

compared this sample to the SVE-FPBA-AL nanoparticles after addition of ascorbic acid (AL+C) with reductive effect and naturally decreased pH to 2.3. We have expected that samples AL pH 7.96 and AL+F day 1 will show the highest intensity fluorescence emission because of the highest amount of bound Alizarin to FPBA in SVE-FPBA-AL micelles. Then, we have expected that the fluorescence emission of sample AL+F day 3 may show weaker fluorescence emission due to a probably very low efficient competitive binding of a few molecules of fructose and AL molecules. Identically, we supposed that also the decrease of pH in sample AL pH 2.2 could induce a minor intensity decrease of fluorescence emission due to hydrolysis of several Alizarin molecules from boron ester. Based on absorbance experiments, we have expected, that the sample AL+C with naturally acidic pH with reductive properties of C will show the lowest emission because of the lowest amount off AL molecules in FPBA-AL boron esters.

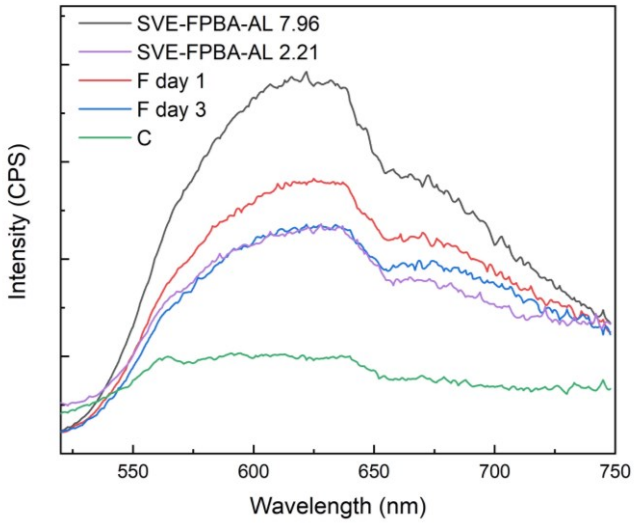

Figure 38: Fluorescence emission measurements of N SVE-FPBA-AL micelles in physiological pH, in acidic pH, in physiological pH with addition of fructose, F, after 1 day and after 3 days, and micelles with naturally decreased pH after addition of ascorbic acid, C.

Figure 38 with steady state fluorescence emission spectra is in accordance with our expectations and theories. In addition, except for the typical bound AL emission maxima at ≈620 nm, the spectra show other maxima at ≈670 nm that could belong to the absorbed AL molecule in form of ion pair between AL hydroxyls and quaternized P4VP units. Thus, we could conclude, that the decrease of pH is not enough strong stimuli to induce the AL release from SVE-FPBA-AL micelles due to extensive hydrogen bonding in micelles. Also, the decrease of pH over the pK_A of P4VP causes that the portion of

P4VP units gain positive charge on nitrogen atoms, that can subsequently form an ion pair with AL molecules. To conclude, we suppose that only a limited number of AL molecules can be released upon decreasing the pH decrease pH=2.2 (violet curve, Figure 38). Also, the competitive binding between sugars and AL molecules cause only a small substitution of AL molecules, (blue cure, Figure 38). Based on our findings, the hydrolysis of Alizarin from our nanoparticles is possible only when the system reaches the red/ox environment, in our case the ascorbic acid, C. These findings highlight the fact, that the circulation time of a potentially used drug until its release prolongates and that the release from our system is induced with specificity to the red/ox environment. the reduction environment induced visualizing of for example tissues when applying the Alizarin molecule to the drug delivery system.[5] In one hand, the oxidizing environment can be found for example in the surrounding of cancerous cells what completely fits to our potential target use of these nanoparticles. In there, our system should release the cargo due to the deboronation reaction.[41] In other hand, micellar system with Alizarin molecules can be applied as a visualization agent for tissues monitoring with response to reducing environment.

7. Conclusion

1. Stimuli-responsive PS-*b*-P4VP-*b*-PEO, SVE, triblock terpolymer was functionalized by post polymerization modification reaction with 2-bromomethyl-4-fluorophenylboronic acid, FPBA, and separately with comparative 2-bromomethyl phenylboronic acid, PBA, in *N,N*-dimethylformamide, DMF, yielding SVE-FPBA and SVE-PBA, respectively. Polymer solution in DMF was changed to water solvent by dialysis and the polymer was isolated in form of light green powder by lyophilization. The quaternization of nitrogen atom on P4VP units brought permanent positive charge to the system and thus, changed the solubility of the polymer. Previously soluble PS-*b*-P4VP-*b*-PEO in *N,N*-dimethylformamide only become soluble in methanol. Polymer modified with fluorinated analogue of phenylboronic acid FPBA shown identical solubility as its parent molecule PBA.
2. The reaction yield was determined from ^{1}H NMR by comparison of integrated area under peak of methylene linker of FPBA and PBA, to the signal of methanol soluble PEO. In SVE-FPBA triblock terpolymer were quaternized 35 % units of P4VP block and in SVE-PBA triblock terpolymer were quaternized 40 % units of P4VP block. ^{11}B NMR confirmed the reaction product by upfield shift of boron signal of both SVE-FPBA and SVE-PBA. Also, infrared spectroscopy shown newly appearing vibrational peak of quaternized vinyl pyridine nitrogen differing from non-quaternized nitrogen atoms of unmodified SVE. The FT-IR spectra of both functionalized triblocks confirmed the co-presence of the quaternized and non-quaternized P4VP units underlying our quaternization percentage calculations based on ^{1}H NMR measurements.
3. Micellar solutions of both SVE-FPBA and comparative SVE-PBA were prepared by solubilization of polymer in methanol followed by quenching to water. Solutions were purified by dialysis and the protocol of self-assembly yielded stable spherical micelles. Stability of nanoparticles was confirmed with positive zeta potential value of +40 mV. The pH responsiveness of P4VP block was studied by analyzing of micelles in acidic solution and in solution with non-adjusted pH near to physiological. Transfer of micelles to basic solution up the

pK_A of boronic acid caused the precipitation due to system destabilization by negative charge of boronic acid. Static and dynamic Zimm plots and dynamic plots giving micellar radius of gyration, aggregation number, diffusion coefficient and hydrodynamic radius showed solvent swelling of P4VP shell in case of nanoparticles transferred to acidic solution of pH near to 5. The decrease of pH below the value approximately 4 did not show further changes in morphology of micelles. Cryo-TEM images together with LS results shown formation of P4VP loops consisting of segments rich in quaternized and soluble P4VP units that interfere with solvent swelled PEO corona. The estimate of micellar composition show nanoparticles with frozen PS core, frozen P4VP shell consisting of non-quaternized P4VP units, then solvent swelled loops consisting from quaternized P4VP segments of P4VP block and by the end solvent swelled PEO corona.

4. First attempt of encapsulation of charged Alizarin Red S as a model drug brought struggles of solubility by additional charge in the system causing destabilization of micelles. ARS was changed to its parent neutral molecule Alizarin. Alizarin encapsulation to SVE-FPBA was successful when performed in methanol followed by micellar transfer to water, as typical for previous self-assembly. Absorbance measurements shown that the encapsulation of 75 % molar equivalent of Alizarin to FPBA molecules occurred quantitatively and that the encapsulated model drug persists bound to micelle until moment of stimuli-induced release. The competitive binding of sugars shown that the release of vicinal diols from our phenylboronic acid containing system is responsive to reductive and oxidative environment.

The specificity of the drug release from our system to both reducing and oxidizing environment showed potential of usage of our functionalized stimuli-responsive triblock terpolymer in field of drug delivery but also as a fluorophore carrier for visualizing of tissues.

Acknowledgment for financial support

This study is a part of a financially supported project by the Czech Science Foundation (GAČR), grant 17-00289Y. Further, I would like to acknowledge the financial support during my master study from the Czech Science Foundation grants 17-00648S and 19-13458S, and from the Ministry of Education of Czech Republic via INTER-EXCELLENCE project grant number LTAIN19078.

8. References

1. Moughton, A. O.; Hillmyer, M. A.; Lodge, T. P. *Macromolecules* **2011**, *45* (1), 2–19.
2. Holder, S. J.; Sommerdijk, N. A. J. M. *Polymer Chemistry* **2011**, *2* (5), 1018.
3. Bates, C. M.; Bates, F. S. *Macromolecules* **2016**, *50* (1), 3-22.
4. Aznar, E.; Oroval, M.; Pascual, L.; Murguía, J. R.; Martínez-Máñez, R.; Sancenón, F. *Chemical Reviews* **2016**, *116* (2), 561–718.
5. Casasús, R.; Marcos, M. D.; Martínez-Máñez, R.; Ros-Lis, J. V.; Soto, J.; Villaescusa, L. A.; Amorós, P.; Beltrán, D.; Guillem, C.; Latorre, J. *Journal of the American Chemical Society* **2004**, *126* (28), 8612–8613.
6. Fernandez-Alvarez, R.; Hlavatovičová, E.; Rodzeń, K.; Strachota, A.; Kereïche, S.; Matějíček, P.; Cabrera-González, J.; Núñez, R.; Uchman, M. *Polymer Chemistry* **2019**, *10* (22), 2774–2780.
7. Willet, N.; Gohy, J.-F.; Auvray, L.; Varshney, S.; Jérôme, R.; Leyh, B. *Langmuir* **2008**, *24* (7), 3009–3015.
8. Hadjichristidis, N.; Iatrou, H.; Pitsikalis, M.; Pispas, S.; Avgeropoulos, A. Linear and Non-Linear Triblock Terpolymers. **2005**, *30* (7), 725–782.
9. Huang, J.; Guo, Y.; Gu, S.; Han, G.; Duan, W.; Gao, C.; Zhang, W. *Polymer Chemistry* **2019**, *10* (25), 3426–3435.
10. Zhang, W.; Shi, L.; Ma, R.; An, Y.; Xu, Y.; Wu, K. *Macromolecules* **2005**, *38* (21), 8850–8852.
11. Skrabania, K.; Laschewsky André; Berlepsch, H. V.; Böttcher Christoph. *Langmuir* **2009**, *25* (13), 7594–7601.
12. Laschewsky, A.; Marsat, J.-N. L.; Skrabania, K.; Berlepsch, H. V. *Macromolecular Chemistry and Physics* **2010**, *211* (2), 215–221.
13. Uchman, M.; Štěpánek M.; Procházka K.; Mountrichas, G.; Pispas, S.; Voets, I. K.; Walther, A. *Macromolecules* **2009**, *42* (15), 5605–5613.
14. Kubowicz, S.; Baussard, J.-F.; Lutz, J.-F.; Thünemann, A. F.; Berlepsch, H. V.; Laschewsky, A. *Angewandte Chemie International Edition* **2005**, *44* (33), 5262–5265.

15. Gröschel, A. H.; Schacher, F. H.; Schmalz, H.; Borisov, O. V.; Zhulina, E. B.; Walther, A.; Müller, A. H. *Nature Communications* **2012**, *3* (1).
16. Schacher, F.; Walther, A.; Ruppel, M.; Drechsler, M.; Müller Axel H. E. *Macromolecules* **2009**, *42* (10), 3540–3548.
17. Berlepsch, H. V.; Böttcher, C.; Skrabania, K.; Laschewsky, A. *Chemical Communications* **2009**, *17*, 2290.
18. Marsat Jean-Noël; Heydenreich, M.; Kleinpeter, E.; Berlepsch, H. V.; Böttcher Christoph; Laschewsky André. *Macromolecules* **2011**, *44* (7), 2092–2105.
19. Talingting, M. R.; Munk, P.; Webber, S. E.; Tuzar, Z. *Macromolecules* **1999**, *32* (5), 1593–1601.
20. Zhu, J.; Hayward, R. C. *Macromolecules* **2008**, *41* (21), 7794–7797.
21. Gohy, J.-F.; Lefèvre, N.; Dhaese, C.; Hoeppener, S.; Schubert, U. S.; Kostov, G.; Améduri, B. *Polym. Chem.* **2011**, *2* (2), 328–332.
22. Plamper, F. A.; Mckee, J. R.; Laukkanen, A.; Nykänen, A.; Walther, A.; Ruokolainen, J.; Aseyev, V.; Tenhu, H. *Soft Matter* **2009**, *5* (9), 1812.
23. Fang, B.; Walther, A.; Wolf, A.; Xu, Y.; Yuan, J.; Müller, A. H. E. *Angewandte Chemie* **2009**, *121* (16), 2921–2924.
24. Schmalz, H.; Schmelz, J.; Drechsler, M.; Yuan, J.; Walther, A.; Schweimer, K.; Mihut, A. M. *Macromolecules* **2008**, *41* (9), 3235–3242.
25. Li, Z.; Hillmyer, M. A.; Lodge, T. P. *Langmuir* **2006**, *22* (22), 9409–9417.
26. Ge, Z.; Liu, S. *Macromolecular Rapid Communications* **2009**, *30* (18), 1523–1532.
27. Swann, J. M. G.; Topham, P. D. *Polymers* **2010**, *2* (4), 454–469.
28. Procházka, K. *Fyzikální Chemie Polymerů*; Univerzita Karlova: Praha, 1995.
29. Israelachvili, J. N.; Mitchell, D. A *Biochimica et Biophysica Acta (BBA) - Biomembranes* **1975**, *389* (1), 13–19.
30. Stuart, M. C.; Boekema, E. J. *Biochimica et Biophysica Acta (BBA) - Biomembranes* **2007**, *1768* (11), 2681–2689.
31. Israelachvili, J. N.; Mitchell, D.; Ninham, B. W. *Biochimica et Biophysica Acta (BBA) - Biomembranes* **1977**, *470* (2), 185–201.
32. Tritschler, U.; Pearce, S.; Gwyther, J.; Whittell, G. R.; Manners, I. *Macromolecules* **2017**, *50* (9), 3439–3463.
33. Yang, J.; He, W.-D.; He, C.; Tao, J.; Chen, S.-Q.; Niu, S.-M.; Zhu, S.-L. *Journal of Polymer Science Part A: Polymer Chemistry* **2013**, *51* (18), 3791–3799.

34. Yan, H.; Teh, C.; Sreejith, S.; Zhu, L.; Kwok, A.; Fang, W.; Ma, X.; Nguyen, K. T.; Korzh, V.; Zhao, Y. *Angewandte Chemie* **2012**, *124* (33), 8498–8502.
35. Ji, W.; Li, N.; Chen, D.; Qi, X.; Sha, W.; Jiao, Y.; Xu, Q.; Lu, J. *Journal of Materials Chemistry B* **2013**, *1* (43), 5942.
36. Xia, L.; Zhou, Z.; Dai, J. *Advances in Polymer Technology* **2013**, *32* (4).
37. Ruhland, T. M.; Reichstein, P. M.; Majewski, A. P.; Walther, A.; Müller, A. H. *Journal of Colloid and Interface Science* **2012**, *374* (1), 45–53.
38. Cammas, S.; Suzuki, K.; Sone, C.; Sakurai, Y.; Kataoka, K.; Okano, T. *Journal of Controlled Release* **1997**, *48* (2-3), 157–164.
39. Li, Q.; Gao, C.; Li, S.; Huo, F.; Zhang, W. *Polym. Chem.* **2014**, *5* (8), 2961–2972.
40. Peer, D.; Karp, J. M.; Hong, S.; Farokhzad, O. C.; Margalit, R.; Langer, R. *Nature Nanotechnology* **2007**, *2* (12), 751–760.
41. Feng, C.; Wang, F.; Dang, Y.; Xu, Z.; Yu, H.; Zhang, W. *Langmuir* **2017**, *33* (13), 3287–3295.
42. Surnar, B.; Jayakannan, M. *Biomacromolecules* **2016**, *17* (12), 4075–4085.
43. Liu, S.; Ono, R. J.; Yang, C.; Gao, S.; Tan, J. Y. M.; Hedrick, J. L.; Yang, Y. Y. *ACS Applied Materials & Interfaces* **2018**, *10* (23), 19355–19364.
44. Stuart, M., Huck, W., Genzer, J. *Nature Mater* **2010**, *9*, 101–113.
45. Ďorďovič, V.; Vojtová, J.; Jana, S.; Uchman, M. *Polymer Chemistry* **2019**, *10* (40), 5522–5533.
46. Billing, M.; Elter, J. K.; Schacher, F. H. *Polymer* **2016**, *104*, 40–48.
47. Humpolíčková Jana; Štěpánek, M.; Procházka, K.; Hof, M. *The Journal of Physical Chemistry A* **2005**, *109* (48), 10803–10812.
48. Valkama, S.; Ruotsalainen, T.; Kosonen, H.; Ruokolainen, J.; Torkkeli, M.; Serimaa, R.; Brinke, G. T.; Ikkala, O. *Macromolecules* **2003**, *36* (11), 3986–3991.
49. Lee, D. H.; Han, S. H.; Joo, W.; Kim, J. K.; Huh, J. *Macromolecules* **2008**, *41* (7), 2577–2583.
50. Belfiore, L. A.; Mccurdie, M. P. *Journal of Polymer Science Part B: Polymer Physics* **1995**, *33* (1), 105–124.
51. El-Hamshary, H.; El-Garawany, M.; Assubaie, F. N.; Al-Eed, M. *Journal of Applied Polymer Science* **2003**, *89* (9), 2522–2526.
52. Kang, N.-G.; Kang, B.-G.; Koh, H.-D.; Changez, M.; Lee, J.-S. *Reactive and Functional Polymers* **2009**, *69* (7), 470–479.
53. Kennemur, J. G. *Macromolecules* **2019**, *52* (4), 1354–1370.

54. Walther, A.; Müller, A. H. E. *Chemical Communications* **2009**, No. 9, 1127.
55. Nghiem, T.-L.; Löbling, T. I.; Gröschel, A. H. *Polymer Chemistry* **2018**, *9* (13), 1583–1592.
56. Mondal, P.; Saha, S. K.; Chowdhury, P. *Journal of Applied Polymer Science* **2012**, *127* (6), 5045–5050.
57. Bicak, N.; Gazi, M. *Journal of Macromolecular Science, Part A* **2003**, *40* (6), 585–591.
58. Medjahed, K.; Tennouga, L.; Mansri, A. *Macromolecular Symposia* **2014**, *339* (1), 130–133.
59. Frere, Y.; Gramain, P. *Macromolecules* **1992**, *25* (12), 3184–3189.
60. Yan, J.; Springsteen, G.; Deeter, S.; Wang, B. *Tetrahedron* **2004**, *60* (49), 11205–11209.
61. Iovine, P. M.; Fletcher, M. N.; Lin, S. *Macromolecules* **2006**, *39* (19), 6324–6326.
62. Marinaro, W. A.; Prankerd, R.; Kinnari, K.; Stella, V. J. *Journal of Pharmaceutical Sciences* **2015**, *104* (4), 1399–1408.
63. Matuszewska, A.; Uchman, M.; Adamczyk-Woźniak, A.; Sporzyński, A.; Pispas, S.; Kováčik, L.; Štěpánek, M. *Biomacromolecules* **2015**, *16* (12), 3731–3739.
64. Su, J.; Chen, F.; Cryns, V. L.; Messersmith, P. B. *Journal of the American Chemical Society* **2011**, *133* (31), 11850–11853.
65. Liu, S.; Ono, R. J.; Yang, C.; Gao, S.; Tan, J. Y. M.; Hedrick, J. L.; Yang, Y. Y. *ACS Applied Materials & Interfaces* **2018**, *10* (23), 19355–19364.
66. Wu, K.; Cheng, R.; Zhang, J.; Meng, F.; Deng, C.; Zhong, Z. *Journal of Materials Chemistry B* **2017**, *5* (28), 5658–5667.
67. Axthelm, J.; Askes, S. H. C.; Elstner, M.; G, U. R.; Görls, H.; Bellstedt, P.; Schiller, A. *Journal of the American Chemical Society* **2017**, *139* (33), 11413–11420.
68. Liang, X.; Trentle, M.; Kozlovskaya, V.; Kharlampieva, E.; Bonizzoni, M. *ACS Applied Polymer Materials* **2019**, *1* (6), 1341–1349.
69. Scorei, R.; Popa, R. *Anti-Cancer Agents in Medicinal Chemistry* **2013**, *13* (6), 901–909.
70. Schumacher, S.; Nagel, T.; Scheller, F. W.; Gajovic-Eichelmann, N. *Electrochimica Acta* **2011**, *56* (19), 6607–6611.

71. Lu, H.; Huang, W. *Shape Memory Polymers for Biomedical Applications* **2015**, 99–132.
72. Sun, X.; James, T. D. *Chemical Reviews* **2015**, *115* (15), 8001–8037.
73. McMurry, J. *Fundamentals of organic chemistry: John McMurry*; Brooks/Cole: Pacific Grove, CA, **2010**.
74. Tošner, Z. *Basics of molecular spectroscopy*, [lecture], Prague, Charles Univerity, Faculty of Science, **2018**.
75. Obšil, T. *Biophysical chemistry I, II,* [lecture], Prague, Charles Univerity, Faculty of Science, **2019**.
76. Schartl, W. *Light Scattering from Polymer Solutions and Nanoparticle: Dispersions*; Springer: Berlin, **2010**.
77. Øgendal, L. H. *Light Scattering Demystified: Therory and Practice;* University of Copenhagen, **2017**.
78. Perkampus, H.-H. *UV-VIS spectroscopy and its applications*; Springer-Verlag Berlin, **2012**.
79. Schrader, E. *Infrared and Raman Spectroscopy, B*. WCH Publishers: Weinheim, **1995**.
80. Štěpánek, J. *Metody absorpční spektroskopie a spektroskopie Ramanova rozptylu v V. Prosser a kol. "Experimentální metody biofyziky"*, Akademia: Prague, **1989**.
81. Lakowicz, J. R. *Principles of fluorescence spectroscopy*, 2nd ed.; Springer: New York, **2006**.
82. Williams, A. T. R. *An Introduction to fluorescence spectroscopy;* Perkin-Elmer: Beaconsfied, **2000**.
83. Albani, J. R. *Principles and applications of fluorescence spectroscopy*; Blackwell Science: Oxford, **2007**.
84. Frank, J. *Single-particle cryo-electron microscopy: the path toward atomic resolution: selected papers of Joachim Frank with commentaries*; World Scientific Publishing Co. Pte Ltd: Singapore, **2018**.
85. Convington, A. K.; Paabo, M.; Robinson, R. A.; Bates, R. G. *Analytical Chemistry*, **1968**, *13* (4), 700–706.
86. Štěpánek, M.; Matějíček Pavel; Humpolíčková Jana; Procházka, K. *Langmuir* **2005**, *21* (23), 10783–10790.
87. Fernandez-Alvarez, R.; Nová, L.; Uhlík, F.; Kereïche, S.; Uchman, M.; Košovan, P.; Matějíček, P. *Journal of Colloid and Interface Science* **2019**, *546*, 371–380.

88. Kubo, Y.; Ishida, T.; Kobayashi, A.; James, T. D. *Journal of Materials Chemistry* **2005**, *15* (27-28), 2889.
89. Stephens, A. J.; Scopelliti, R.; Tirani, F. F.; Solari, E.; Severin, K. *ACS Materials Letters* **2019**, *1* (1), 3–7.
90. Gul, F.; Khan, A. M.; Shah, S. S.; Nazar, M. F. *Coloration Technology* **2010**, *126* (2), 109–113.
91. Schumacher, S.; Nagel, T.; Scheller, F. W.; Gajovic-Eichelmann, N. *Electrochimica Acta* **2011**, *56* (19), 6607–6611.
92. Smith, M.; March, J. *Marchs advanced organic chemistry: reactions, mechanisms, and structure*; John Wiley & Sons: Hoboken, NJ, **2007**.
93. Huglin, M. B. *Light scattering from polymer solutions*; Academic Press: London, **1972**.